University of Cape Town

Department of Mechanical Engineering

Design and Construction of a Pulsed Linear Induction Motor

by

Braam Maxim Daniels [DNLBRA003]

braamdaniels@gmail.com

supervised by

Dr. Andrew Wilkinson

26th December 2007

Abstract

A small single stage pulsed co-axial linear induction motor was designed and constructed to verify the computational simulation used in its development and to determine the feasibility of the operation concept at low operating voltages and energy inputs of 400 Volts and of 25 Joules respectively. The suitability of the Insulated Gate Bi-polar Transistor (I.G.B.T) in such a launcher system was also investigated. Moreover the system uses wire wound helical armature coils as opposed to conventional conducting rings to greatly enhance the mutual induction between the stator and armature.

Research was conducted through a comprehensive literature review providing detailed and concise information regarding the theoretical modeling of the system and important design considerations. Information was extracted from research published in the IEEE Transactions on Magnetics and similar journals, supplemented by numerous books and device data sheets/application notes.

In practice the operation of the device was compared to the theoretical model mainly in terms of the tank circuit current magnitude, oscillation frequency and qualitative observations of the mechanical performance. Despite much of the theoretical model being to some extent verified, this project has found that pulsed co-axial linear induction motors are not effective if designed to operate at low voltages. It is also concluded that the idealized assumptions which neglect mechanical friction and more specifically the IGBT on state resistance are not valid at these low energy inputs.

Declaration

1. I know that plagiarism is wrong. Plagiarism is to use another's work and pretend this it is one's own.
2. I have used the Harvard convention for citation and referencing. Each significant contribution to, and quotation in, this thesis from the works(s) of other people has been attributed and has been cited and referenced.
3. This thesis is my own work.
4. I have not allowed and will not allow anyone to copy my work with the intention of passing it off as his or her own work.

Signature.....

Braam Maxim Daniels

Acknowledgments

I would like to specifically thank the following individuals for the assistance and support they offered not just during the course of this thesis but indeed over the last four years study which I have enjoyed at the University of Cape Town.

Firstly I would like to give a huge thanks to Mr. Chris Wozniak, whose subtle guidance, provision of laboratory equipment and general assistance in the Machines Laboratory has made this projects laboratory testing phase an enriching and educational success. I would also like to extend great gratitude to Mr. Barry Hansen whose unconditional support, advice and availability for long in-depth discussions regarding the subject of electromechanical launchers has played a significant role in the completion of this project.

The Mechanical Engineering Workshop Staff for manufacturing the few parts required in this project and for their support and guidance offered during other projects I have had to complete during my stay at U.C.T. In particular Mr. Glen Newins whose dedication, patience and caring support of this project while simultaneously demonstrating similar behavior to all the other students is both highly commendable and greatly appreciated.

To my Mother and Father whose endless love and support has not only guided me through this project but through my entire university career. I gratefully thank you for everything you have done for me in the past and during this project by eliminating all the unfortunate obstacles which life throws at one. Most notably was my computer crashing midway through the course of this project. Your swift reaction to the many events such as this is most gratefully noted and appreciated.

I would also like to thank my thesis supervisor, Dr. Andrew Wilkinson for supporting this project and allowing me the freedom to research a topic of my own choosing. Without you faith, support and subtle guidance I would never have come so far and learned so much.

I would also like to thank Mr. Julian Meyer who assisted me greatly in equipment and parts purchasing. Similarly I would also like to thank Mr. Alburt Martin who has provided me with all the electronic components and companionship I have ever needed while working on this and other projects in The White Lab. Mrs. Tembi Dlyakia who's the Departmental Secretary of the Mechanical Engineering Department at U.C.T, for your supportive and joyful manner which has made all my administrative dealings with the department over the last four years an absolute pleasure.

To my fellow students with whom I have had the pleasure of studying alongside, for providing the endless entertainment, support and camaraderie which was greatly enjoyed and required over the last four years. I'm sure the relationships forged will lead to many joyous encounters in the future. During the course of my studies I have obviously made many social sacrifices, for this reason I'd also like to give thanks to all my other friends and family for their endless understanding and patience during the course of my studies, this has been a strong motivator over the years and has allowed me to enjoy my studies in the fullest.

Summary

Introduction

A typical coil gun converts electrical energy to linear kinetic energy by using a wire wound stator coil and electro-mechanical principles to accelerate a ferromagnetic or wire wound coil armature. Of particular interest to this study however is the operation of a multistage pulsed or capacitor driven linear induction motor/launcher which is shown conceptually in Figure 1 below.

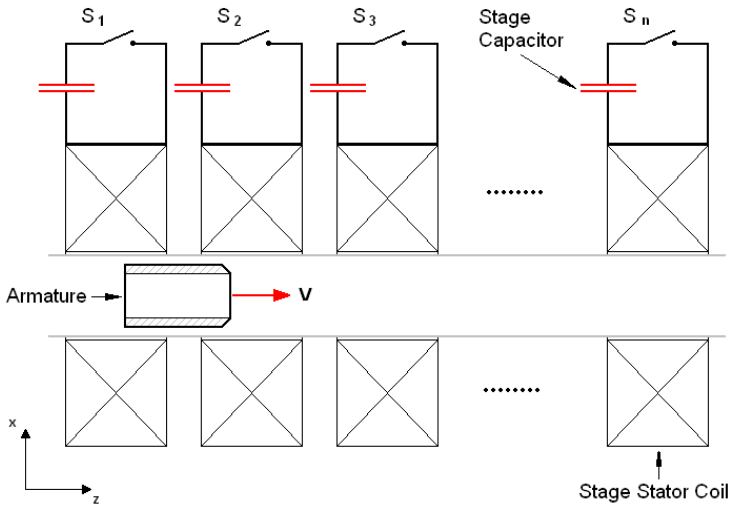

Figure 1: Schematic diagram of a muti-stage capacitor driven linear induction motor/laucher system.

These systems offer a variety of attractive features over other coilgun and railgun systems but despite this research into the technology remains a study of advanced electro-mechanical research groups only. Much of the current literature available describes these devices typically operating at voltages and energy levels exceeding 10^3 Volts and 10^3 Joules, operating at efficiencies well above 50%. However despite the impressive performance of these systems they are typically very large and bulky. It is because of the impressive performance that these devices can achieve when scaled in size and operating energy that very little research has been focused system miniaturization, resulting in high research and development costs which only a handfull of research programs can actually afford. Therefore certain critical engineering and design issues such as lightweight design and system miniaturization of these systems has not received much attention [1].

At lower energies and operating voltages the cost of the equipment required in building such a system is greatly reduced. The availability of desktop computers also plays a significant role in that for the first time large supercomputers are no longer required to carry out the complex simulations required to model and develop such a device. These and many other technological advances now make the study of linear

induction launchers feasible within the scope of a small undergraduate project. The aim of this research project is to develop a linear induction motor system capable of operating at 400 Volts with an initial energy of 25 J to investigate the low energy feasibility of the operating concept and to verify the design procedure used in its development. If successful further research may be conducted into the expansion and optimization of the system.

Procedure

A detailed launcher model/simulation program was first written in Matlab and served as a most important tool used throughout the development and design of the single stage pulsed linear induction motor. Based on the initial inputs provided by the user, the simulation would calculate a specified coil pairs inductance parameters, resistance and mass. These results are used by a numerical method based on two coupled differential equations derived by applying KIRCHOFF'S VOLTAGE LAW to the equivalent armature and stator coil circuits (shown below in Figure 2), thus allowing for many of the systems time varying parameters to be quite readily solved over a specified time period.

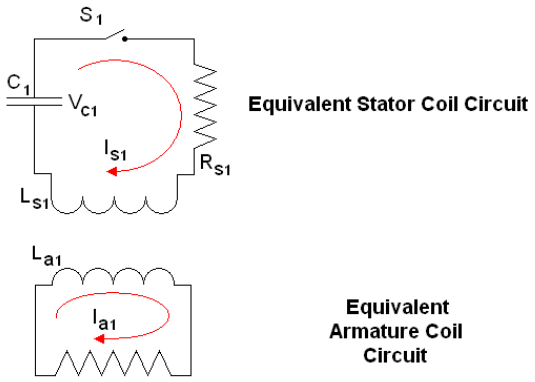

Figure 2: Equivalent stator and armature coil circuits used to develop the differential equations describing the launcher system.

This simulation was then used to develop a feasible launcher system based on initial performance requirement specifications, project goals and extensive research on the systems important design considerations. The complete launcher system on which tests were conducted is shown below in Figure 3.

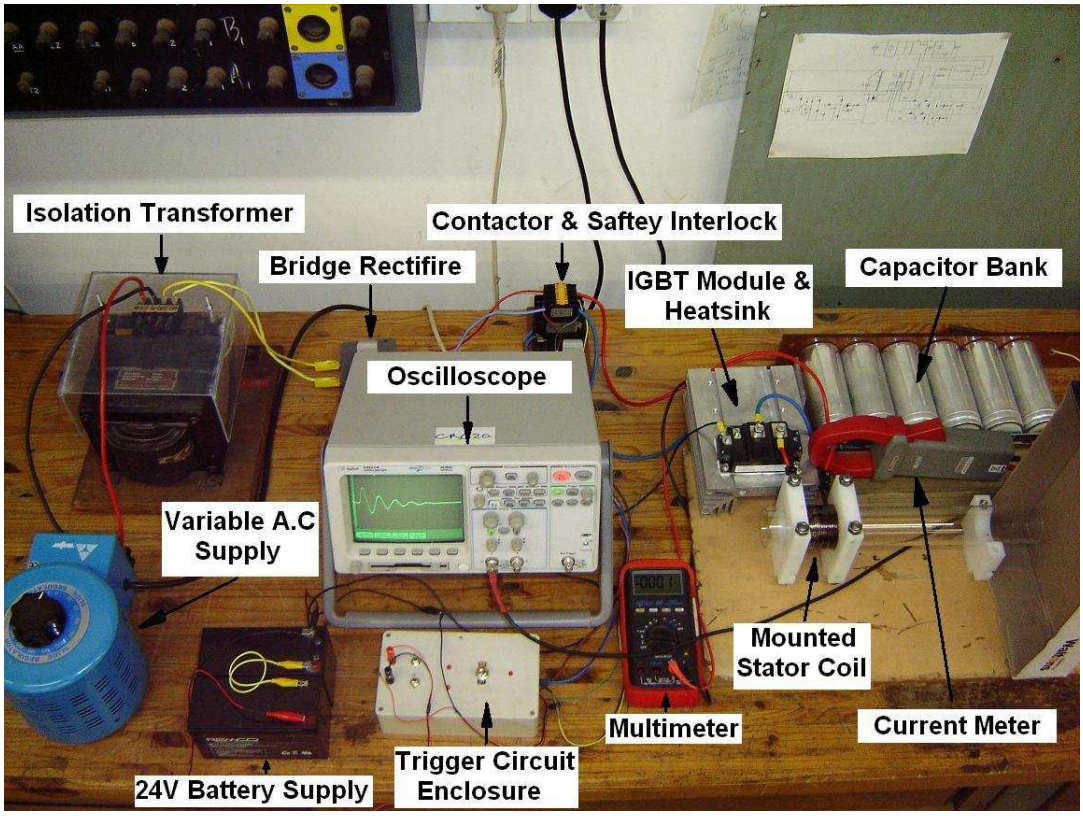

Figure 3: Experimental system used to test the pulsed linear induction launcher concept.

Current waveforms produced by the system in practice and by the theoretical simulation are compared to each other, in addition to qualitatively observing any motion of the armature coil. If the velocities achieved by the armature warrant it, optical methods may be used to determine armature velocity between two points to more accurately compare the theoretical and actual mechanical performance of the system.

Results

Despite the less than impressive mechanical performance of the device, the actual current plots were very much similar to that predicted by the computer simulation with any differences being reasonably well explained. Figure 4 shows for comparison the typical tank circuit current waveform seen in practice and the waveform predicted by the computer simulation of the launcher system for a similar system parameters and operating conditions.

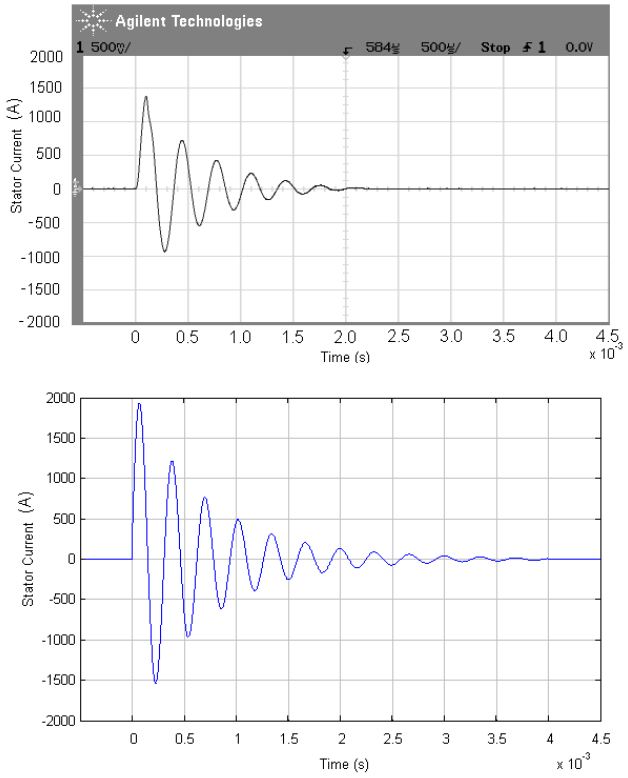

Figure 4: Actual (top) and theoretical (bottom) plots of the tank circuit current during the capacitors discharge into the stator coil for an initial voltage of 350 Volts.

Analysis/comparison of these waveforms clearly reveals that damping of this oscillatory waveform in practice is far more severe than theoretically expected, however the magnitudes of currents and oscillation frequency are very close to that predicated by the simulation. Furthermore at voltages above 300 Volts, obvious motion of the armature was achieved, thus to some extent proving the operating concept.

Finally when switching the tank circuit with a mechanical contactor as opposed to the IGBT, it was found that the mechanical performance (armature displacement and velocity) of the system was greatly improved. The current magnitudes and decay period was in practice also far closer to that predicted by the computer simulations. These tests confirmed the conclusions made regarding IGBT usage in the system (as discussed in brief below).

Conclusions

The fact that that the actual launcher's electrical performance was predicted with good accuracy suggests that the simulation code is to some extent valid. Therefore the poor mechanical performance of the launcher is attributed to the invalid assumption of an ideal system (neglecting mechanical friction and IGBT/diode on state resistance within the tank circuit) on which the system model was developed. The

validity of this conclusion, specifically regarding the usage of the IGBT was confirmed when the tank circuit was switched using a mechanical contactor, as opposed to the IGBT.

It was also learned that low operating voltages and input energies will result in launcher designs where the tank circuit is inherently limited by a very small oscillation envelope leading to poor system performance. Operating at much higher voltages will allow for much larger stator coils with higher inductances to be used which will make the system much more resilient to damping by increasing the envelope of oscillation. Numerous recommendations are made in light of these and other conclusions to facilitate any further research.

Contents

List of Figures

List of Tables

Glossary of Terms

A.C Acronym for Alternating Current.

Adiabatic An Adiabatic Process is one where no heat is transfered to or from a working material or fluid. In the case of this project the temperature rise of the stator and armature coils happens so quickly (the time period is in the order of 3 m.sec) that it is assumed that all the energy lost due to ohmic heating is absorbed by the armature and stator coil windings and not to the surrounding atmosphere.

Armature Coil Unlike the stator coil, the armature is not fixed. The armature can be either a solid conducting ring or in the case of this project a wound coil whose ends are shorted to maintain the induced current's flow. Interaction of this induced current with the current in the stator coil results in an acceleration of the armature.

Average The average value of a time varying quantity taken as $F_{avg} = \frac{1}{T}\int_0^T f(t)\,dt$ and normally used to determine average power dissipation over time period T.

B.G.A Acronym for Breeder Genetic Algorithm. A computing technique used to find optimized design solutions for difficult/multivariable systems. These optimization algorithms are inspired by principles of evolutionary biology, such as replication, breeding, natural selection, mutation and inheritance to name but a few.

Bore This is the inner diameter of the stator coil form and represents the maximum diameter which the armature coil may be.

Capacitor A passive electrical component which stores electrical energy as charge between to oppositely charged plates. Capable of short duration high rate of energy release (i.e high power output) they form an excellent isolated power source to drive the stator coil.

Coil gun Any electromechanical launcher which operates by energizing a stator coil which accelerates ferromagnetic masses or wire wound helical armature coils using magnetic principles such as reluctance, induction and or the Lorentz force.

Corona Discharge This is an electrical discharge where the potential difference or electric field is high enough to ionize the fluid around a conductor but not enough for the formation of a spark/arc . Coronal discharges are typically found in high voltage and high frequency systems. This makes linear induction launchers particularly susceptible to this phenomenon which may over time break down the stator coil winding insulation and the dielectric material of the capacitor bank, resulting in failure of both these devices.

D.C Acronym for Direct Current.

Dielectric Losses These are non ideal losses which occur in a capacitors non-ideal dielectric and is usually related to the frequency and operating voltage of the device.

Diode Reverse Recovery After a diode finishes conducting in its forward state, a significant amount of charge is built up in parts of the diode. The amount of charge built up is proportional to the forward current the diode has conducted. At turnoff this additional charge results in a momentary reverse biased current flow through the diode. This is known as the diodes reverse recovery and the time duration of reverse biased current flow is known as its reverse recovery time. Although a small problem the reverse recovery may often cause faults in power electronic circuitry.

E.M.F Acronym for Electro Motive Force (similar to voltage).

E.S.R Equivalent Series Resistance is the non ideal resistance found in non resistive passive components e.g. A capacitor's E.S.R.

E.T.O Acronym for Earth to Orbit.

Envelope of Oscillation In the context of a decaying oscillatory voltage and current waveforms which exist in the P.L.I.M tank circuits. The oscillations of current and voltage are never outside of this envelope which is essentially a decaying exponential function as shown in Figure 5 below.

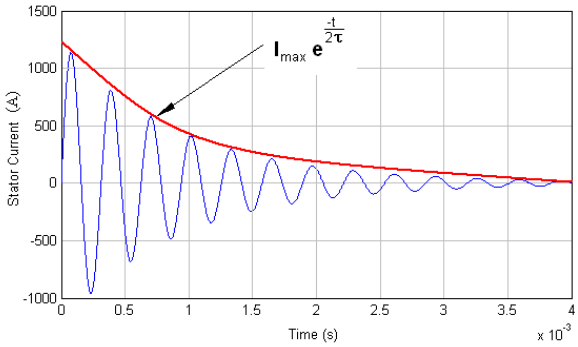

Figure 5: Typical envelope of oscillation for the stator coil current.

Excitation Specifically to coil guns this is the chosen method of armature coil energization. Typically and in the case of this project the armature coil is excited through induction. It may also however be excited using the same current which energizes the stator coil, in this case brushes are required.

F.E.M.M Acronym for Finite Element Magnetic Model, a freely available open source Finite Element Analysis Package for magnetic problems.

Ferromagnetic Ferromagnetic is a material property related to feromagnetism, the magnetic effect we see in everyday day life. It is responsible for Ferromagnetic materials such as ion becoming magnetized in the presence of an external magnetic field. Permanent magnets themselves can be made of a Ferromagnetic material as well.

H.D.P.E Acronym for High Density Polyethylene a commercially available plastic.

Induction A process where by a time varying magnetic flux through a coil induces an EMF or voltage across the coil in accordance with FARADAY'S LAW OF INDUCTION.

Inductor A passive electrical component used in circuits for its property of inductance. When a capacitor is discharged into an inductor an oscillatory current flow is produced with the capacitor and inductor exchanging energy. This oscillatory current in the stator coil inductor is suitable for inducing a current flow in the armature coil which is in close proximity.

Magnetic Coupling This is a measure of how well one magnetic circuit is coupled to another, normally in context of two coils which are coupled to together to create a transformer or in this case a linear induction launcher. The higher the coupling the higher the mutual inductance of the two coils.

Magnetic Flux Flux is a measure of the quantity of magnetism, taking into account the strength of the magnetic field. A changing magnetic flux through the circular area bound by a coil's windings results in the induction of voltage across that particular coil.

Mutual Inductance The mutual inductance of two coils is the ratio of the product of the number of turns on a coil and flux through that coil to the current flowing in another coil which is providing the flux through the first coil, expressed as $M = \frac{N_1 \cdot \phi_{12}}{I_2} = \frac{N_2 \cdot \phi_{21}}{I_1}$.

O.E.M Acronym for Original Equipment Manufacturer.

P.L.I.M/P.L.I.L Pulse Linear Induction Motor or Pulsed Linear Induction Launcher.

P.T.F.E Acronym for Polytetrafluoroethylene, more commonly known as Telflon. Widely used to reduce friction because of its typically low coefficient of friction when in contact with other materials.

Pole Pitch This is the spacing between stator coils on a traveling wave type induction launcher.

R.M.S Acronym for the Root Mean Square value of a time varying quantity taken as $F_{RMS} = \left[\frac{1}{T}\int_0^T \left(f\left(t\right)\right)^2 dt\right]^{\frac{1}{2}}$ over a time period T. Normally used when working with an alternating voltage or current.

Radius Ratio This is the ratio of the mean armature coil winding radius to the mean stator coil winding radius, expresses as $\frac{r_a}{r_s}$.

Rail gun An electromechanical launching device which operates using to rails at a potential difference and an externally provided magnetic field. The armature which is typically a conducting material has a current that flowing through it, provided by it being in contact with the aforementioned rails. This current flow which is perpendicular to the external magnetic field results in an force on the armature that is perpendicular to both the flow of current and the external magnetic field, in accordance with Lorentz Force Law.

Reluctance As described by Maxwell's Equations, magnetic flux always forms a closed loop. However the amount of flux which flows is dependent on the reluctance of the loop. Lines of magnetic flux always try to flow through paths of low reluctance than through paths of high reluctance. This concept is exploited in the design of a reluctance operated coil guns.

Saturation Saturation occurs when ferromagnetic material cannot be magnetized any further, and the increase of the external magnetic field results in no further increase in magnetization. This is a design limitation of reluctance launchers, if poorly designed the external magnetic field produced by stator coils energization is wasted once the the ferromagnetic launching material has reached saturation. This energy is then goes directly to heating the stator coil greatly lowering device efficiency.

Self Inductance The self inductance of a circuit/coil is the ratio of magnetic flux through the circuit/coil to the current that is flowing in the circuit/coil.

Skin Effect The skin effect is a phenomenon which occurs at high frequencies and results in current flowing on the outside of conductors, reducing the effective cross-sectional area available for current flow. In some cases this may greatly increase a conductor's resistance and thus the associated ohmic/heating losses as well.

Stator Coil The stator coil is fixed, the oscillatory current which flows through it when the a capacitor is discharged induces a similar current in the armature coil. These currents interact and result in a repulse force between the stator and armature coils. Since the armature is not fixed and free to move this force results in an appreciable acceleration of the armature.

Suck-Back This is a phenomenon which occurs in reluctance based launcher systems. Since the ferromagnetic material is always attracted to the center of the stator coil, if the stator coil's power supply is not interrupted when the armature or mass being projected has passed the half way through the stator coil, the launched mass will experience a significant amount of unwanted deceleration, returning it to the stator coil center.

Tank Circuit The tank circuit is another term for the stator coil circuit, and generaly refers to any circuit where a capacitor is connected in parallel to an appreciable inductance as is the case with

the stator coil circuit. Any initial electrical energy stored in the capacitor when the circuit is closed is exchanged between the stator coil inductance and the capacitor.

Transformer A passive electrical component which transfers electrical energy from one circuit to another through the process of induction. These are also A.C devices and will not work on a constant D.C voltage, as a changing primary coil current is needed to induce a voltage in the secondary coil.

U.P.S Acronym for Uninterpretable Power Supply.

List of Symbols

a armature acceleration; Subscript to denote x, y, z direction [m/s]

B magnetic field strength/induction [A/m]; Subscripts x, y, z denoting direction

C tank circuit capacitance [F]

c_p specific heat [J.kg^{-1}.K^{-1}]; Additional subscripts denoting material

E electric field strength [V/m]

E_{cap} capacitively stored energy [J]

$E_{magnetic}$ magnetic energy stored in armature and stator coils [J]

E_{ohmic} energy which is lost/dissipated as heat [J]

E_{work} useful work energy which accelerates the armature [J]

F armature acceleration force [N]; Subscripts x, y, z denoting direction

f frequency [Hz]

f_0 resonant frequency [Hz]

f_d damped frequency of oscillation [Hz]

G_{sa} stator/armature mutual inductance gradient [H/m]

I_a armature coil current [A]

I_s stator coil current [A]

L self inductance [H]

L_{aa} armature coil self inductance [H]

L_{ss} stator coil self inductance [H]

l_b induction length [m]

M mutual inductance [H]

M_{as} armature/stator mutual inductance [H]

M_{sa} stator/armature Mutual Inductance$M_{sa} = M_{as}$[H]

m_a armature coil mass [kg]

m_s stator coil mass [kg]

N number of turns on an inductor coil; Subscripts $_s$ and $_a$ denote stator or armature coil

n number of stator coils in multiple stage launcher

n_a radial divisions on armature coil inductance calculation mesh

n_s radial divisions on stator coil inductance calculation mesh

P instantaneous power dissipation [W]; Subscripts $_{IGBT}$, $_{Diode}$, $_{RMS}$ and $_{Avg}$ denote IGBT or Diode components and RMS or Average value respectively.

p_{mag} radial magnetic pressure [Pa]

q charge [C]

R resistance [Ω]

R_{aa} armature resistance [Ω]

R_{ss} stator resistance [Ω]

$\frac{r_a}{r_s}$ stator/armature winding radius ratio

r_{ai} armature coil winding inner radius [m]

r_{ao} armature coil winding outer radius [m]

r_{si} stator coil winding inner radius [m]

r_{so} stator coil winding outer radius [m]

s armature displacement [m]; Subscript x, y, z to denote direction

T temperature [K]; Subscript to denote usage

V_{GE} IGBT gate emitter voltage [V]

V_s instantaneous tank circuit capacitor voltage [V]

v armature velocity [m/s]; Subscript x, y, z to denote direction

v_s traveling wave velocity [m/s]

W_{aa} armature coil width [m]

W_{ss} stator coil width [m]

x, y, z Refer to axis referenced by the coordinate system shown in Figure 6 below.

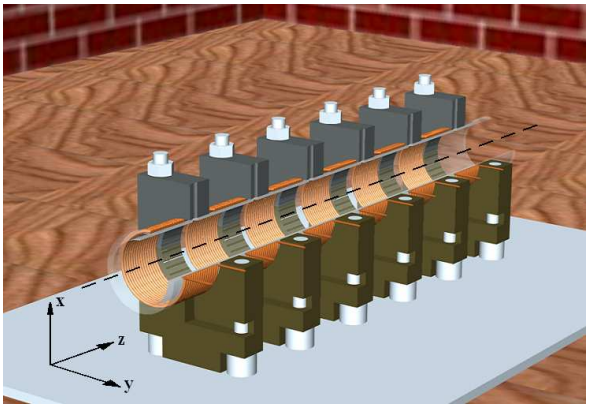

Figure 6: Coordinate system used to describe the launcher system.

Z transient thermal impedance [^{o}C/W]; Subscripts $_{IGBT}$ and $_{Diode}$ denote the transient thermal impedance of a specific device

α damping factor

ε induced Electro Motive Force [V]

Θ pole pitch [m]

μ_0 permeability of space $4\pi \times 10^{-7}$[N/A^2]

ρ resistivity [Ω/m]

σ_h hoop stress [Pa]; Subscripts;$_{aa}$or $_{ss}$denoting armature or stator support structures respectively

τ L.C.R damped oscillation decay time constant [L/Ω]

Φ magnetic flux [Wb]; Subscript to denote x, y, z direction

ω_0 resonant frequency [rad.s^{-1}]

ω_d damped frequency of oscillation [rad.s^{-1}]

1 Introduction

There are many different types of electro-mechanical coil launchers (listed below) each distinguished by their own method of operation and construction.

1. Reluctance Launchers
2. Induction Launchers
3. Helical/Commuted Launchers

After doing thorough research on all of these operation and construction variations it was determined early in the design process that a capacitor driven coaxial linear induction motor, driving wire wound armature coils would be the most interesting launcher system to investigate, model and build. Aside from consisting of only a few passive electrical components P.L.I.M (Pulsed Linear Induction Motors) also have a very elegant method of analysis discussed at great length in Appendix A.4 on page A-17.

The operation of a typical linear induction motor is fairly simple to inderstand Figures 7 & 8 below show the schematic outline of a general multi stage P.L.I.M (excluding the capacitor charging circuits) followed by a simplified representation of the two coils with anti-parallel currents flowing in them for conceptual purposes. When each of the capacitors shown in Figure 7 are discharged into the stator coil inductance an oscillatory current waveform is produced in the stator coil. This time varying oscillatory current will induce a current in the armature coil which flows in the opposite direction (in accordance with Lenz's Law) as shown in Figure 8. These anti-parallel currents in armature and stator coils results in a repulsive force F_z between the two coils in acordance with the Lorentz Force Law.

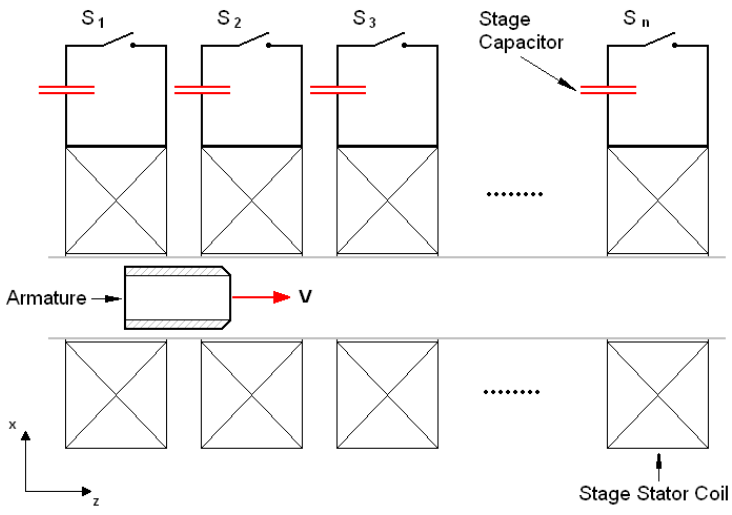

Figure 7: Sectioned schematic of the stator and armature coils of a mulitstage capacitor driven linear induction motor/launcher.

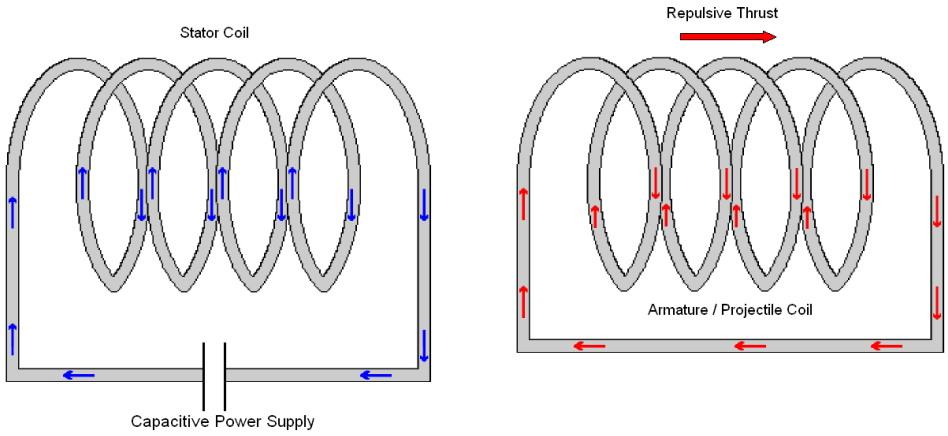

Figure 8: Illustrating the principle of operation of an induction based coil gun.

This armature can either be a single turn ring of conducting material, or it can be made of a wire wound coil with both ends shorted to allow current flow as shown in Figure 8 above.

The concept of a pulsed coaxial linear induction motor capable of driving a large mass to very high velocities has existed for quite some time, however despite the very attractive performance attributes over rail gun technology research in P.L.I.M remains a subject of advanced electromechanical research groups. Much of the literature describes launchers operating with current, voltage and energy levels that are in the order of 10^3 Amps, Volts and Joules. These excessive power requirements mean that very few people actually end up studying or researching P.L.I.M with intent to miniaturize and improve the technology, despite its incredibly attractive attributes for applications including mass transport, overhead factory gantries, earth to orbit launching, conveyer systems, aircraft launching catapults and long range artillery. For this reason it is of major interest to determine whether or not a pulsed linear induction launcher could in fact be operated at much lower voltages and energy levels, opening up the field of research to independent researchers and amateurs.

The challenge in developing a P.L.I.M is largely due to the shear number of design variables involved in the system and the extent to which these variables themselves are interrelated. This makes finding feasible system designs based on a "trial and error" method almost impossible. It was thus required that this project conduct thorough research on the topic to acquire credible information regarding the systems modeling and design considerations to aid the design process ensuring that an operating system could be developed within the first construction iteration.

The primary objectives of this project are summarized below

1. Conduct thorough research on the topic.
2. Create a computer simulation to model and developed a 6 Stage P.L.I.M with an efficiency greater than 3.5% (electrical to mechanical energy conversion).

3. Design/develop a feasible low energy laboratory scale test launcher using the computer simulation.

4. Build and test this launcher to verify accuracy of model and prove concept.

The test device must be able to feasibly and safely demonstrate the operating principle and when combined with the report must be of such a quality that further research on the topic will be greatly enriched or facilitated through this work. Figure 9 shows a rendered impression of what the proposed 6 stage linear induction launcher developed in this project would look like, it also shows the armature coil for a scale comparison.

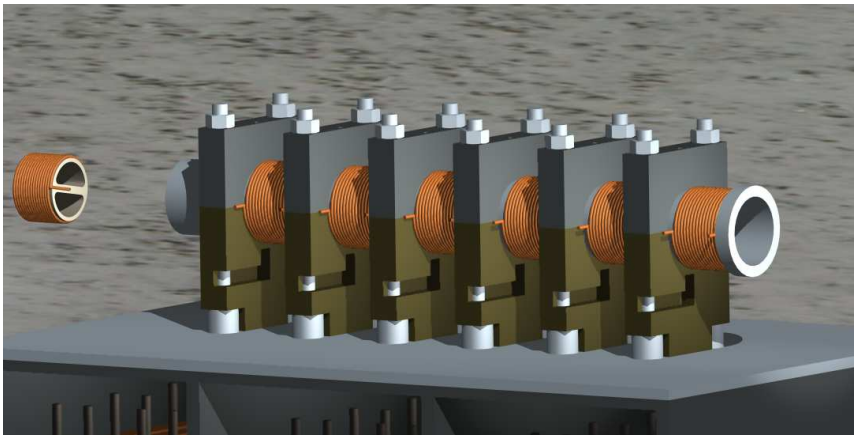

Figure 9: 3D visual rendering showing the concept of the 6 stage induction launcher also visible (the object on the left) for size comparason is the concept armature.

This project requires a broad set of skills and knowledge in power electronics, mechanics, basic physics, computer programming, measurement and numerical methods to achieve the said goals. As electro-mechanical engineering student this project effectively exercises the expertise and knowledge learned in the last four years.

The report begins with a brief executive summary which will effectively outline what this project has achieved. In addition to this introduction it then presents the specifications of the laboratory scale P.L.I.M which was tested to verify the theoretical model and simulation used to develop the system. After which the theoretical design approach which was followed in developing the launcher is described. The report will then describe the construction/selection/assembly process for each of the test rig's important items and systems. Thus with a general but firm grasp of the devices expected capabilities and components, the report will present and discuss the experimental performance results of the test launcher in Section 5 on page 31. This is followed by an in depth discussion and comparison between the theoretical Matlab simulation results (found in Appendix B on page B-1) and the results achieved in practice by the test launcher while also suggesting possible reasons for any differences or unexpected anomalies encountered in practice.

The report will then present the many findings and conclusions which were made in light of this investigation. This conclusion will also will reflect on the extent to which the project's objectives have been achieved in addition to outlining some of the projects limitations and constraints which may have impeded progress.

The Section 8 on page 60 will present the recommendations and project direction which should followed in light of this work's findings to ensure the likelihood of further advancement/progress in this field of study.

In addition to all of the above this project includes many additional appendices which may be of interest to the reader. Appendix A on page A-1 provides an excellent and in depth literature review covering almost every aspect of the pulsed linear induction motor design, physics of operation, computer simulation, numerical analysis including a detailed introduction of the technology. Appendix A.4 on page A-17 is most important as it presents the theory on which the entire theoretical model is based. It is thus also referenced extensively throughout Appendix B on page B-1 which presents the test launchers predicted simulation performance calculations and results which essentially form the theoretical hypothesis of the test P.L.I.Ms performance. Appendix C on page C-1 furnishes the complete list of test launcher specifications and their respective justifications. Finally all parts drawings and a complete electrical circuit diagram can be found in Appendix E on page E-1. Included also is a compact disk containing all of the information and data used in compiling this project in addition to all the matlab simulation codes and a soft copy of this report.

2 Main Specifications

A full list of the laboratory test launchers specification are presented in Appendix 2, shown here for quick reference is the list of main specifications drawn up at the start of the laboratory scale launchers development. The location column in Table 1 below refers to where the specification's justification can be found within Appendix C on page C-1.

Table 1: List of main specifications.

D/W	Requirement	Desired	Actual	Rev	Location
D	Modular construction	Yes	Yes	0	C.3.1.1.1
D	Operating energy	150 J	144 J	0	C.3.1.1.2
D	Stage energy	25 J	24 J	0	C.3.1.1.3
D	Stage efficiency	3.5 %	N/A	0	C.3.1.1.4
W	Operating voltage	<500V	400V	0	C.3.1.1.5
W	Total length	< 1m	500mm	0	C.3.1.1.6
W	Total cost	<R1500.00	R3800.00	0	C.3.4.1
D	Robust and sturdy test rig	Yes	Yes	0	C.3.1.1.7

NOTE:

D = Demand

W = Wish

TBC = To Be Confirmed

3 Theoretical Design Approach

3.1 Introduction

The design of a working P.L.I.L (Pulsed Linear Induction Launcher) is a task which requires an intermit understanding of the devices operation and a general "feel" for the relationships or tradeoffs that exist between variables. It is the shear complexity of the system and the number of variables involved that makes any kind of hand written design calculations highly impractical. For this reason the first step in designing a linear induction launcher is to write a computer program capable of calculating of all the important performance variables (Most of which are dynamic and the instantaneous values of these variables must be found over a given time period) for a specified launcher system. This computer simulation must itself be based on a verified analysis of the system, which once written will serve as an invaluable design tool allowing the performance of a specified launcher to be estimated and studied. However the results of such a computer simulation are still subject to the system limits determined by the specified coil geometry, voltage and capacitor size. It is because the design input variables themselves are so numerous that chances of finding/guessing an "optimal" design is highly unlikely. This project however is not necessarily aiming to find an optimum design but is however more interested in qualitative results of the comparison between the theoretical computer simulated launcher system and an actual laboratory test launcher system built to the same specifications which are used as inputs for the computer simulation. To ensure that a feasible or working launcher is constructed initial system inputs/specifications of the computer simulation were based on design considerations and careful study of the subject through a detailed and comprehensive literature review. This literature review can be found in Appendix A on page A-1 and includes extensive and detailed sections regarding the considerations for design and synthesis of L.I.L (Linear Induction Launchers) with specific relevance to a small scale test launcher. This section will elaborate more specifically on the design process which was undertaken in developing the laboratory scale P.L.I.M.

3.2 Launcher Simulation

As mentioned, the first step in designing a linear induction launcher is writing the computer code needed to simulate and quantify a given design's performance. The simulation was implemented in Mathworks Matlab and had two important components as listed below and illustrated in Figure 10.

1. Stator/Armature Inductance Parameter Calculator
2. Coil Performance Numerical Solution

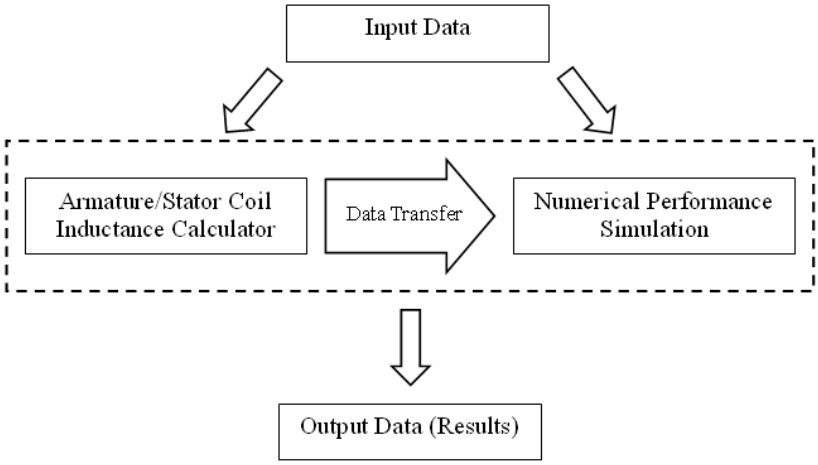

Figure 10: Conceptual illustration of how the launcher simulation operates. All operations occurring within the dashed box represent the total actual simulation code. Outside the box are simply the user defined variable initialization and simulation output results.

The input data which is made up of coil geometries and initial system conditions is written into a Matlab .m-File. The stator/armature inductance calculator uses the specified coil geometries and wire diameters to determine each coil's self inductance in addition to calculating the mutual inductance and mutual inductance gradient between the coils over a specified range of axial separation. The calculator also estimates the armature and stator coil's mass and resistance. The numerical performance simulation then uses this data and the predefined initial system conditions solve the coupled differential equations (shown below), from which all other launcher performance parameters (e.g. circuit currents, instantaneous armature acceleration and velocity) are quite easily derived as discussed in great detail in Appendix A.4.1 on page A-17.

$$V_s = I_s R_s + L_{ss}\frac{dI_s}{dt} + M\frac{dI_a}{dt} + I_a\left(\frac{ds_z}{dt} \times \frac{dM}{dz}\right)$$

$$0 = I_a R_a + L_{aa}\frac{dI_a}{dt} + M\frac{dI_s}{dt} + I_s\left(\frac{ds_z}{dt} \times \frac{dM}{dz}\right)$$

The theory required to develop both facets of this model was carefully researched and for the sake of brevity is not discussed here but can be found in Appendix A.4 on page A-17. However it is interesting to know that the differential equations were derived from applying KIRCHOFFS VOLTAGE LAW on the equivalent stator and armature coil circuits as shown in Figure 11 below.

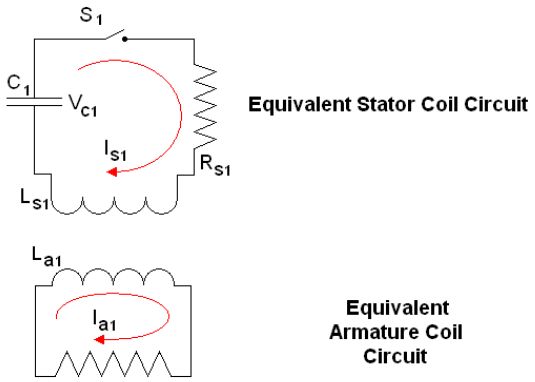

Figure 11: Equivalent tank circuit and armature coil circuits used to derive the systems coupled differential equations.

The purpose of this brief simulation description is to simply reveal how the theoretical tests and ultimate design of the single stage launcher was conducted. The corresponding detailed simulation results which formed many of the specifications of the launcher constructed in practice can be found in Appendix B on page B-1 which also provides excellent exposure to the typical outputs of the simulation implemented in Matlab.

3.3 Initial Energy & Operating Voltage

The initial energy stored in the capacitor before it's discharged into the stator coil is what determines the amount of energy available for the acceleration of the armature (assuming for simplicity a fixed efficiency, which simulations indicate may not be true). Using the initial specification requirements of the system and the relationship between capacitance, the energy stored and the voltage to which it is charged (expressed as $E_{cap} = \frac{1}{2}CV^2$) the tank circuit capacitor bank can be completely specified. The initial stage energy input was specified as 25 J. Since one of this project's important objectives is that the launcher may be operated off readily available A.C power supplies, the maximum assumed voltage at which the device can operate was specified as 400 V. Since both the capacitor banks energy content and maximum voltage charge have been specified, the tank capacitance could be calculated and specified.

Figure 12 below shows a typical instantaneous plot of all the system energies during operation event of a pulsed linear induction motor and effectively illustrates that losses in the system are largely due to ohmic/resistive heating only. Figure 12 also shows that while energy is dissipated as heat, it is also transfered between the capacitor and inductor.

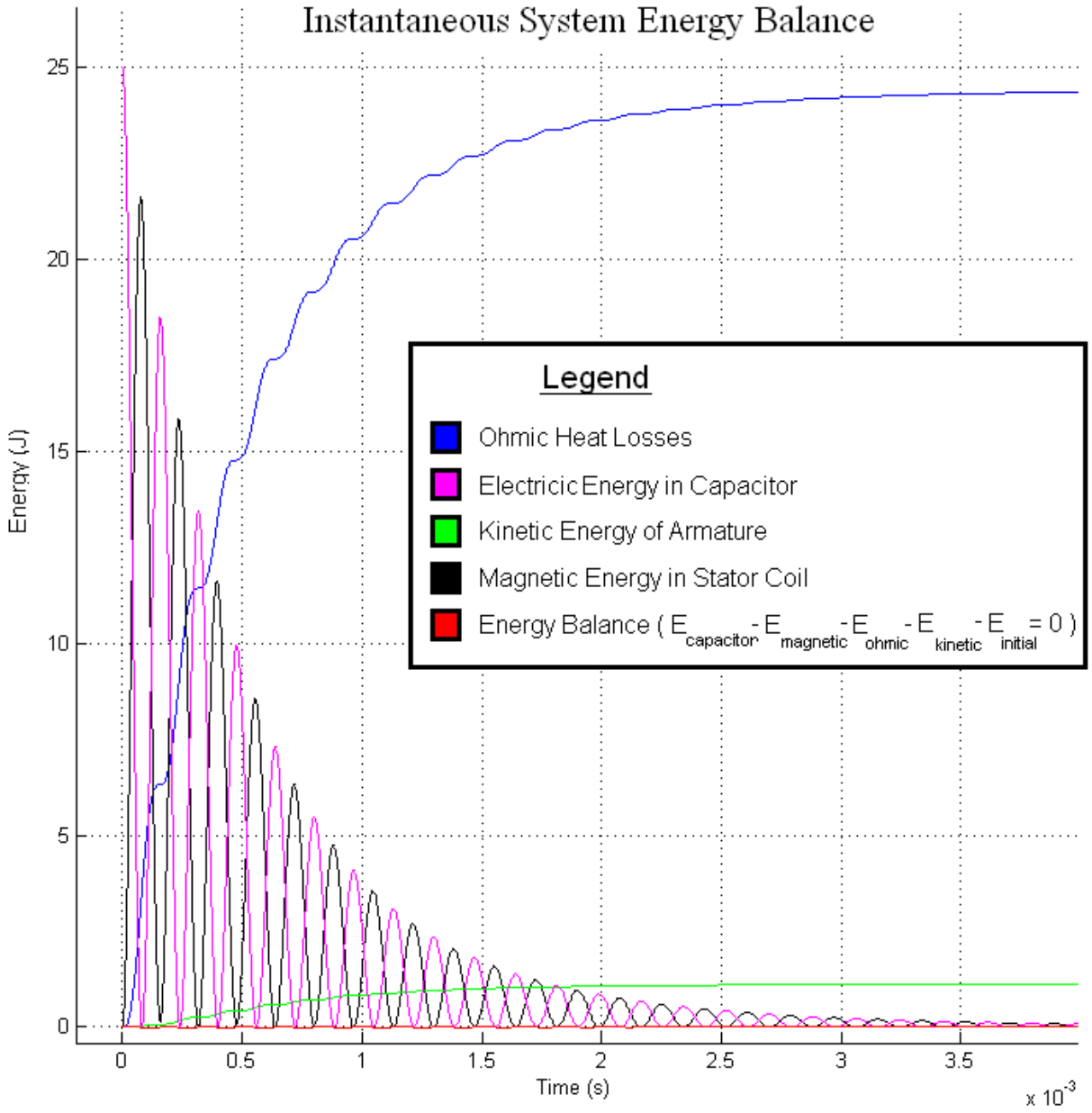

Figure 12: Typical instantaneous plot of all the energies stored or converted by the launchers components.

It is for this reason that one of the main implications of driving the launcher with a voltage less than 500 V is that the stator, tank circuit and armature coils have to be designed such they have the least resistance to decrease or lessen the extent of the resistive/ohmic losses in the launcher system. The specified design parameters determined at this stage are shown in Table 2 below.

Table 2: Design specifications the tank circuit capacitor energy source

Initial Stage Voltage	V	400
Stage Capacitance	μF	315
Stage Energy	J	25.2

3.4 Coil Geometry and Associated Specifications

The stator and armature coil geometry specifications were determined by first choosing a coil pair radius ratio $\frac{r_a}{r_s}$ followed by the armature bore diameter. Based on extensive research (presented in Appendix A.5.1 on page A-29 & A.5.2 on page A-32) it was quickly learned that increasing the armature bore diameter would greatly increase the systems performance. Since the objective is to maximize the amount of kinetic energy delivered to the armature coil there exists a trade off, in that increasing a given armature bore diameter also results in a much larger coil turn circumference and (ceterus parabus) the armature weight will increase accordingly thus significantly decreasing its acceleration and overall launcher performance. The existence of this tradeoff was correctly predicted by the system simulation (where both the stator coil and armature weight including its associated form was estimated by the simulation, based on user defined coil geometries). Another consequence of increasing armature/stator diameter is that the overall coil resistance is greatly increased with each turn and thus an excessive number of turns on both coils undesirable. In an attempt to reduce the resistive losses in the coils large wire diameters have been chosen to reduce the resistance per turn on both coils. However because the frequency of oscillation (of voltage and current in the tank circuit when capacitor is discharged into the tank circuit) is expected to be in the order of 5kHz, increasing coil wire diameter can only be done up until a point where the additional cross section of the wire will serve no useful purpose due to the skin effect which may actually result in a decrease of effective current conducting area in the wire resulting in greater ohmic losses and "dead weight" on the armature coil. Table 3 below shows the specifications of the wire used in the armature and stator coils.

Table 3: Design data of wire used for winding launcher coils [3].

	Diameter (mm)	mΩ/m	Maximum freqency for uniform current density in wire
Stator Coil (AWG 11)	2.30	4.13	3.2 kHz
Armature Coil (AWG 13)	1.83	6.57	5.3 kHz

Table 3 above shows that the maximum allowable frequency of current and voltage in the tank circuit should not exceed 3.2kHz. This is important because the frequency of operation is approximately depen-

dant on the tank circuit capacitance and the inductance of the stator coil, a relationship expressed as $f \approx \frac{1}{2\pi\sqrt{L_{ss} \cdot C}}$. Since the capacitance has already been specified an approximate estimation of the stator coil's inductance could be made such that frequency of current and voltage oscillation would not exceed 3.2 kHz.

Studies show that breeder optimization routines applied to L.I.L (Linear Induction Launcher) simulations would typically converge on coil pairs that have more or less the same length in addition to both coils being thin rather than thick [2]. The latter result is quite expected as thicker layer of coils will reduce the overall radius ratio $\frac{r_a}{r_s}$ of the two coils resulting in reduced coupling and poorer performance.

The acceleration of the armature is greatly dependant (for a specified coil pair) on the initial axial separation of the two coils when the stator coil is energized. This is explored later in more detail in Section 3.6 on page 17. Since it has been chosen to determine the armature coil's position relative to a stage stator coil using optical sensors an additional design objective for the coil geometry was that when the armature is in its optimum position for the associated stage stator coil to be energised, part of the armature must be outside of the stator coil in order for the armature coil to break the optical beam. The breaking of this optical beem results in a control signal being sent to a suitable control circuit allowing the stator coil to be energised at the right time. This concept is better understood in looking at Figure 13 below.

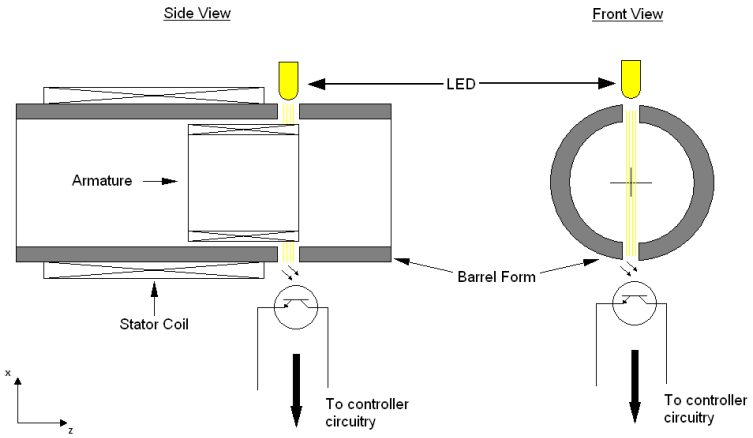

Figure 13: Showing the stage stator coil to be energized and the armature in transit. The beam has been positioned such that as soon as the armature breaks the light beam, it is in its optimum position for stage stator coil to be energized.

It was realized very early in the design process that the stator coil forms would not be able to be machined from plastic stock material as the required wall diameter of 2 mm (to maximise the radius ratio) is far too thin to be machined from plastic stock. The stator coil form was thus bought off the shelf. The most convenient coil form diameter found and used in this project had an outer diameter of 50 mm and a wall thickness of 2 mm and is made of Perspex.

In light of all these mechanical and electrical considerations made in designing the coil pair, much of the coil pair geometry was already specified, starting with the coil diameters and the wire diameters specified in Table 3. A feasible working coil geometry was quickly established using the described launcher simulation program. The diameters were chosen such that the radius ratio would be maximized while maintaining at least 1.5mm of clearance between the stator coils inner form and the armature coil windings when the armature is co-axially located within the stator coil.

The full details of the armature and stator coils are far too numerous to mention here but can be found in the launchers detailed specifications, found in Appendix C on page C-1. For this reason a summary of the important mechanical and electrical specifications of the armature and stator coils pairs are presented in Table 4 below followed by Figure 14 showing a plot of the coil pairs inductance mutual inductance and mutual inductance gradient at various positions of axial coil separation, determined by the computer simulation.

Table 4: Important design specifications for the laboratory scale pulsed linear induction motor.

	Mechanical Specifcations			
	Coil Diameter	Turns	Length	Weight
Stator Coil	52.3 mm	16	36.9 mm	N/A
Armature	43.38 mm	15	27.4 mm	58 g
	Electrical Specifications			
	Self Inductance		Resistance	
Stator Coil	10.9 μH		10.9 mΩ	
Armature	9.39 μH		13.7 mΩ	
	Combined Coil Pair Specifications			
	Max Mutual Inductance		Radius Ratio $\frac{r_a}{r_s}$	
	7.53 μH		0.8380	

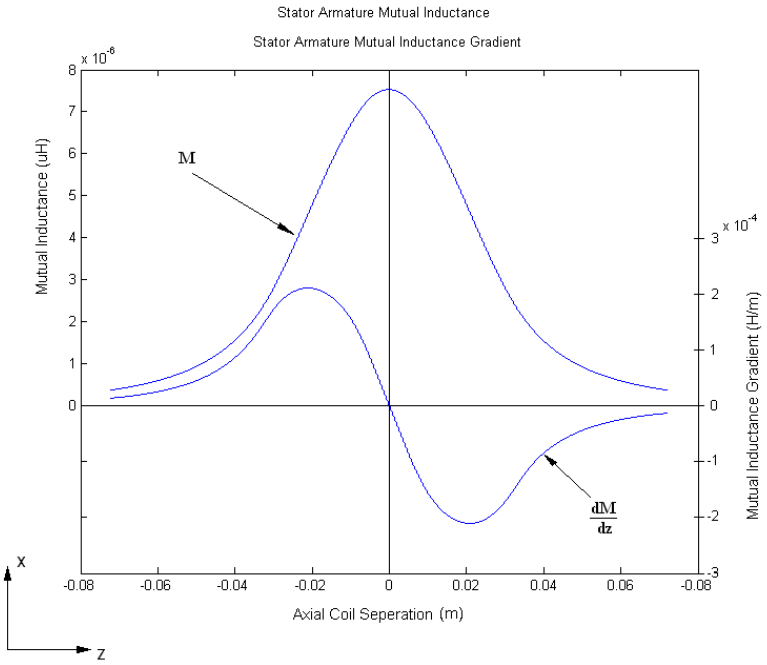

Figure 14: Inductance parameters corresponding to the specified coil geometries of the laboratory scale test launcher.

3.5 Circuit Resistance and Damping

During discharge of the capacitor into the stator coil inductance the tank circuit of the linear induction launcher effectively forms an LC oscillator. In the absence of any circuit resistance the frequency of oscillation would almost be equal to resonant frequency of the circuit expressed as $f_{res} = \frac{1}{2\pi\sqrt{LC}}$. Also in the absence of any tank circuit resistance the current and voltage would oscillate forever (no resistive losses). However, in practice, the tank circuit including the stator coil will have some resistance. This resistance is what causes the dissipation of energy (in the form of heat), resulting in oscillatory current and voltage waveforms which decay over time. Thus for a specified tank circuit the extant of this damping is dependant on the tank circuit resistance and determines how quickly the current and voltage waveforms will decay, effectively controlling the envelope of oscillation. The reason for this is that increasing the resistance increases the ohmic losses resulting in the quicker decay of the current and voltage in the circuit due to increased energy dissipation through resistive heating. Therefore this damped response is most undesirable in the operation of a linear induction launcher because the greater the damping (quicker the decay) the greater the resistance losses thus reducing the total amount of electric energy available which could be converted to kinetic energy in the armature. Figures 15 & 16 below comparatively illustrate the effects of resistive damping on stator coil current and armature acceleration for the most extreme cases of under damping and over damping as well as a typically damped response. A comparison of performance for the various levels of damping investigated in Figures 15 & 16 is provided in Table 5 below.

Table 5: Comparison of several of tank circuit oscillation responses. Note that the damped case only takes the stator coil into account in the LRC circuit. Also note that a mere 0.5 ohms of connection resistance is enough to cause excessive damping, significantly reducing performance.

	Max Velocity	Efficiency	Circuit Resitance	Tank Resistance
Under Damped	14.98 ($m.s^{-1}$)	31.73 %	0 Ω	0 Ω
Damped	5 15 ($m.s^{-1}$)	03.74 %	0 Ω	10.9 mΩ
Over Damped	0.13 ($m.s^{-1}$)	0.002 %	0.5 Ω	0.5109 Ω

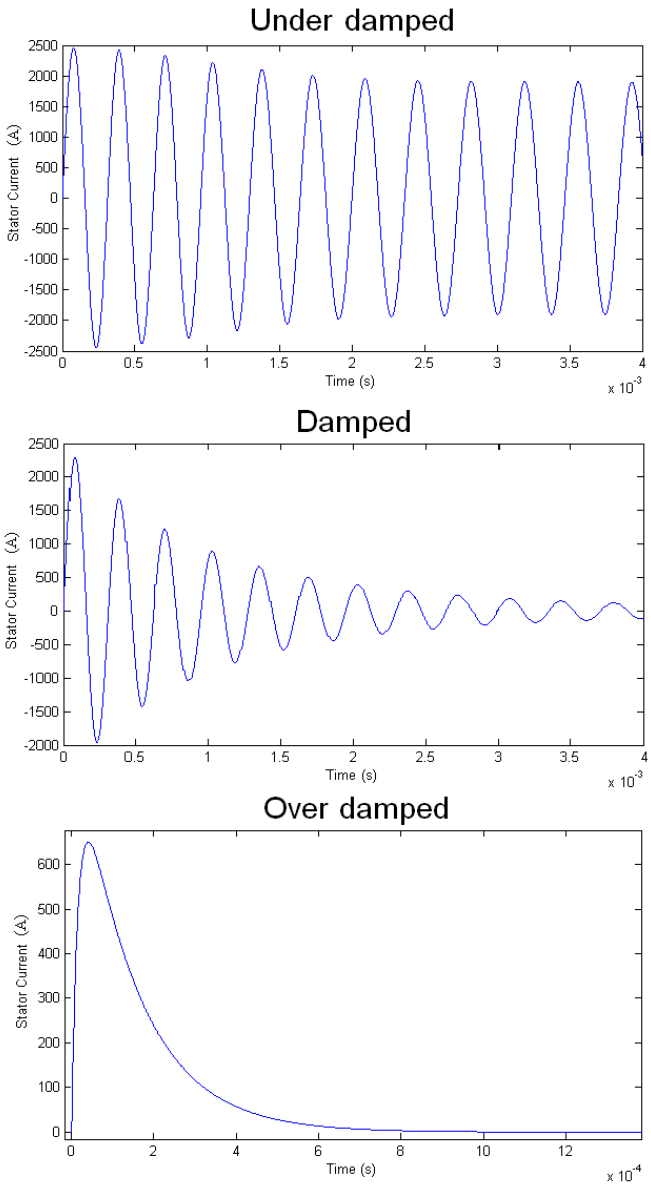

Figure 15: Stator coil current response to the capacitive discharge for 3 separate cases. Starting from the top; under damped, damped and finally over damped.

Figure 15 above clearly illustrates that current will continue to oscillate forever if no circuit resistance is present, however as soon as there is resistance present the waveform will begin to decay. Note the greatly reduced peak stator coil current in the stator coil for the over damped case.

Figure 16 below shows the associated acceleration profiles for these various levels of damping. It is clearly evident that the maximum acceleration occurs with under damping, however in practice the best which can be achieved is that of the damped case. Figure 16 also reflects the very poor acceleration achieved when the circuit response is over damped.

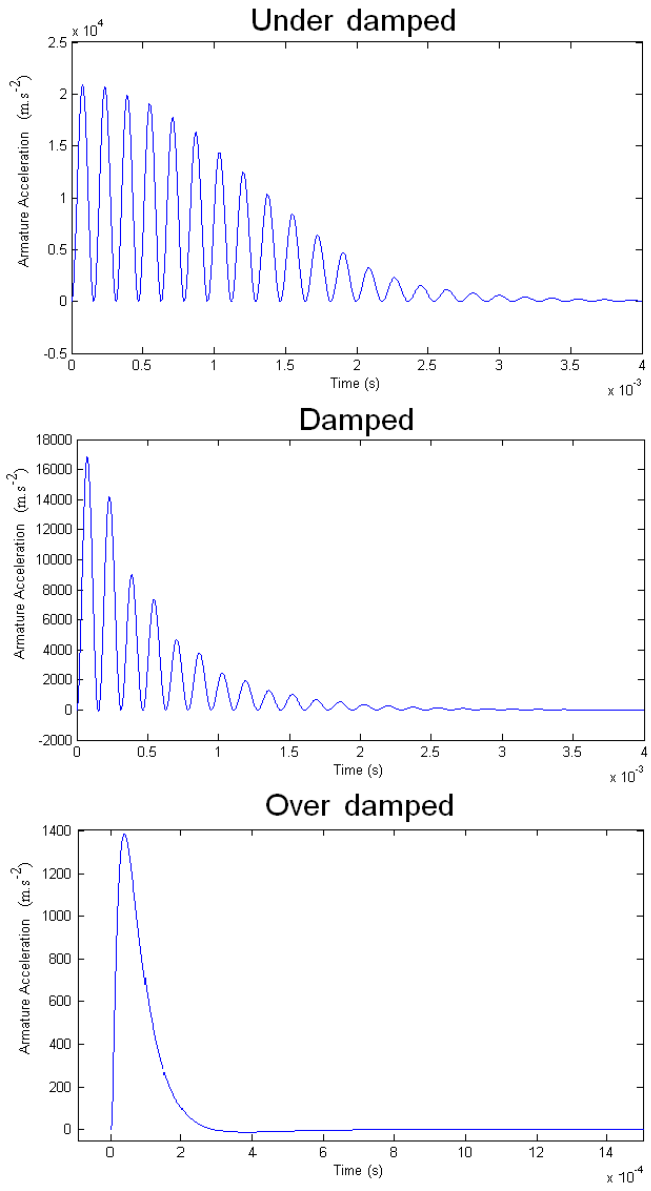

Figure 16: Predicted armature accelerations associated with the current plots of Figure 15, clearly illustrating the decrease in armature acceleration as the extent of damping is increased.

Since the stator coil itself is not ideal and has a resistance around 11 mΩ it is expected that the test launcher will have a damped oscillatory response. The extent of this damping must be minimized by reducing the circuit connection resistance, to do this all wires must be as short as possible, if crimp joints are used, the wire must be soldered in addition to being crimped onto the lugs. Ideally copper ground strapping or buss bars must be used to connect capacitors in parallel. Simulations show that even a tank circuit resistance of 25 mΩ(excluding stator coil of 11 mΩ) will lead to excessive damping and thus poorer performance, again reinforcing the urgency and importance of keeping the tank circuit resistance to a minimum. Every precaution that can be taken must be taken to ensure optimum performance of a given launcher.

3.6 Initial Armature Coil Position

To achieve a given linear induction launchers optimum performance the first and successive stator coil stages need to be energized when the stationary or moving armature is its optimal position (relative to the stator coils), to fully take advantage of the induction length of the coil pairs. Determining the optimum position for the specified coil pairs was accomplished using the computational launcher simulation. Since one of the inputs to the numerical simulator is the initial coil separation when the stator coil is energized, a simple "for-loop" was implemented in Matlab which would simulate the launcher performance at various initial axial separations (ceterus paribus). Figure 17 below shows plots of launcher performance for various initial positions of the armature coil.

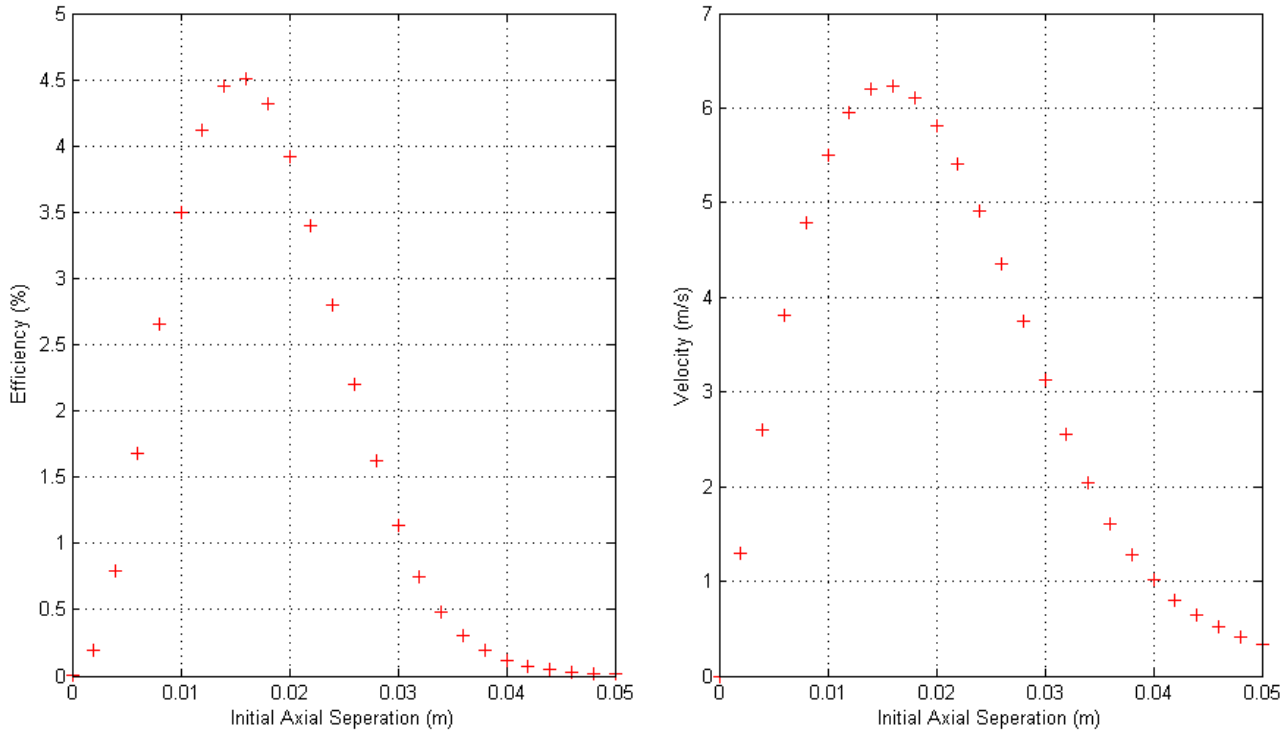

Figure 17: Single stage launcher performance vs. initial axial separation.

The results of this simulation indicated that the optimum spacing of the coils (of this system) is 16 mm as shown in Figure 18 below. This is an important design specification in that it determines the positioning of the optical sensors required to detect the armature coils position before the stator coil can be energized. Since the barrel form (onto which the stator coil is wound) is located firmly by mounting clamps, these optical sensors will be mounted within the mounting clamps. This specification thus determines the positioning of the diametrically opposite holes in both mounting blocks to accommodate the optical sensors as well as the positioning of the stator coil relative to the mounting clamps.

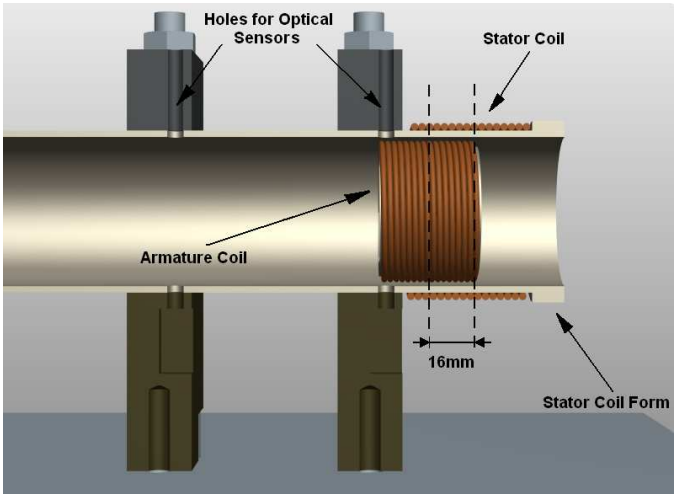

Figure 18: Section through stator coil, barrel and mounting clamps. This figure effectively demonstrates the optimum axial separation of the two coils and how the holes must be made in the mounting blocks to accommodate the optical sensors.

4 Launcher Construction

This section provides an overview of the construction process, highlighting key design features for each of the important systems found in the laboratory linear induction launcher system. Detailed parts drawings and a full circuit schematic can be found in Appendix E on page E-1.

Aside from the electronic components in the control circuit the launcher system makes use of two very important O.E.M components listed below in Table 6 below. The selection of these devices was based on thorough research of the respective devices data sheet, application notes and detailed operation calculations all of which are presented in Appendices A on page A-1 & B on page B-1.

Table 6: O.E.M components used in the launcher tank circuit.

Item	Description
Tank Capacitors	Afcap 440 Volt ; 50 μF C.V.T Polypropylene A.C capacitors
Discrete IGBT & Diode Module	Mitsubishi CM600-12H 600 V @ 600 A (continuous)

4.1 Armature Coil

In light of thorough research it was decided early on in the conceptual design of the test launcher that it would accelerate wire wound armature coils whose ends are shorted allowing current to flow. These armatures offered easier system modeling and reduced ohmic losses however their design and fabrication would offer some interesting challenges [16]. Since the armature coil was designed to use a single winding layer (as apposed to multiple winding layers) shorting the wire ends would require that at least one of the wire ends be routed through the center of the coil as shown in Figure 19 below, also shown is a multilayer winding which allows the coil wiring ends to be shorted on the windings surface.

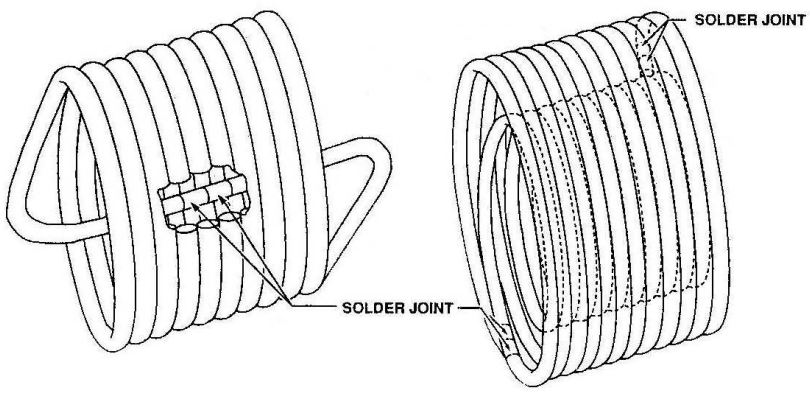

Figure 19: Possible armature coil winding techniques. Showing single layer and multilayer coils on the left and right respectively.

The design of the armature coil form was based on the coil geometry specifications as summarized in Table 4 on page 12. A further design goal for the armature was to minimize its weight, besides accomplishing this goal through varying the actual coil geometry and wire specification (indeed most of the armature weight is due to the wire windings of the coil) additional measures were taken in selecting the armature coil form material and shape. The armature was made from Polypropylene, the lightest of the commonly available plastics and quite coincidently the same material used in manufacturing the capacitors. Furthermore since the coil requires wire to be passed through its center axis as shown in Figure 19 above, it was possible to remove much of the unnecessary material greatly reducing the coil forms weight while keeping it balanced. The final stator coil design concept is shown in Figure 20 with a comparison of the actual armature coil alongside.

Figure 20: ProEngineer 3D rendering of the armature coil on the left, while the actual armature coil before varnishing is shown on the right. This figure illustrates many details of the armature coil form and the similarity between design concept and implementation.

Figure 20 illustrates the key design features of the coil form quite effectively such as the grooves on the flat end surfaces of the coil form, their purpose being to effectively locate the copper wire which is routed through the central axis of the coil. Also obvious is the extensive material removal from what would have been a solid polypropylene cylinder which serves to reduce the weight of the armature coil form.

The winding process started with routing the wire through the axial hole of the coil form, after which the free end of the wire would be positioned onto the surface groove locating the wire onto the coil form allowing the required 15 turns to be wound onto the form. Once wound the windings were secured to the coil form using painters tape, the enamel coating at the two ends of the wound coil could be removed using sand paper. After the enamel coating was removed the ends were permanently joined together with a solder joint. Great care was taken in making each of the solder joins making sure that the solder

had "flowed" into the exposed copper at the two wire ends. The solder joint implementation is shown in Figure 21 below.

Figure 21: Close up view of the solder joint implementation, the exposed copper wire can be seen on the wire which emerges from the coils center. Also reflected quite well in this figure is the wire location groove.

Since the current flowing in one turn of the a coil is anti-parallel to the same current flowing in the adjacent turn what often happens in coils is that the individual turns tend repel each other, to prevent this from distorting the coil during the devices operation the armature coils were coated in 6 coats of clear varnish thus "binding" the turns together and to securing the coil to form. A complete varnished armature coil is shown in Figure 22 below.

Figure 22: Close up view of an armature coil complete after being coated in 6 coats of varnish.

The addition of the varnish increased the total weight of the coil by 10 grams beyond the design weight predicted by the ProEngineer model. However the simulation code suggests that this extra 10 grams would have a minor effect on the performance of the launcher.

4.2 Stator Coil and Associated Mounting

The stator coil, its form and the mounting blocks effectively make up the barrel of the launcher. Figure 23 below shows the concept of the 6 stage linear induction launcher from which the laboratory test scale launcher is derived.

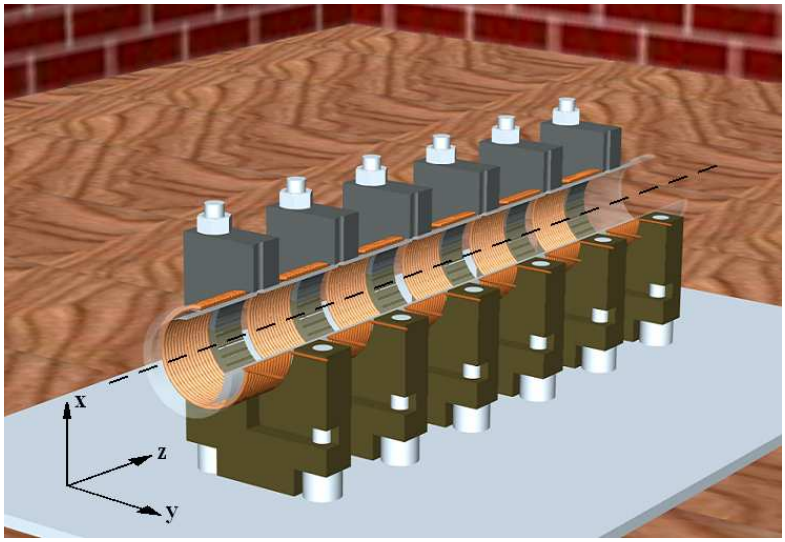

Figure 23: A conceptual 3D rendering of the full 6 stage modular linear induction motor sectioned to show stator coil location on the form and cutouts in mounting clamps for optical sensors.

Figure 23 also effectively reflects the simplicity of the linear induction launcher (aside from the armature) in that very few parts are actually required to construct the device. The stator coil form was purchased off the shelf as a 50 mm outer diameter/46 mm inner diameter clear Perspex tube shown in Figure 24 below.

Figure 24: Clear Perspex tubing (50mm Outer Diameter and a 2mm wall thickness) used in the construction of the laboratory scale test launcher.

The mounting clamps were easily machined from H.D.P.E (High Density Polyethylene), another readily available plastic. These mounting clamps are effectively two parts which clamp down to secure the stator coil form as shown in Figure 25 below.

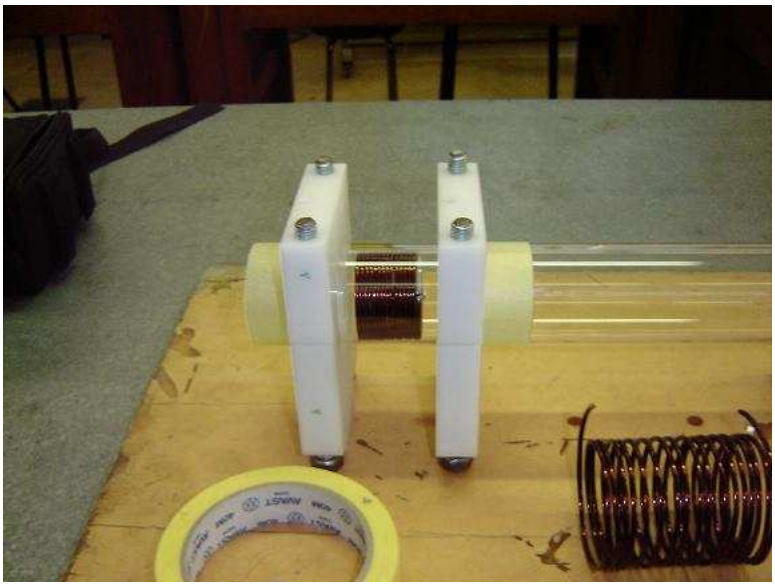

Figure 25: Stator coil form clamped between mounting blocks. Also shown is the armature coil which loosely fits in the Perspex form and the pre-wound stator coil (discussed later).

The clamps would also house the optical sensors to determine when the armature is in the optimum position for the corresponding stator coil to be energized. Figure 26 shows the design features of the mounting blocks to accommodate optical sensors.

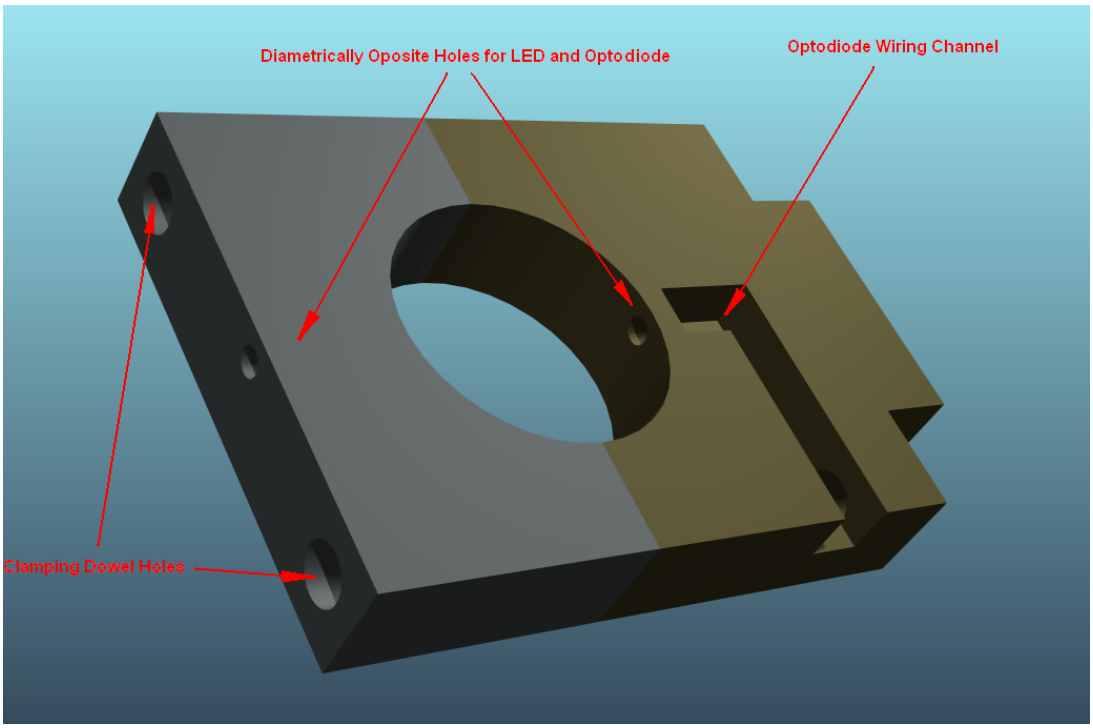

Figure 26: Stator coil form mounting block showing diametrically opposite holes for armature coil optical sensors.

The stator coil was to be wound from enameled copper wire with a specified diameter of 2.3 mm which is quite thick and difficult to wind by hand as it requires a large winding torque to make the windings as uniform as possible. Since the Perspex (a brittle material) tubing only had a 2 mm wall thickness winding the stator coil directly onto this form may have resulting in cracking or breaking of the form. For this reason the armature coil was pre-wound onto a wooden form which had a similar diameter to the Perspex tubing. The pre-wound coil was then easily secured to the Perspex coil form using painters tape as shown in Figure 27 below.

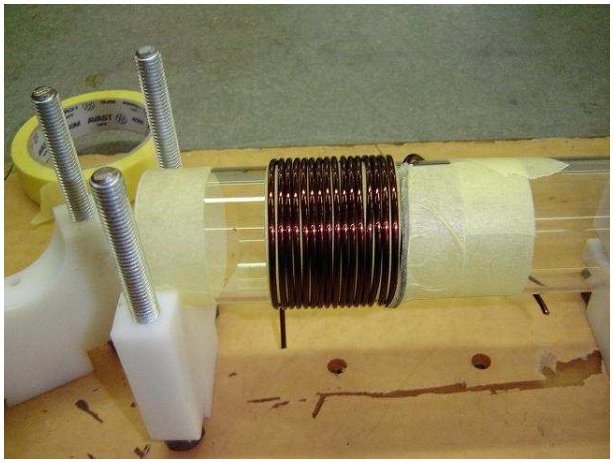

Figure 27: 16 Turn stator coil secured onto the Perspex form with painters tape.

Once secure, the stator coil was compressed to improve uniformity and then coated in varnish to bind the turns and secure the coil to the form. The completed single stage laboratory test launcher is shown in Figure 28 below.

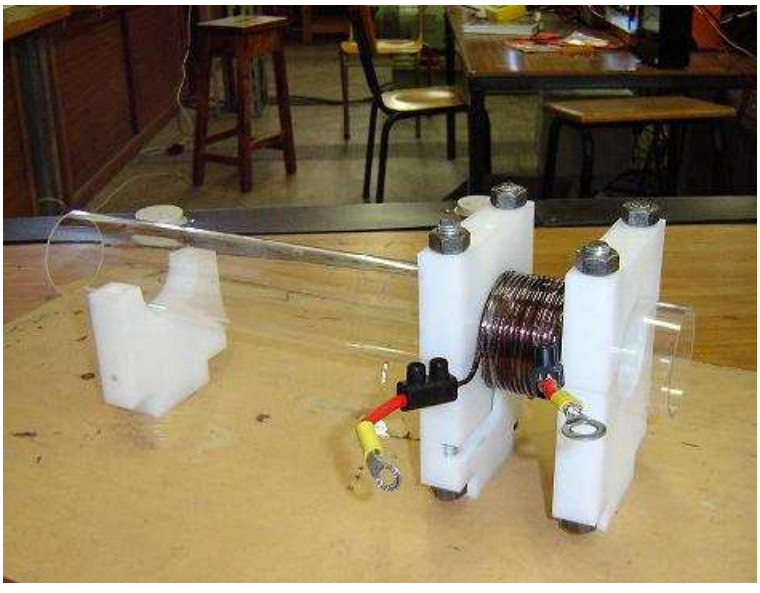

Figure 28: Complete single stage stator coil showing crimped & soldered connection leads which are connected directly to the IGBT module and capacitor bank.

4.3 IGBT Implementation and Drive Circuitry

The IGBT behaves much like a switch which keeps the tank circuit open allowing capacitor to be charged and closes the circuit when the stator coil needs to be energized. One of the most important systems found on the launcher is therefore the IGBT drive circuitry.

The device is turned on by applying a voltage to the gate of the device allowing current to flow from its collector to emitter. If not designed properly the drive circuit can cause failure of the IGBT. This is in fact just what happened during the initial testing phase of the launcher, in light of this unfortunate loss modifications have been made to the drive circuit and its layout. The circuit shown in Figure 29 is the most recent drive circuit reflecting the neccessary changes to prevent failure of the IGBT, discussed in depth in Section 5.1 on page 31.

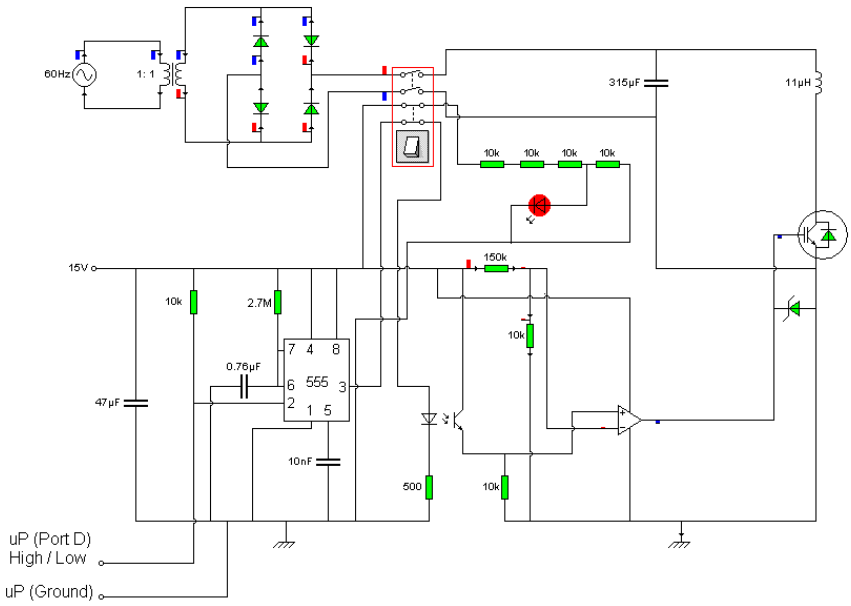

Figure 29: The complete launcher electrical schematic, showing the IGBT gate drive control, tank circuit, and capacitor charging circuit..

The entire energizing event of the stator coil is expected to take place in less than 10 msec based on a complete simulation of the launcher system shown in Appendix B on page B-1. The pulse generated by the 555 Timer IC (used as a mono-stable vibrator) was set to 2 seconds for two reasons. It would ensure that the 555 IC would be high (on pin 3) for the entire discharge event while in addition serving as some measure of switch de-bouncing.

The circuit in Figure 29 also reflects the opto-coupler used to isolate the control circuit from the heavy current tank circuit. An additional safety feature is the interlock, which decouples the charging circuit (connected to mains electricity) allowing current to flow from pin 3 to the opto-coupler. This prevents damage of the bridge rectifier, VARIAC (variable A.C) supply and mains wiring which may occur if the capacitor was ever discharged while still connected the charging circuit. Trigger pulse from the 555 IC results in the op-amp output swinging high (15 V), raising the IGBT gate voltage and thus turning the IGBT on and energizing the stator coil. The circuit in Figure 29 also shows the zener diode connected across the IGBT gate and emitter which protects the gate from any over voltage which may occur (discussed at length in Section 5.1.2 on page 36).

The IGBT was carefully mounted on large aluminium heat-sink (150mm x 200mm x 100mm) as shown in Figure 30 below. Adequate Silicon heat transfer compound was also used to ensure efficient heat dissipation from the device. Since the IGBT is a M.O.S device the gate and emitter were kept shorted as shown in Figure 30 below to prevent any damage which may occur during installation due to electrostatic discharge .

Figure 30: The Mitsubishi IGBT securely mounted onto heat-sink and heat transfer paste used.

4.4 Capacitor Bank and Charging Circuit

The capacitor bank was made out of six AFCAP 440 V 50 μF Polypropelene A.C Capacitors connected in parallel initially with 6mm Litz wire and crimp connectors as shown in Figure 31 below. The suporting theory justifying the choice of capacitor and the bank design for this application is discussed in great detail in Appendix B.9 on page B-19.

Figure 31: Prototype capacitor bank with capacitors connected in parallel using crimped 6mm wire.

However in light of initial testing which emphasized the need to minimize tank circuit resistance, these crimped wire connectors were scrapped and replaced with Nickel plated copper buss bars as shown below in Figure 32, followed by Figure 33 showing the improved capacitor bank.

Figure 32: Nickel plated copper motor connection bars which replaced crimped capacitor connectors as shown in Figure 31.

Figure 33: The complete capacitor bank after modifactions.

The capacitor bank was charged through a variable A.C power supply (VARIAC) which was isolated using a 1:1, 2kVA isolation transformer. The output from the isolation transformer was rectified using a 10 A bridge rectifier. The maximum output voltage from the Variable A.C supply was 260 V A.C. Since the A.C was rectified using a bridge rectifire, we can expect the peak D.C voltage ouput to be $\sqrt{2} \times 260\text{V}$ thus the maximum voltage to which the capacitors could be charged 360V, slightly less then the design specification of 400 V. The charging circuit is shown in Figure 34 below, including the interlock which decouples the charging circuit during the launcher operation. Figure 34 also shows where 10 Amp saftey fuses were used in the circuit.

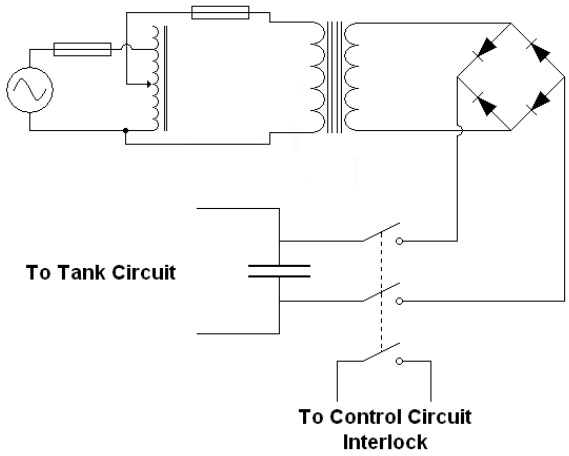

Figure 34: Capacitor charging circuit.

4.5 System Integration & Complete Test Setup

By integrating all the aforementioned systems the single stage test launcher was constructed. For initial testing it was decided that additional measurement systems would be constructed and implemented once the launcher concept had proved successful, this was the case with the optical velocity sensors. The tank circuit current was measured using a commercially available current meter. This device conveniently had a 1mV/Amp output and was capable of measuring the tank circuit current while outputting the data into a digital storage oscilloscope for recording. Initial tests revealed the importance of minimizing circuit resistance to prevent damping. As such the tank circuit components were all physically located as close as possible to each other to reduce the length of circuit wiring and thus resistance. The complete Test Area is shown in Figure 35 below, the microprocessor is not shown here as it was never implemented into the final test set up.

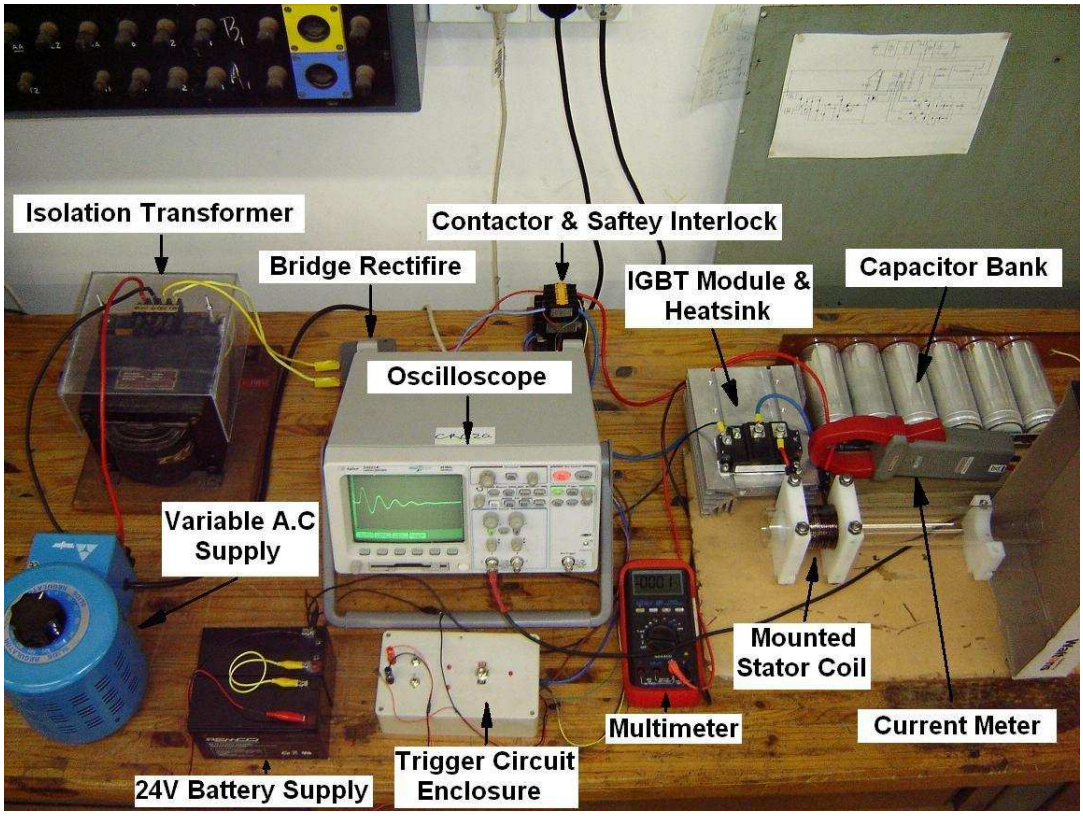

Figure 35: Laboratory test area, showing all equipment used to conduct tests on the single stage pulsed linear induction launcher.

The capacitor is charged with a through a variable A.C power supply which is coupled to an isolation 1:1 transformer whose output is rectified to get a D.C charging current. During charging of the capacitor the supply will see the capacitor as a dead short in the circuit, thus providing the maximum available current. To prevent excessive current draw the charging voltage was "ramped" up steadily on the variable the A.C supply preventing a rapid inrush of current to the capacitors, which may harm the bridge rectifier or any other component in the charging circuit. The initial charge on the capacitor was measured using a digital multi-meter. Finally the IGBT drive or trigger circuit was enclosed in a project box for safety and neatness. The power supply for the drive circuit was provided by a 24 V battery supply.

5 Experimental Results

5.1 Initial Tests and IGBT Failure

Initial operation tests were conducted at a low voltage, to ensure that the test rig was working correctly before high energy tests could be conducted these initial tests form part of the commissioning of the test rig for safe usage. Any problems or failures encountered here will provide data allowing for circuit modification to be made in adition to making initial comparisons between theoretical and actual performance. Table 7 below sumarises the conditions of the initial tests.

Table 7: Launcher preliminary testing details.

Test No.	Voltage Charge	Energy	Expected Theoretical Peak Current	Actual Peak Current
3	150 V	3.43 J	858.02 A	800 A
4	200 V	6.10 J	1144.00 A	1125 A

These tests ultimately resulted in failure of one IGBT modules. The possible reasons for this failure were thoroughly considered allowing for possible solutions and circuit modifications to be developed and implemented. All of which is discussed in much greater detail in Section 5.1.2. However before the failure of the IGBT module occoured some operation data was captured by the digital storage oscilloscope. Analysis of this data shows some correlation between theoretical and actual electrical performance of the device which is the subject of the Section 5.1.1 below.

5.1.1 Circuit Resistance & Damping

Despite failure of the IGBT in the preliminary trials of the device, data was still acquired which allows for a critical comparison between theoretical and practical results to be made. Using the digital storage scope and a Hall Effect current to voltage transducer (which has a 1mV/A output) the current in the stator coil was measured during the discharge event. Figures 36 & 37 comparatively show the actual and theoretical plots of the tank circuit currents for initial capacitor voltage charges of 150 V and 200 V respectively.

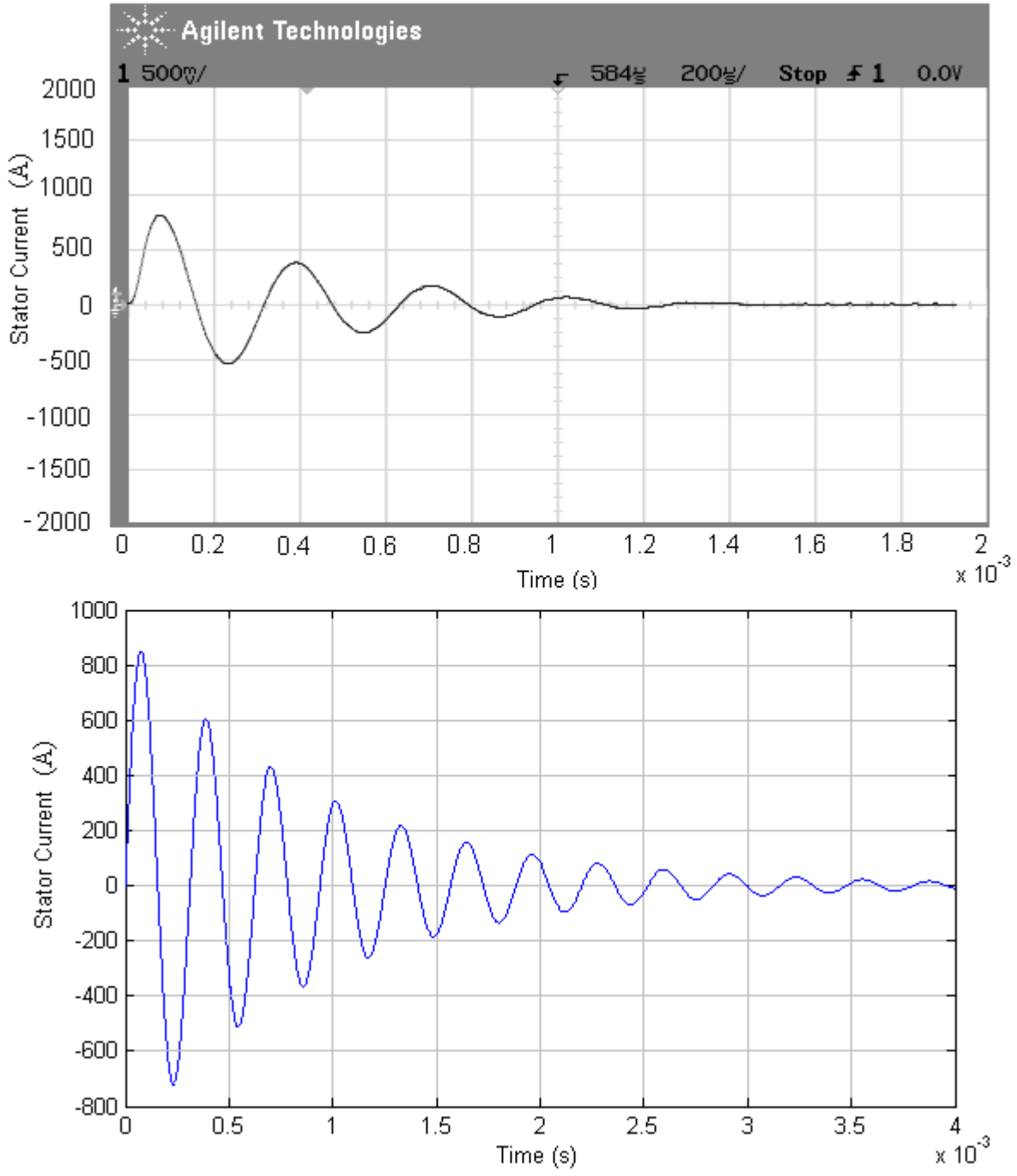

Figure 36: Actual and theoretical current waveform for an initial capacitor charge of 150 V

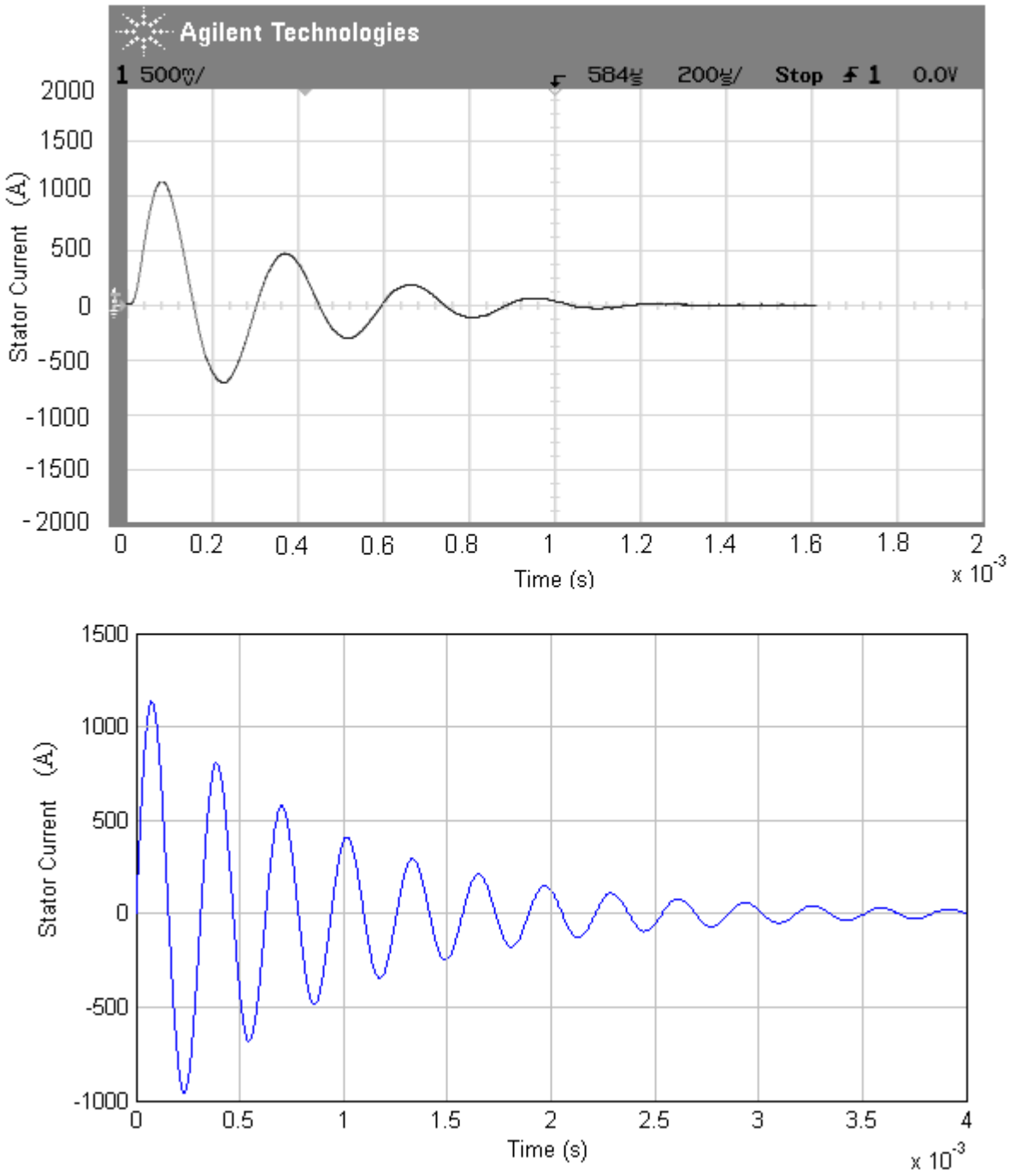

Figure 37: Actual and theoretical current waveforms for an initial capacitor charge of 200 V.

Table 8: Frequency of oscilation comparison for waveforms in Figures 36 & 37.

Test Voltage	Theoretical Frequency	Actual Frequency	Error
150	3205 Hz	3125 Hz	2.6 %
200	3205 Hz	3205 Hz	0 %

A comparison of the theoretical and actual data presented in Figures 36 & 37 and Tables 8 & 7 above reveals that the current magnitude & frequency of oscilation in the tank circuit is very accuratly predicted by the theoretical model. This serves as excellent validation of the computer code, in that it must atleast have been able to correctly predict the coil pairs self inductace.

It is however quite clear that in practics extent of damping in the circuit is quite severe. Is should also be noted that the theoretical currents plots shown above in Figures 36 & 37 were modeled under the assumption of ideal conditions, that said the circuit resistance was modeled taking only the stator coils resistance and not the resistance of connecting wires or capacitive E.S.R (which is in practice small enough to be ignored) into account. For this reason it is believed that the theoretical results will far better match the results in found in practice if the circuit connection resistance is included in the computer simulation. Figure 38 below shows a similar comparison as that found in Figure 37 for an initial capacitor charge of 200 V however the theoretical results shown in Figure 38 do take into account an assumed circuit wiring resistance of 25 mΩ in addition to the stator coils resistance of almost 11 mΩ.

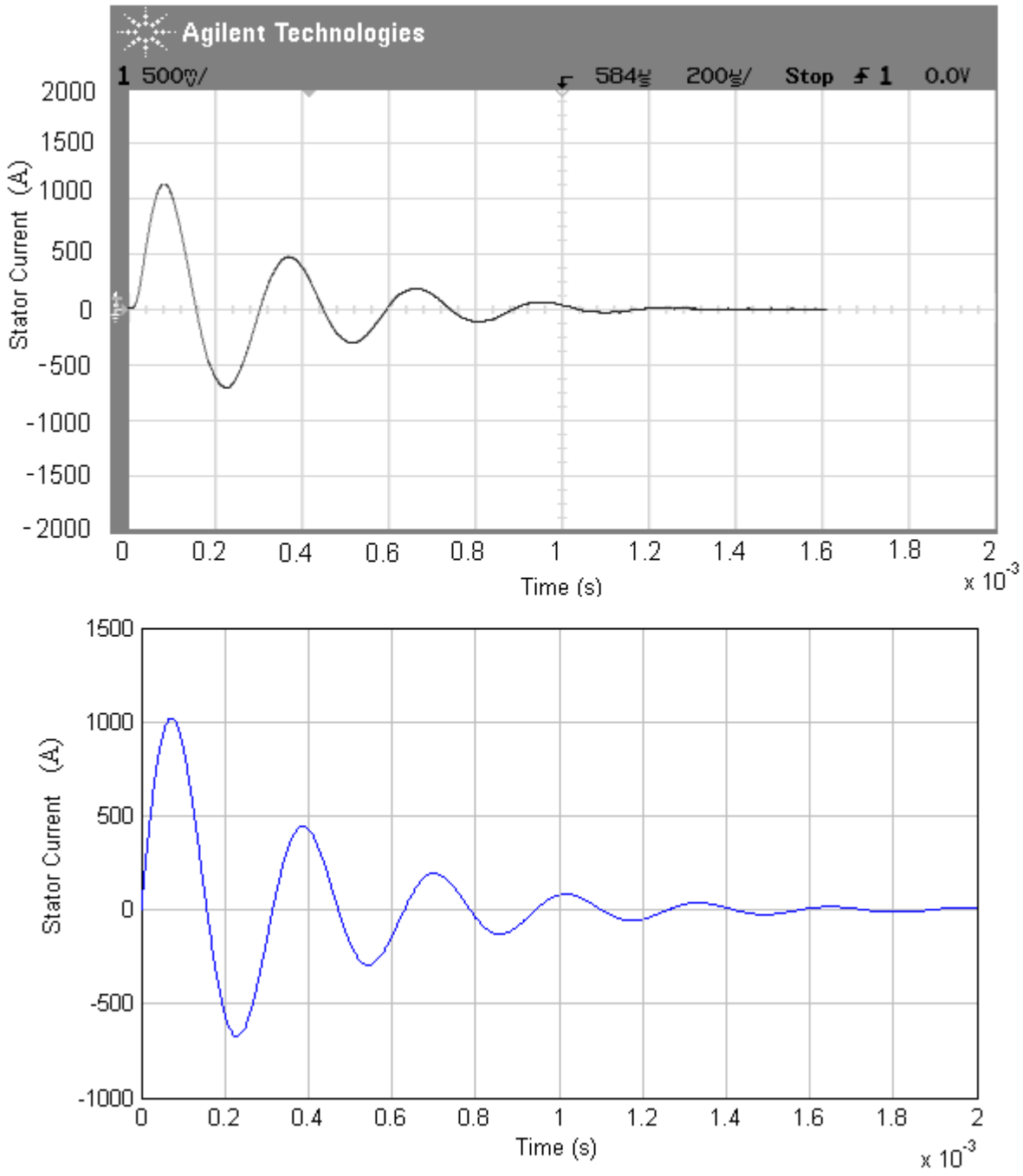

Figure 38: Current waveform for operation with an initial capacitor charge of 200 V. However theoretical results were modeled taking into account the circuit wiring resistance assumed to approximately 25 mΩ.

The theoretical and practical results shown in Figure 38 above match very closely again in terms current magnatude of the frequency and this time the time period in which the waveforms decay, nevertheless the graphs in Figure 38 are not identical as the circuit resistance was only estimated in the simulation.

As described in Section 3.5 on page 14 the performance of a linear induction motor is greatly dependant on the extent of resitive damping in the system and as such every precaution must be taken to minimize circuit resistance. Despite poor performance at this low energy input (approximately 6 Joules) which was to some extent expected (one can only hear the armature coil rattling in the barrel) these tests do serve as excellent validation of the computer simulation used to develop the launcher. Simulation and practical tests both clearly emphasize the necessity of minimizing circuit resistance, and it is expected that the loop resistance can by minimized at least 4 fold through the following techniques.

- Connecting capacitors with copper buss bars.
- Reducing tank circuit wiring by physically moving all circuit elements closer together.
- Soldering all crimp joints (i.e. solder the wire to the lug).

5.1.2 IGBT Failure

During the launchers initial testing the IGBT used for switching the tank circuit had failed. It is noted that the Failure of the device was non-violent and could not even be heard. The failed device was unable to block current flow from the collector to emitter; thus acting as a short circuit making it impossible to charge the capacitor bank. Even shorting the gate and emitter to ensure the device would not conduct failed to stop it from conducting. Since the device was operating within its save operating limits throughout the testing phase it is believed that devices gate had been damaged, the most likely causes are discussed in this section. Important and relevant data regarding the devices operation is shown below in Figure 39, and will be referred to during this failure discussion.

CM600HU-12F

MITSUBISHI ELECTRIC

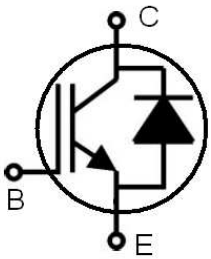

MAXIMUM RATINGS (T_j = 25°C)

Symbol	Parameter	Conditions	Ratings	Unit
V_{CES}	Collector-emitter voltage	G-E Short	600	V
V_{GES}	Gate-emitter voltage	C-E Short	±20	V
I_C	Collector current	T_C = 25°C	600	A
I_{CM}		Pulse (Note 2)	1200	
I_E (Note 1)	Emitter current	T_C = 25°C	600	A
I_{EM} (Note 1)		Pulse (Note 2)	1200	
P_C (Note 3)	Maximum collector dissipation	T_C = 25°C	1420	W
T_j	Junction temperature		–40 ~ +150	°C
T_j	Junction temperature		–40 ~ +150	°C

ELECTRICAL CHARACTERISTICS (T_j = 25°C)

Symbol	Parameter	Test conditions	Limits Min.	Limits Typ.	Limits Max.	Unit
$V_{GE(th)}$	Gate-emitter threshold voltage	I_C = 60mA, V_{CE} = 10V	5	6	7	V
I_{GES}	Gate leakage current	V_{GE} = V_{CES}, V_{CE} = 0V	—	—	80	µA
$V_{CE(sat)}$	Collector-emitter saturation voltage	T_j = 25°C, I_C = 600A, V_{GE} = 15V	—	1.6	2.2	V
		T_j = 125°C, I_C = 600A, V_{GE} = 15V	—	1.6	—	
$t_{d(on)}$	Turn-on delay time	V_{CC} = 300V, I_C = 600A, V_{GE1} = V_{GE2} = 15V, R_G = 3.1Ω, Inductive load switching operation	—	—	600	ns
t_r	Turn-on rise time		—	—	400	
$t_{d(off)}$	Turn-off delay time		—	—	900	
t_f	Turn-off fall time		—	—	250	
t_{rr} (Note 1)	Reverse recovery time	I_E = 600A	—	—	300	ns
Q_{rr} (Note 1)	Reverse recovery charge		—	11.7	—	µC
V_{EC} (Note 1)	Emitter-collector voltage	I_E = 600A, V_{GE} = 0V	—	—	2.6	V

Note 1. I_E, V_{EC}, t_{rr}, Q_{rr}, die/dt represent characteristics of the anti-parallel, emitter to collector free-wheel diode. (FWDi).
2. Pulse width and repetition rate should be such that the device junction temp. (T_j) does not exceed T_{jmax} rating.
3. Junction temperature (T_j) should not increase beyond 150°C.

Figure 39: Data sheet summary of the important parameters for the IGBT (Mitsubishi CM600HU-12F) used to switch the test launchers tank circuit[37].

To give the reader a better understanding of the systems being analyzed the tank circuit is shown in Figure 40 below, incl. the IGBT switching circuitry. The items in red represent stray (non-ideal) inductances and capacitances found in the circuit, due to wiring or in the case of the IGBT actual construction.

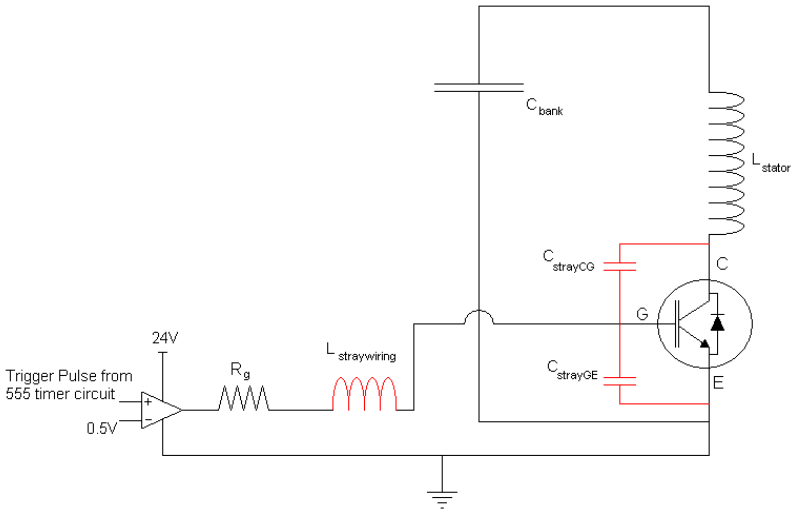

Figure 40: Tank ciruit of the launcher showing capacitor bank C_{bank}, stator coil L_{stator}, associated stray capacitances and inductances and the IGBT drive circuit with gate resistance R_g.

When the IGBT gate is turned on, the capacitor is effectively discharged into the stator coil inductance L_{stator}, this results in an bi-polar oscillatory waveform as shown in Figure 41 below. The diode conducts the negative half cycle protecting the IGBT from any reverse voltage. The IGBT gate is kept high even when the device is not conducting.

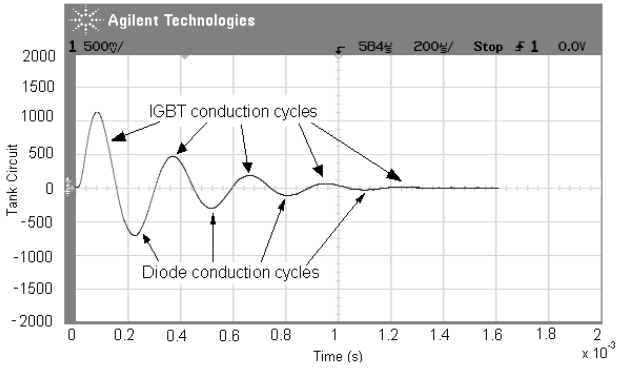

Figure 41: illustration of how the oscillatory wave is conducted through the IGBT device (with built in anti-parallel diode).

The orientation of the IGBT is critical, had the device been orientated the other way around, the diode would act as a dead short circuit immediately conducting any charge which tries to accumulate in the capacitor during charging.

It was found that the gate of the IGBT had blown through to the emitter. This was determined by rising gate voltage and measuring the V_{GE} across the gate and emiter with a multimeter which registered 0 V, clearly indicating that the gate had infact been damaged.

It is also worth mentioning that none of the devices control circuitry was damaged during the fault and the op-amp used to control the gate voltage pulse was unaffected and in working condition after the failure occurred.

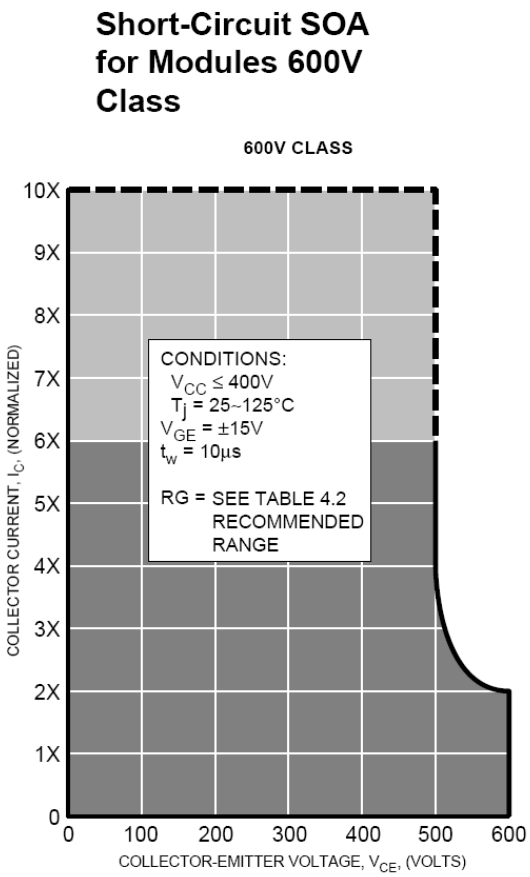

Figure 42: Safe operating area of the IGBT device[37].

Figure 42 above shows the safe operating area of the device illustrating its maximum voltage and current limits. During these initial tests the launcher was not operated beyond 200V and the measured current never exceeded 2 times the rated collector emitter current. Furthermore because the diode always conducts (its purpose is actually for reverse bias protection of the IGBT) failure most likely occurred at a time when the IGBT was in (or switched to) its off state when it should have been in its on state. The three most likely causes of failure are discussed below, these discussions are very theoretical and for good reason. The entire event duration of the fault which resulted in the IGBT failure is such a short event that it is difficult to say with any certainty what happened. The best that can be done within the scope of this project is to identify the possible causes based on the symptoms of failure observed in the system. Once done, the likelihood of failure occurring due to any one of these theories can be estimated and effective attempts to mitigate these failure causes can be undertaken.

5.1.2.1 Current Failure Theories

1. Gate turn off during IGBT conduction cycle would result in rapid fall in collector current, this fall in current is associated with a very high $\frac{dI}{dt}$ which could have caused a "back" E.M.F across the

stator coil inductance L_{stator}. This back E.M.F would have been coupled directly to the gate drive circuit through the IGBT's stray capacitance $C_{strayCG}$ possibly exceeding the maximum allowable gate emiter voltage V_{GE}. It is also possible that the high turnoff $\frac{dI}{dt}$ was coupled to the stray wiring inductance $L_{straywiring}$ of the drive circuit through the stray capacitance $C_{strayGE}$which also would have resulted in a "back" E.M.F that could have damaged the gate/emitter of the device.

2. If the IGBT were off when it should have been on the voltage it was supposed to conduct would've caused a voltage rise at the collector, it is possible that the rate of voltage rise $\frac{dV}{dt}$ (dependant on tank circuit frequency of oscillation & operating voltage) applied to the stray capacitance $C_{strayCG}$ may have resulted in a flow of current from the gate to the the now low output of the driving op amp. This would have could have caused a current to flow across the gate resistor resulting in a voltage at the gate which may have exceeded the devices V_{GE} specifiaction.

3. Also less likely but equilly possible is that during the IGBT's off state, when the diode finishes its conduction cycle, the *reevrvse recovery* of the diode is associated with a rapid positive rate of rise of current or $\frac{dI}{dt}$, this $\frac{dI}{dt}$ could possibly have caused a back EMF when applied to the stator coil inductance L_{stator}. Again this back EMF coupled through the stray capacitance C_{CG} to the gate may have raised the gate voltage V_{GE} beyond specification resulting in failure.

All of these failure theories have 2 things in common. Firstly and most importantly failure is ultimately a result of gate destruction (through over voltage). Secondly all of these failure theories occur because either the IGBT is off or is turned off when it should be on. Since the oscillatory wave form applied to the device decays (as shown in Figure 41), the degree of severity of many of the failure theories above are greatly dependant on when the device is turned off. For instance a turn off of the IGBT very early (before the wave has decayed) in the case of Theory 1 would result in a much larger $\frac{dI}{dt}$ transient and consequently a much larger gate voltage overdrive.

Figure 40 shows that the op-amp was controlled using a 555 Timer IC operating in mono-stable mode. The pulse period generated by the 555 timer IC was approximately 2 seconds long, in contrasts to the time it takes for the tank circuit current to completely decay which is in the order of milliseconds. It is believed that the interlock contactor which disconnects the charging circuit and electrical wiring of the 3 prong wall socket and applies power to the op amp source (allowing the device to only be triggered when the charging circuit is disconnected) may have resulted in the op amp in going high and suddenly falling to low, momentarily triggering the IGBT and turning it off, when it should have continued in its on state. This is believed to be the root cause of the failure.

5.1.2.2 Solutions & Modifications Fortunately because all the failure theories above are ultimately a result of exceeding the gate voltage failure can possibly be prevented by implementing a few a simple

drive circuit modifications as discussed below. These modifications relate mainly to the drive circuit as there is nothing that can be done about the stray capacitances in the IGBT modules which is a consequence of the devices construction.

1. *The voltage at the gate needs to be "clamped" or fixed to a value not exceeding device specifiaction.*
   One easy method of doing this is to use a zener diode across the gate and emmiter of the device as shown in Figure 43 below. The zener diode conducts a forward current but also conducts when the its reverse voltage exeeds a specied value known as the zener voltage.

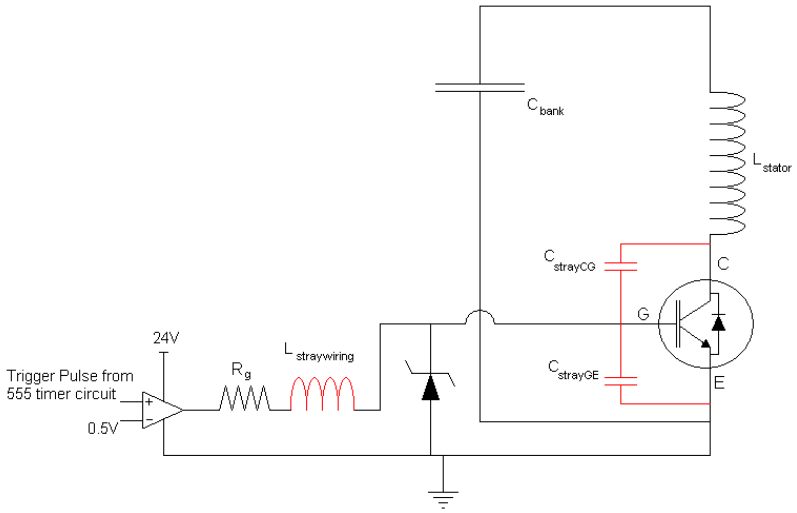

Figure 43: Modified drive circuit showing the included zener Diode for over voltage protection.

   Once the reverse voltage has been exceeded, voltage across the zener diode will be clamped or fixed to this zener voltage and any voltage spikes above the zener voltage will be shorted directly to ground. Using the zener diode preferably mounted on the IGBT device terminals (to minimize the loop inductance) will protect the gate from any voltages which exceed the zener voltage, which is chosen to be lower than the IGBT gate emitter V_{GE} voltage specification, effectively protecting the device from the three causes of failure discussed in Section 5.1.2 on page 36.

2. *Minimising gate drive wiring inductance $L_{straywiring}$.*
   The high rate of change of current at the collector of the IGBT (when it is turned off during its conduction cycle) applied to the gate drive wiring inductance $L_{straywiring}$ throught the stray capacitance $C_{strayCG}$ can potentially result in a "back" E.M.F to the IGBT gate. Reducing this unwanted wiring inductance $L_{straywiring}$ will go a long way in reducing the IGBTs vulnerability. Decreasing the wiring inductance can be done by minimizing the drive circuit loop area, represented by the shaded area in Figure 44 below. If this is not possible it is recomended in the Mitsubishi Application notes that the wires leading up to gate and emiter must be twisted with at least 3 twists per inch [46].

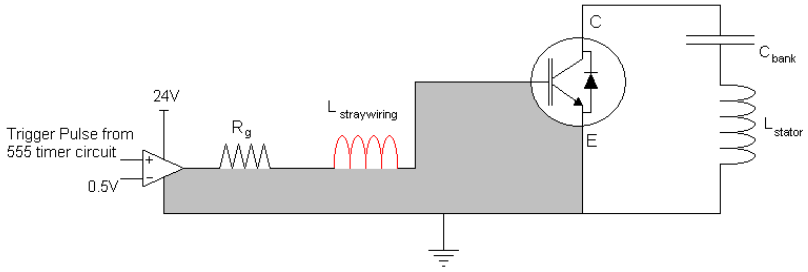

Figure 44: Shade area represents drive circuit wiring loop. This larger this area the greater the stray wiring inductance $L_{straywiring}$.

3. *Minimising gate drive resistance R_g.*

   The purpose of the gate resistance is to controll the turn on and turn off speed of the IGBT. A smaller resistance allows the device to turn off or turn on faster. The device data sheet specifies a minimum and a maximum gate resistance as shown in Table 9 below.

Table 9: Minimum and maximum recommended gate resistances[37].

Min	Max
1 Ω	10 Ω

   Initial tests were conducted with a gate resistance of 10 Ω . However in light of the failure theories it believed that minimizing this gate resistance would also minimize the possible voltage rise across it and possibly limit the extent to which the gate voltage could be exceeded under failure Theory 2.

4. *Modifying Interlock wiring*

   Figure 45 shows how the charging circuit and control circuit were initially interlocked so that the gate cannot be triggered with out first disconnecting the tank circuit from the charging circuit which is connected to the 220 volt mains socket, albeit through a 1:1, 2 kVA isolation transformer. Figure 45 also illustrates how this interlock controls the supply power to the op-amps source.

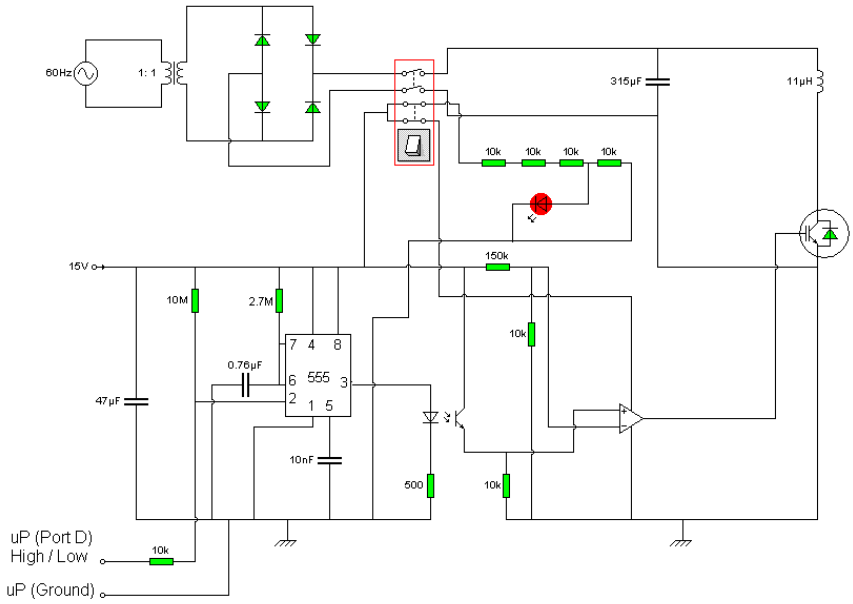

Figure 45: Complete circuit showing the tank circuit, capacitor charging circuit and gate control circuitry. Also shown is the interlock preventing tank circuit energization while it is still coupled to the charging circuit. The LED is simply to indicate the status of the interlock.

As discussed in Theory 3 it is believed that the initial supply of power to the op amp source momentarily sets its output high. Since the 555 Timer IC has not been triggered the device falls to low again. This momentary pulse would have momentarily turned the IGBT and then returning it to its off state during its conduction cycle causing many of the failures discussed in Section 5.1.2 on page 36. This interlock must be modified to interrupt the current pulse at the IGBT gate during the capacitors charging phase without interfering with critical components such as the op-amp or 555 IC. This can by done by disconnecting the opto-coupler on control side of the circuit as show in Figure 46 below. This would prevent unintentional momentary turn on of the IGBT when ever the interlock is switched.

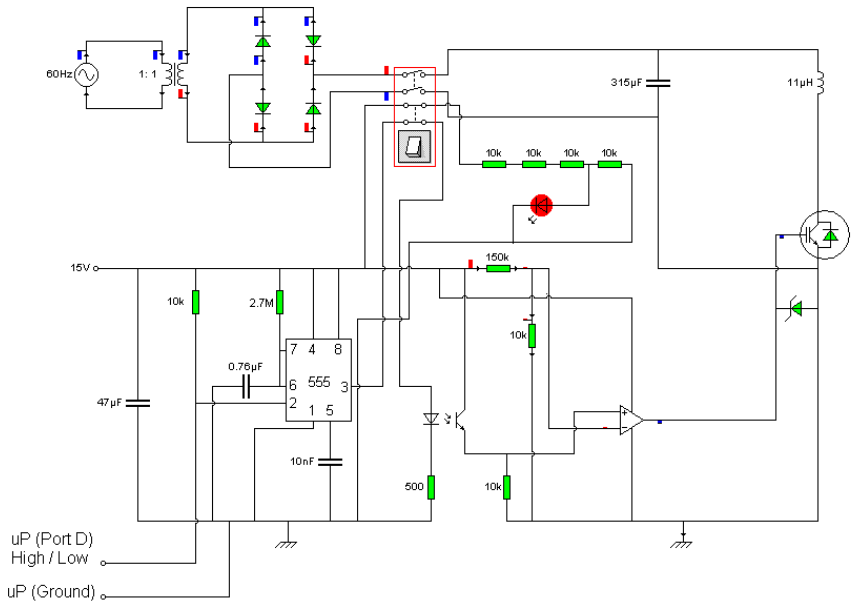

Figure 46: Modified circuit showing interlock now interrupting the opto-coupler current flow as opposed to the supply of the op-amp Also shown is the gate protection zener diode.

Failure of the IGBT was a most unfortunate event. However much was learned about IGBT application, protection and control in linear induction motor systems. The failure emphasizes the important design considerations and precautions which must be made to avoid future failures. As such the circuit modifications will be carried out on the test launcher circuitry before any further testing is conducted using the last remaining IGBT.

5.2 Further Device Testing

Having implemented a few modifications, testing continued with the last remaining 600 A IGBT module. A major improvement in addition to the control circuit modifications was that of reducing the tank circuits overall resistance by replacing capacitor connectors with Nickel plated copper buss bars and physically locating all tank circuit components close to each other to reduced the tank circuit loop resistance and hopefully the extent of damping. Figure 47 comparatively shows two tank circuit current plots for two separate tests.

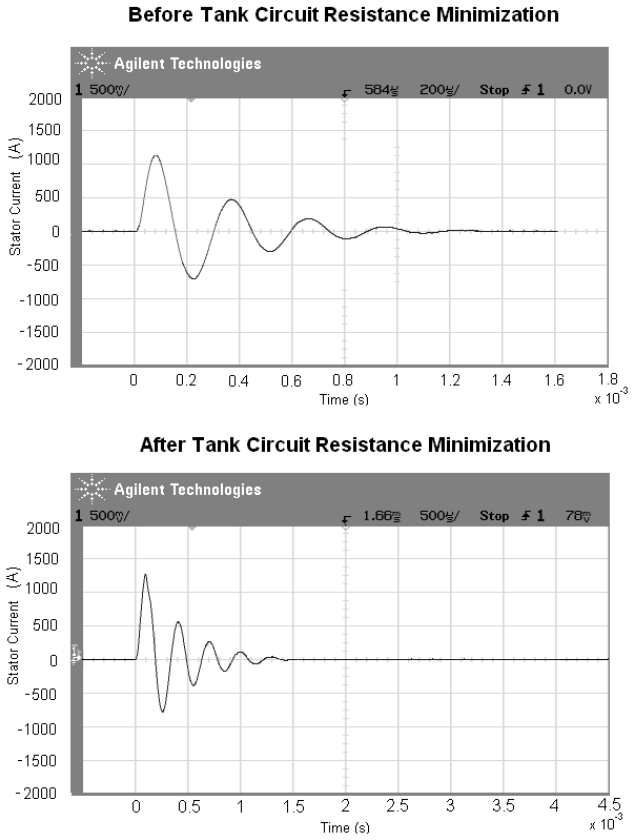

Figure 47: Stator coil currents before and after the tank circuit resistance was minimized to reduce damping, clearly illustrating a less than significant reduction in damping.

Both these tests had an initial capacitor voltage charge of 250 V however the first test (above) was before circuit resistance was minimized and the second (below) was conducted on the same test rig after attempting to reduce the circuit resistance. Figure 47 shows that the improvements gained were hardly significant although the peak current was increased by approximately 100 A.

It was during these tests that obvious motion of the armature coil was achieved. At a maximum tested initial capacitor charge of 350 V representing approximately 19 J the armature coil would move approximately 15 mm hardly enough to practically measure its velocity but enough to verify that the concept does in fact work. Unfortunately only 8 tests were conducted before the last remaining IGBT also failed. The full results and parameters of these tests are included in Appendix D on page D-1.

Despite minimal movement of the armature the simulation plots for stator current closely match those of the laboratory scale model in that the frequency of oscillation of the current in the stator coil was very close to that predicted by the model, in addition to the general magnitude of the actual tank circuit current which was also very much similar to that predicted by the simulation code. This suggests that the computer simulation had correctly predicted the coil pairs inductance parameters. The extent of damping found in the actual tank circuit however was much greater than expected. Since the capacitors

E.S.R was less than 2 mΩ and having minimized the tank circuit resistance as much as possible showed little improvements it is believed that the resistance of the IGBT and the Diode during their respective conduction cycles were significant enough to greatly limit the performance of the launcher. Unfortunately these resistance parameters are not reflected in the devices data sheet and could not have been known before hand.

6 Discussion

6.1 Introduction

The theoretical simulation of the launcher system correctly predicted the electrical performance in the sense that the theoretical current waveforms matched those found in practice in terms of magnitude and more importantly frequency of oscillation. Since the frequency of oscillation is dependant on the stator coils inductance and the tank circuit capacitance which is specified, the correct predication of the frequency of oscillation indicates that the simulation has at least correctly approximated the stator coils inductance parameters. Mechanically however the actual results varied greatly to what was predicted by the simulation program. This section will discuss some of the key reasons and factors which may have resulted in such a marked difference between the actual and theoretical mechanical performance of the launcher. Also if possible, methods around these launcher limitations are also discussed.

6.2 Tank Circuit Resistance & Damping

It is currently believed that the main reason for the launchers poor mechanical performance is at root caused by the extent of damping, which is a result of resistance somewhere in the tank circuit. As discussed in Sections 5.1.1 on page 31 & 3.5 on page 14 resistive damping of the oscillatory discharge current in the tank circuit severely limits the acceleration of the armature. An additional implication of the damping is that if the forward accelerating forces of the armature coil are inadequate, then it is also very likely that the radial forces acting circumferentially on the armature coil are also inadequate meaning that the centralizing force which was to hold the armature more or less in the center of the barrel form thus greatly minimizing the armature/barrel contact and friction was absent. This would have allowed the armature coil to touch the barrel form, severely limited the acceleration of the armature through friction.

As mentioned in the results section, many efforts were made to reduce the circuit resistance, including minimizing the physical spacing between tank circuit components. This was thought to be an effective means of reducing resistance, because of the linear relationship between a wire's length and its resistance. All connecting wire lengths were more than halved in length, in addition to using Nickel plated copper buss bars to connect capacitors in parallel. Also every effort was to improve the quality of connection points in the tank circuit. After the ends of the stator coil were also sanded down to remove the enamel coating, after which they were coated with solder, to prevent any oxidation of the copper over time. Figur 47 on page 45 shows that these measures did very little to reduce the extent of system damping. Fortunately there are only 4 sources of resistance within the tank circuit (listed below), allowing for a critical consideration of each to determine which one is the culprit.

1. *IGBT & Anti-parrallel diode.*

   A likely contributor to tank circuit resistance is believed to be the IGBT module which is used to reliably, efficiently and safely switch or energize the stator coil at specific instants in time (as required in a multiple stage launcher). Both the IGBT and Anti-parallel diode have an associated voltage drop across themselves during the conduction of current. This voltage drop has a typical specified value and in the case of the IGBT module used can be as high as 2.8 V (for both diode and IGBT). During the design of the launcher, the contribution to current damping as a result of this voltage was not included in the simulation of the launcher. Subsequently this voltage drop has been included in the launchers simulation revealing that is does in fact play a minor but still significant part in damping the tank circuit current. This is discussed at length in Section 6.5 on page 54.

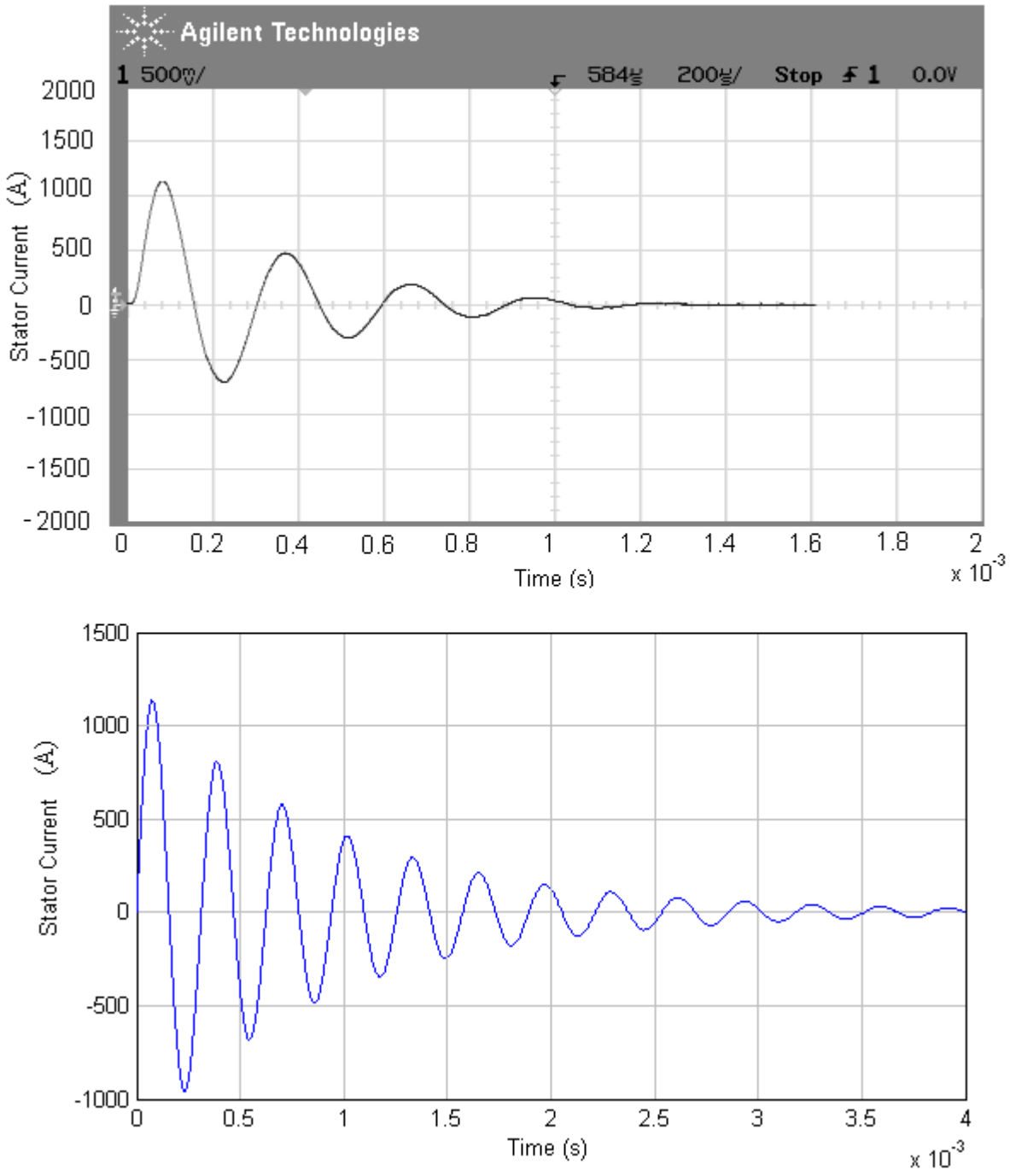

Figure 48: Theoretical and actual current waveforms for an initial capacitor charge of 250 V, showing a peak current of just over 1125 A.

Figure 48 shows both actual and theoretical plots of what the current waveform should look like, (ideally in the absence of any circuit resistance except that of the stator coil). The current should have decayed completely in around 4 m.s instead in practice it is found that the current decays in less than 2 m.s, reflecting a considerable amount of damping. Since the IGBTs internal resistance which is typically very low was not quoted in any of the devices datasheets or application notes,

the test launcher was modeled assuming that the resistance across the IGBT and its associated diode would be negligible. For this reason the nominal circuit resistance used in the modeling and development of the device was that of the stator coil only. In light of the current waveforms seen during the operation of the test launcher (shown in Figure 48) and the small amount of resistance required to drastically increase the effects of damping it is believed to be quite possible that the circuit resistance contributed by the IGBT may in be significant. In fact computer simulations have shown that even 10 mΩ of resistance would enough to result in significant current damping.

2. *Capacitor Bank*

   The Afcap capacitors used to construct the tank circuit capacitor bank each had an internal series resistance of only 10mΩ [35], which is a significant amount of resistance on its own. However the capacitor bank was made by connecting six of these capacitors in parallel, the series resistances of the bank was therefore equal to six 10 mΩ resistors in parallel. The internal resistance of the bank was thus approximately only 1.67 mΩ (resistors in parallel), this resistance was included in the simulation model which showed that its contribution would not significantly effect the tank circuit current damping. In addition to the equivalent series resistance capacitors also have some small equivalent series inductance and while not specifically quantified in the device data sheet it is mentioned that these capacitors have a low equivalent series inductance [35], a trait typical of polypropylene capacitors [27]. Furthermore serries inductances for the total bank inductance will be much less than the inductance of one capacitor (inductors connected in parrallel). In addition was learned that losses in these capacitors decrease as the frequency of operation is increased [31]. Thus making the capacitor an unlikely contributor to circuit resitance and damping.

3. *Stator Coil*

   The resistance of the stator coil was actually conservatively estimated through modeling as 11 mΩ, however in practice using a Wheatstone Galvanometer based current measuring kit the stator coil resistance (including some wiring) was much closer to 6 mΩ . This means that that stator coil and tank circuit wiring had a very minor contribution to the systems damping, suggesting that that in practice the extent of damping should have been much less severe. In consequence the likely hood of the major resistance contribution coming from the IGBT module is increased.

4. *Circuit Connnections & Wiring Resistance*

   In developing the simulation model of the test launcher it was assumed that the device would operate under ideal conditions and that the tank circuit resistance was negligible. In practice every effort had been made to reduce the circuit resistance and that comparative tests before and after these improvements showed little improvements in reducing circuit damping, therefore it is believed

that the major contribution of tank circuit resistance coming from the circuit connection and wiring resistance is unlikely, even more so since the stator coils resistance was less than that estimated by the model.

In light of this it most likely that the much of the circuits additional damping is largely a consequence of the on state resistance in the IGBT module. This was a most unexpected outcome, but in light of the above considerations is still the most likely cause for the tank circuits resistance. This is a most unfortunate result which cannot be worked around on the current test launcher design. However the effects of damping can be reduced if a higher stator coil inductance could be used, but this will require some revision of the initial performance requirement specifications and project objectives as discussed in the following section.

6.3 Low Tank Circuit Inductance Due To an Inadequate Operating Voltage

The design specification that the launcher be operated at a low voltage imposed a serious limit on the test launchers design which resulted a system inherently susceptible to current decay. Figure49 shows the exponential function which serves as the oscillation envelope within which the discharge current in the tank circuit decays.

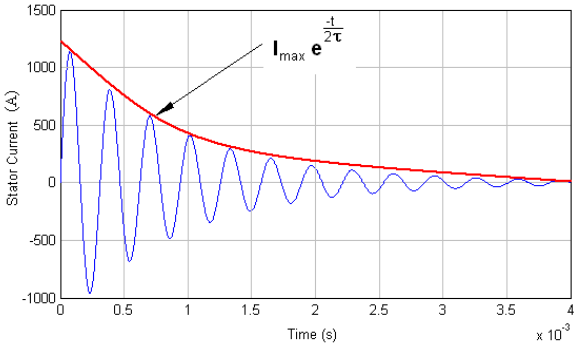

Figure 49: Exponential function which determines the rate of stator coil current decay or the boundary of envelope of oscillation.

This exponential function is greatly dependant on the LCR time constant $\tau = \frac{L}{R}$, the greater this time constant the longer it takes for the current to decay to zero, the opposite also being true. Thus if the stator coil was designed with an inherently small inductance, then the reducing the circuit resistance will do much less to increase the time constant. Therefore ideally a high stator coil inductance is preferred. However since the stator coils inductance is directly proportional to the number of turns, the goal of achieving a higher coil inductance often results in increasing stator coil resistance. Not only does this

resistance mitigate the effects of increasing the coil inductance on the time constant but it also greatly increases the given systems ohmic losses assuming the capacitive power supply remains unchanged (in initial voltage charge and size).

The armatures acceleration is proportional to the product of the armature and stator coil currents which must therefore be maximized in order to improve performance. Unfortunately the current in the stator coil is also inversely proportional to the inductance as shown by the following relationship describing instantaneous current in the tank circuit [13].

$$I(t) = \frac{V_{initial}}{\omega_d \cdot L_{ss}} \exp^{\frac{1}{2\tau}} \cdot \sin(\omega_d \cdot t)$$

Therefore in order to maintain tank circuit current as the stator coil inductance is increased (Thus increasing the envelope of oscillation) the voltage much be increased accordingly in order to maintain a feasible operating current. These findings suggest that the initial low voltage specification of 400 V may in fact have constrained or limited the scope of possible design configurations resulting in stator coil which is inherently susceptible to damping (has a small envelope of oscillation). The reason for this is that since the capacitors initial voltage charge and its energy content (specified by the systems intial performance requirement specifications) effectively fixed the tank circuit capacitance. The stator coil inductance thus had to be chosen such that that the frequency of oscillation would be approximately equal to 3 kHz to avoid complications and losses due to the skin effect. Choosing this inductance resulted in an inherently low inductance giving rise to a small oscillation envelope. If however voltage was not a design specification or limit, choosing a higher voltage would enable a much smaller capacitance to be used for the same energy requirement and frequency of oscillation. A smaller capacitance would mean that a larger inductance could be used while keeping the operating frequency within tolerable limits. Again operating at a high voltage will maintain the operating current when the stator coil inductance is increased. This will allow for launcher configurations with much more attractive inherent time constants that are more resilient to circuit damping.

6.4 Friction

As mention in Appendix B on page B-1 it was assumed in the theoretical modeling of the single stage test launcher that the system was in many cases ideal, electrically in the sense that the circuit connections would contribute no additional resistance and that the resistance across the IGBT would be negligible. Idealized mechanical assumptions were also made, most notably that the friction between the armature coil and the stator coil would be negligible and not included in the acceleration force modeling. This assumption was at first thought to be reasonable because during the launchers operation there would

be a radial force component which acts circumferentially on the armature coil surface. This radial force would effectively center the armature coil in the stator coil form during launching, thus reducing contact and friction between the armature coil and stator coil surfaces. In the case of the laboratory test launcher performance is greatly worsened since the damping which is currently believed to be limiting the forward acceleration of the coil will also reduce the radial/circumferential acceleration or force which locates the armature coil resulting in increased contact and friction.

Ideally this centering force must be very much greater than the weight of the armature, failure to meet this condition will cause the armature coil to remain in contact with the stator coil form thus greatly increasing the force of friction which reduces the net acceleration on the armature greatly effecting velocity and displacement profiles. Aside from the consequences of damping this is considered to be the most likely reason for the difference between the actual and theoretical mechanical performance of the launcher.

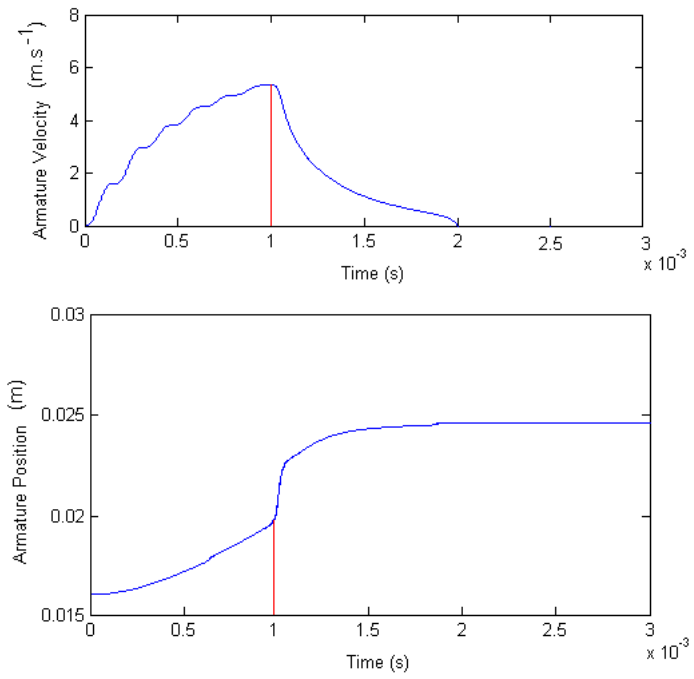

Figure 50: Theoretical velocity and displacement profiles of the armature illustrating how the effect of friction between the armature and the stator coil form may possibly affect the launchers performance.

Figure 50 above illustrates the affect which friction may have had on the launchers mechanical performance, for a launcher operated at 400 V and assuming that any appreciable induction acceleration ends after t = 1msec. Even though Figure 50 represents a very rough "guess" as to what frictions effects could be it does show that the actual armature displacements achieved in practice (approximately 10 mm - 18 mm) might well be very close to what the simulation would have predicted if mechanical friction was taken into account.

6.5 IGBT & Diode Voltage Drop

The effect of the voltage drop across the IGBT and its associated diode was also considered and investigated as it was believed to be responsible for the more sever damping which occurs later in the oscillatory discharge time period. Since the two coupled differential equations on which the numerical simulation based are derived using KIRCHOFF'S VOLTAGE LAW applied to the tank circuit current loop, the IGBT and diode voltage drop was easily included in the simulation model in order to model the effect that the voltage drop across the IGBT module has on the tank circuits behavior.

Figure 51 below shows two stator coil current plots. The current plot in red represents the simulation where the IGBT and Diode voltage drops were not considered. The plot in blue illustrates the resulting stator coil current waveform when the IGBT and Diode voltages were included in the tank circuit model. Figure 51 clearly shows that taking the IGBT module voltage drop into account results in a minor but still significant reduction of the envelope of oscillation, particularly towards the end of the discharge oscillation period, resulting in a much quicker tank circuit current decay.

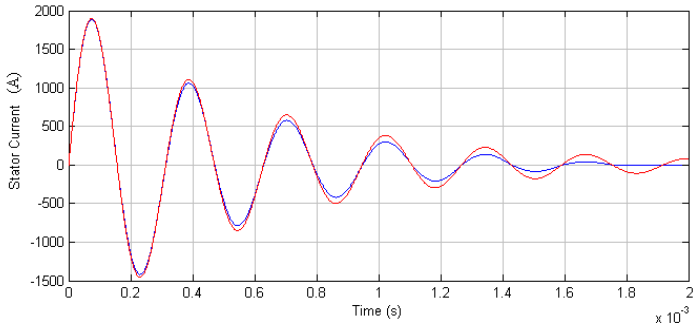

Figure 51: Comparative simulation results illustrating the theoretical difference made when the IGBT module voltage drop is taken into account in the numerical launcher simulation (Both plots assume a 25 mΩ circuit restance in addition to the estimated stator coil resistance).

This effect or symptom of the IGBT module voltage drop is seen in practice as reflected by Figure 52 below showing a sudden flatting out of the decaying waveform after the 4th oscillation cycle. For the sake of comparison both the practice and computer simulation results (for both plots in Figure 51 and that of Figure 52 respectively) the initial voltage charge on the capacitor was 350 V, furthermore the IGBT and diode voltage drops were assumed to be the maximum value of 2.8 V as quoted by the IGBT device data sheet [37].

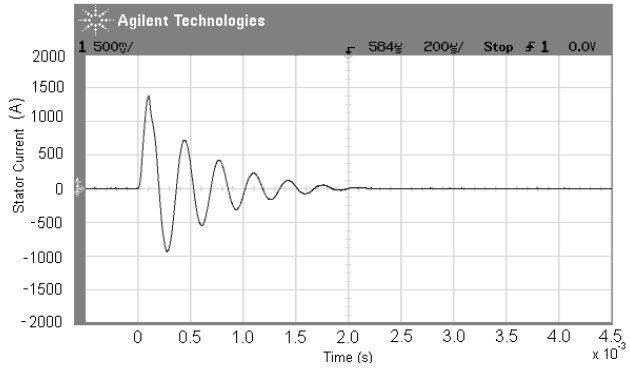

Figure 52: Actual current plot over time for the single stage laboratory test launcher. Note the similar rapid current decay after the 4th cycle, very similar to what was predicted by the simulation.

However the extent to which this effect may have reduced the armature coils acceleration is hardly significant. This is largely due to the fact that most of the armature coils acceleration takes places long before the 4th oscillation ends. This is largely due to the fact that the armature coil is well outside its induction length of the coil pair for the effect to cause any significant change in performance. The comparison of the maximum theoretical velocities in Table 10 for the two cases modeled and shown in Figure 51, confirms that this effect is of minor significance.

Table 10: Comparative theoretical performance of the two cases modeled (reflected in Figure 51).

	Efficiency
Ignoring IGBT & Diode Voltage Drop	1.61 %
Considering IGBT & Diode Voltage Drop	1.24 %

6.6 Summary

The major reasons as to why the launchers performance (electrically and mechanically) did not match the theoretical performance predicted by the computer simulation have been discussed. The effects or phenomena which worked against the test launcher were both electrical and mechanical and were not unaccounted by the model due to the simplifications or assumptions made when developing the theoretical launcher computer simulation and final test launcher system. In summary the major reasons discussed for the single stage launchers poor performance are listed below.

1. Armature/Stator Coilform Friction

2. Circuit Resistance and Damping

3. Limitations of Low operating voltage

4. IGBT voltage drop

The theoretical design approach, construction and tests conducted on system have been so far been discussed. This section has critically discussed the results of the test launcher and the reasons for the deviation in system performance when compared to the theoretical model. It is now possible to draw some definite conclusions, even more so in light of the experience gained during the completion of this project. The following section contains the concluding remarks of this project which is followed by recommendations for further study in this field.

7 Conclusions

A complete computational simulation was written and used to develop a single stage pulsed linear induction motor that was ultimately constructed and tested to verify the concept of operation and validate the simulation code which was a key tool used in the design and development of the device itself.

Unfortunately tests showed that in practice the constructed launcher failed to perform mechanically as theoretical simulations predicted it should. However careful study of the tank circuit current waveforms for the launcher system suggests that the simulation code had correctly predicted the typical decaying oscillatory current waveform which occurs in practice as well as the magnitude of these currents. In addition actually achieving motion of the armature coil does prove the concept of inductive acceleration. These findings conclusively indicated that the simulation model had correctly predicted the armature/stator coil inductance parameters, a significant step in the modeling and development of any system operating on the concept of induction. Furthermore there is also substantial evidence to suggest that many of the theoretical models shortcomings are purely the result of the initial simplifications used in creating the simulation, and when taken into account the practical performance of the launching system can be reasonably well explained.

It is interesting to learn that even though many of the simplifications made in the model on their own would have an insignificant affect on the launchers performance, it seems that all of these effects combined is enough to significantly affect the launchers performance. For this reason it is believed that it is not the validity of the launchers simulation which limited the practical performance but instead the initial assumptions made in developing the induction launcher system. Also despite the launchers poor mechanical performance a review of this projects initial objectives show that many of the goals have to some extent been achieved despite many of the initial specifications not being met.

1. Conduct thorough research on the topic.
2. Create a computer simulation to model and developed a 6 Stage P.L.I.M with an efficiency greater than 3.5% (electrical to mechanical energy conversion).
3. Design/develop a feasible low energy laboratory scale test launcher using the computer simulation.
4. Build and test this launcher to verify accuracy of model and prove concept.

For this reason in terms of the purely academic motivation of this project it is still be viewed as a educational success leaving behind a detailed summary of the most important design considerations, a complete and verified computer simulation (although simplified) and a test rig or procedure which all serves as an excellent starting point for any further research on this topic.

A notable omission to this projects final scope was the microprocessor control of the test launcher system was never implemented. The reason for this is that microprocessor control would only have been necessary if the launcher made use of more than one accelerating stage.

In hindsight the most notable limitation of this project was the projects initial goals. As discussed the requirement that the launcher operate with and initial capacitor charge of 400 V severely limited or reduced the number of possible launcher designs. The experiment also suggests that the low stage energy (25 J) is believed to be only enough for the launcher system to overcome the non-ideal operating conditions and effects which are found in practice. It is concluded therefore that at higher energy levels these non-ideal effects would play much less of a significant role in affecting the launchers performance both electrically and mechanically. This conclusion does seem to be quite a valid finding that is supported in the literature regarding the subject and although not strictly mentioned in the published literature, it is found that the general trend of designing linear induction launchers to operate at high voltages and energy levels is very common. To put this in better perspective many of the launchers described in the literature review operate at a voltage exceeding 10 kV and stage energies well above 5 kJ, which is more than two orders of magnitude greater than the specified energies in this project

From an economic perspective it is also noteworthy that even for a small project such as this the costs had greatly exceeded the originally specified budget. This was largely due (and somewhat unexpected) to the high cost of the IGBT modules used for efficient, safe and precisely switching the tank circuit. However it was quite fortunate that the capacitors required for the launcher are infact used for Laboratory work in the Machines Laboratory at U.C.T, eliminating cost relating to their purchase. Some light materials manufacturing/machining was required for making the mounting blocks and armature coil forms but it is noted that the material requirements for the test P.L.I.M system were minor.

All components which were integrated to form the test launcher functioned well and much was learned about their detailed selection for special applications usage. It was also unexpectedly learned that while providing precise and excellent switching characteristics that are considered ideal in high power applications the IGBT was most vulnerable in the tank circuit with both devices ultimately failing. Most likely being even more vulnerable to failure at higher voltages and energies. Further as discussed it is more than likely that the largest contribution to tank circuit resistance was due the IGBT and its ant-parallel diode's onstate resistance. All this suggests IGBTs may not be the best device suited for linear induction launcher tank circuit application. The Afcap capacitors used in the capacitor bank in contrast performed very well. They were capable of meeting the required currents while operating at a frequency far beyond that found in its intended application withought failure.

The armature coil is one of the projects most notable features. The fabrication of a projectile made from a wire wound coil that is shorted on itself presented some extra design considerations. Its design and

construction was indeed a highlight in the project. It was only noted that the varnish used to bind the armature windings to its form added and additional 10 grams to its total weight. It is also believed that the varnish may have increased the coefficient of friction between the Perspex stator coil form and the armature windings. Achieving movement of the armature coil also shows that the method of shorting the winding coil using a solder joint is feasible.

Despite the poor performance of the launcher the overall project and study is still viewed as a success. Much was learned in terms of this devices design, construction & component selection and even the reasonable correlation between the theoretical and practical results has provided an excellent starting point from which to critically analysis and explain the performance. It must also be considered that this launcher was the first iteration design solution to a very complex problem which leaves behind a detailed design process of a linear induction launcher and deffinate conclusions made in light of the research.

Clearly much was learned during the desiging, development and testing of this prototype model and as such there are several recommendations which may improve the current launchers performance and more importantly assist any further research on the topic after this project is completed. These recommendations will be presented in the following section.

8 Recommendations

There are a number of recommendations that can be made in view of the experience gained from the development of this test launcher. These recommendations would likely greatly improved the performance of future launchers and could possibly verify the theoretical model even further. It should be noted that implementation of some of these recommendations would require a project whose objectives differ slightly from this projects. Nevertheless many of these recommendations could be easily implemented within the scope of a typical MEC4061Z undergraduate thesis project.

8.1 Higher Operating Voltage

As mentioned, the initial performance requirement specification and goal of this project to operate on a low voltage power source severely limited the possible designs of launcher systems leading to a design which is inherently plagued by excessive tank circuit current damping. Operating at a much higher voltage results in a greatly reduced capacitor size if energy content is to remain the same allowing the stator coil inductance to be much larger (while maintaining operation frequency and current). Enabling the design of tank circuits which have much larger oscillation envelopes thus greatly improving launcher performance capability. An additional benefit of operating at a high voltage is that it enables the tank circuit to be switched using triggered spark gaps, which is probably the best method as the cost of semiconductor switching devices increases greatly as the operating voltage increases.

8.2 Higher Stage Energy

The current performance of the single stage launcher would suggest that a stage energy of 25 J is only enough for the launcher to overcome the non-ideal conditions found in practice such as mechanical friction and circuit resistance. Thus operating at higher initial energies would result in launchers where the armatures mechanical performance would be enough to warrant measurement and comparison of its actual and theoretical velocities. It should be noted that because of the interdependence of all the many variables involved in a linear induction motor simply changing the capacitor banks size or voltage to increase the energy might not yield effective results for an already existing launcher. Any significant changes in operating voltage and energy would require a whole new launcher (stator and armature coil pair) to be designed around the new operating point.

8.3 Tank Circuit Swithing

Suprisingly a huge limitation of this project was the use of IGBT semiconductor devices to switch the oscillatory tank circuit currents. These devices allow for precision switching of the circuit that and can be control by some very simple circuitry and a microprocessor which makes them ideal for multiple stage P.L.I.Ms. This project used discrete IGBT modules which included an anti-parallel diode connected across the gate and the collector allowing conduction of the alternating currents. These devices were very expensive and are the primary reason for the project running over budget, they also seemed to be very vulnerable to failure and it is believed that their on state resistance was the greatest contributor/or cause of tank circuit current damping. Therefore aside from semiconductor switching techniques there are two further alternatives should be investigated should further study be pursued.

1. *Mechanical Switches*

   A form of mechanical switch can also be used to switch the tank circuit and although this implementation would most likely be far cheaper than any semiconductor devices, a mechanical switch (similar to a relay) would have to be carefully designed for this application and will still have its limitations and drawbacks. At high energy levels discharging a capacitor by physically connecting circuit contacts will result in excessive arcing and sparking which is accompanied by extremely loud "BANG" noise. The amount of energy lost when the contactors touch would have to be carefully researched as well. This almost explosive release of energy is obviously an operational hazard which must be avoided if possible. Furthermore these devices would not be suitable for a complete multistage launcher as there mechanical turn on time would be far to slow to precisely energize the stator coils during the transit of the armature coil through the launchers barrel.

2. *High Voltage Spark Gap Switches*

   Following the recommendation to operate at a much higher voltage a much more suitable means of switching the tank circuit is then made possible. The device is known as a high voltage spark gap switch. Its use has been well noted in the literature regarding P.L.I.M where the launchers typically operate at voltages capable of ionizing and discharging through air. Sustaining current flow through an electrical arc of ionized gas, the resistance of this path is incredibly small. Thus conducting the high voltage high current tank circuit energy, until the voltage drops below the ionization voltage of the given spark gap configuration. Such a device could be built at a cost much lower than purchasing cost of a semiconductor device but greater than the cost of developing a mechanical switch. They would also have to be carefully designed and there effect on the launchers performance for a given voltage would need to be critically considered.

8.4 Optimum Launcher Development Using BGA

The number variables and the extent of their interdependency has most defiantly made the development of the laboratory test launcher challenging, whose final design by no means represents a so called "optimum". The reason for this is that optimization of such a complex multivariable problem would have been outside the scope of this project, where the aim was more to develop a model or simulation which could be verified with a simple test scale launcher. It is now strongly recommended that any further study should implement what is known as a Breeder Genetic Algorithm to seek out and rank all possible launcher designs, thus optimizing the single stage design in a process similar to natural selection. Literature regarding pulsed linear induction launcher design would indeed suggest that this is the most effective method of designing a linear induction launcher [2, 22]. It is suggested that this algorythm be developed from the computer simulation model developed in this project.

Due to the large computing times required to accurately simulate a given launcher design, it should be made apparent that implementation of this optimization algorithm will require a significant amount of computing power, furthermore a detailed ranking method based on the projects goals will need to be established and implemented into the software to allow a computer to autonomously critically compare various launcher designs. Using this technique high efficiency launchers can be developed which operate "optimally" around a user defined operating point (e.g. voltage, frequency and armature mass etc...).

8.5 Armature/Stator Barrel Form Friction Tests

Although it is expected to be much less of a problem at higher operating voltages and energies it would still be interesting to quantify the friction that occurs between current the armature coil and the stator coil form. This will perhaps help to aproximate more or less the energy requirements for the losses due to friction allowing a stage energy to be chosen such the frictional losses are insignificant in comparison to the kinetic energy gained by the armature coil. These tests can easily be performed on the current launcher setup using the tilted surface method of friction testing to give a crude estimation of how badly dynamic friction affects the launchers performance [15].

9 References

[1] Andrews, J.A. ; 1993, "Coilgun Structures", IEEE Trans. on Magnetics, vol. 29, no. 1, pp 637-642.

[2] Bresie, D.A. ;Andrews, J.A & Ingram, S.W. ; 1991, "Parametric Approach to Linear Induction Accelerator Design", IEEE Trans. on Magnetics, vol. 27, no. 1, pp 390-393.

[3] Lund Instrument Engineering, Inc. ; 2007, "Wire Gauge and Current Limits", [Online; Last Accessed 06 September 2007] Available at: http://www.powerstream.com/Wire_Size.htm

[4] Kolm, H. & Mongeau, P. ; 1996, "Basic Principles of Co-Axial Launch Technology", IEEE Trans. on Magnetics, vol. MAG-50, no. 2, pp. 227-230.

[5] McKinney, K. & Mongeau, P. ; 1984, "Multiple Stage Pulsed Induction Acceleration", IEEE Trans. on Magnetics, vol. MAG-20, no. 2, pp. 239-242.

[6] Coilgun Systems; 2004, "Coilgun Basics", [Online; Last Accessed 20 July 2007] Available at: http://www.coilgun.eclipse.co.uk/coilgun_basics_1.html

[7] Barry's Coilgun Design Site; 2007, "Interaction of magnetic field and projectile", [Online; Last Accessed 20 July 2007] Available at: http://www.coilgun.info/theory/magneticfield.htm

[8] Wikipeadia; 2007, "Faraday's Law of Induction", [Online; Last Accessed 22 July 2007] Available at: http://en.wikipedia.org/wiki/Faraday's_law_of_induction

[9] Wikipeadia; 2007, "Lorentz Force", [Online; Last Accessed 22 July 2007] Available at: http://en.wikipedia.org/wiki/Lorentz_force

[10] Coilgun Systems; 2004 "Electromagnetic Basics", [Online; Last Accessed 23 July 2007] Available at: http://www.coilgun.eclipse.co.uk/electromagnetic_basics_1.html

[11] Coilgun Systems; 2004, "Coilgun Basics", [Online; Last Accessed 23 July 2007] Available at: http://www.coilgun.eclipse.co.uk/coilgun_basics_2.html

[12] He, J. ;Levi. E. ;Zabar, Z. & Birenbaum, L. ; 1989, "Concerning the Design of Capacitively Driven Induction Coil Guns", IEEE Trans. on Plasma Science, vol. 17, no. 3 , pp 429 -437

[13] Zabar, Z. ;Naot, Y. ;Birenbaum, L. ;Levi. E. & Joshi P.N. ; 1989, "Design and Power Conditioning for the Coil-Gun", IEEE Trans. on Magnetics, vol. 25, no. 1, pp 627 - 631.

[14] Bresie, D.A. & Ingram, S.K; 1993, "Coilgun Technology at the Center for Electromechanics, The University of Texas at Austin", IEEE Trans. on Magnetics, vol. 29, no. 1, pp 649-654.

[15] Williamson, S. & Leonard, P.J ; 1986, "Analysis of Air-Cored Tubular Induction Motors", IEE Proceedings, vol. 133, pt. B, no. 4, pp 285 - 290.

[16] Andrews, J.A. & Devine, J.R. ; 1991, "Armature Design for Coaxial Induction Launchers" , IEEE Trans. on Magnetics, vol. 27, no. 1, pp 639 - 643.

[17] Burgess, T.J. ;Cnare, E.C. ;Oberkampf, W.L. ;Beard, S.G. & Cowan, M. ; 1982, "The electromagnetic θ Gun and Tubular Projectiles", IEEE Trans. Magnetics, vol. MAG-18, no. 1, pp 46- 55.

[18] Coilgun Systems; 2004, "Coilgun Basics", [Online; Last Accessed 24 July 2007] Available at: http://www.coilgun.eclipse.co.uk/coilgun_basics_3.html

[19] Elliot, D.G. ; 1989, "Traveling-Wave Induction Lauchers", IEEE Trans. on Magnetics, vol. 25, no. 1, pp 159-163.

[20] Grover, F.W; 1946, "Inductance calculations", Dover Publications, New York.

[21] Williamson, S. & Horne, C.D. ; 1995, "Design of Pulsed Coil Guns", IEEE Trans. on Magnetics, vol. 31, no. 1, pp 516- 521.

[22] Hainsworth, G. & Rodger, D. ; 1995, "Design Optimisation of Coilguns", IEEE Trans. on Magnetics, vol. 31, no. 1, pp 473-477.

[23] Knoepful, J.E. ; 1970, "Pulsed Magnetic Fields", North Holland Publishing, Amsterdam.

[24] Young, W.C. ; 1989, "Roark's Formulas for Stress and Strain, 6th Edt. ", McGraw-Hill, pp 638-639.

[25] Hearn, E.J. ; 19997, "Mechanics of Materials No. 1, 3rd Edt.", Butterworth Heinemann, Oxford ; pp 198-233.

[26] Cnare, E.C. ;Widner, M.M. & Duggin, B.W. ; 1991, "A 10-Stage Reconnection Demonstration Launcher", IEEE Transactions on Magnetics, vol. 70, no.1, pp 644-646.

[27] Byers T.J, ; 2007, "Bypass Caps Demystified", Nuts and Bolts, January, pp 18-19.

[28] Westcode Semiconductors Ltd ; 2004, "Capacitors for Power Electronics", [Online; Last Accessed 05 August 2007] Available at: http://www.coilgun.eclipse.co.uk/coilgun_basics_3.html.

[29] Avelar, V. ; 2004, "How APC designs AC Power capacitors into large UPS systems", APC (American Power Conversion) Application Notes, no.46, pp 1-4. [Online; Last Accessed 08 August 2007] Available at: http://www.apcmedia.com/salestools/

[30] Illinois Capacitor, INC ; 2006, "Film capacitor technical information and selection", [Online; Last Accessed 08 August 2007] Available at: http://www.illcap.com.hk/products/pdfs/

[31] Mohan, N. ; Underland, T.M. & Robbins, W.P. ; 1995, "Power Electronics: Converters, Applications and Design, 2nd Edt.", John Wiley & Sons, Inc.; New York, pp728

[32] Driga, M.D., Weldon, W.F. & Woodson, H.H. ; 1986, "Electromagnetic Induction Launchers", IEEE Trans. on Magnetics, vol. MAG-22, no. 6, pp 1453-1458

[33] Marder, B. ; 1993, "A Coil Gun Design Primer", IEEE Trans. on Magnetics, vol. 29, no. 1, pp 701-705.

[34] Angel, R. ; 2006, "Feasibility of cooling the earth with a cload of small spacecraft near the inner Lagrange point.", Proceedings of the National Academy of Sciences of the United States of America, vol. 103, no. 46, pp 17185-17189.

[35] African Capacitors (Pty) Ltd. ; 2007, "Afcap Product Catalogue", [Online; Last Accessed 12 August 2007] Available at: http://www.afcap.co.za/catalogues.asp

[36] Ledwich, G. ; 1998, "IGBTs Basics", Power Designers, LLC, [Online; Last Accessed 15 August 2007] Available at: http://www.powerdesigners.com/InfoWeb/design_center/articles/IGBTs/igbts.shtm

[37] Mitsubishi Electric ; 1999, "Mitsubishi IGBT Modules CM600HU-12F", [Online; Last Accessed 24 August 2007] Available at: http://www.mitsubishichips.com/Global

[38] Mitsubishi Electric ; 1998, "Mitsubishi High Power Semiconductors Symbology", [Online; Last Accessed 24 August 2007] Available at: http://www.mitsubishichips.com/Global/note/power.html

[39] Mohan, N. ; Underland, T.M. & Robbins, W.P. ; 1995, "Power Electronics: Converters, Applications and Design, 2nd Edt.", John Wiley & Sons, Inc. ; New York; pp 30.

[40] Semikron Semiconductors ; 2004, "Application Notes: Thermal Behaviour", [Online; Last Accessed 28 August 2007] Available at: http://www.semikron.com/internet/index.jsp?sekId=13

[41] NDT Rescource center ; 2001, "Techniques and Select Industrial Applications of Thermal Imaging", [Online; Last Accessed 29 August 2007] Available at: http://www.ndt-ed.org/EducationResources/CommunityCollege/Other%20Methods/IRT/IR_Applications.htm

[42] Mohan, N. ; Underland, T.M. & Robbins, W.P. ; 1995, "Power Electronics: Converters, Applications and Design, 2nd Edt.", John Wiley & Sons, Inc. ; New York; pp 730-737.

[43] Silvester, P. ; 1968 ; "Modern Electromagnetic Fields", Prentice Hall, Inc. London; pp 153-167

[44] Girardi, C. ; 2004, "Variometer Design", [Online; Last Accessed 02 September 2007] Available at: http://www.qsl.net/in3otd/variodes.html

[45] Abramowitz, M. & Stegun, I.A. ; 1965, "Handbook of mathematical functions", Dover Publications; New York.

[46] Mitsubishi Electric ; 1998, "Mitsubishi Semiconductors Power Modules Mos - Using IGBT Modules", [Online; Last Accessed 31 October 2007] Available at: http://www.mitsubishichips.com/Global/note/power.html

[47] Wikipeadia; 2007, "Copper", [Online; Last Accessed 01 August 2007] Available at: http://en.wikipedia.org/wiki/Copper

[48] Wikipeadia; 2007, "Polypropylene", [Online; Last Accessed 01 August 2007] Available at: http://en.wikipedia.org/wiki/Polypropylene

Appendicies

A Literature Review

Figures

Tables

A.1 Introduction to Technology

Coil gun technology has existed since the 1930's when Professor Northrup of Princeton University built the first mechanically synchronized launcher as a means of accelerating projectiles or payloads to hyper-velocities. He predicted the possibility of using these devices for launching vehicles into space [4]. However at the time due their somewhat complex modeling and operation much more attention and research was done on railgun technology instead which offered a simpler operation, that said it was only natural that railguns were developed first ahead of coilguns. Despite the research being slow there have been numerous technological leaps and insites in understanding of coilguns, particularly in the early and late 1980's. It was in 1978 when the Soviet researcher N. Bondaletov accelerated 2 gram aluminium rings to 5 km/s over a distance of 1 cm [4]. In the period following Bodaletov's achievement much research was done at Sandia Laboratories, Massachusets Institute of Technology (M.I.T) and The University of Austin Texas's Center for Electromechanics (CEM-UT) which resulted in the development of many novel methods of operation for the coilgun, described in more detail in Section A.2 on page A-5.

The current popularity in the develpoment of railguns by no means makes them superior to coilguns, infact coilguns offer the following very attractive advantages over railguns.

- No physical contact with projectile and barrels required
- Potentially zero mechanical wear
- Impressive increasing returns to scale
- Thrust acts over entire projectile length
- Up to 100 times more thrust on the projectile for a given current
- Efficiencies of well above 50%
- Possibility of modular construction
- Can be operated under open loop or closed loop control
- Launchers can be made such that the projectile fits around the launching barrel (increasing feasibility of E.T.O launchers)

Coilguns certainly do have their dissadvantages [5] (listed below), many of these can and have been overcome by the parallel technological advances in semiconductors, computers and materials manufacture.

- Fast control and electrical switching systems
- Drive coils must be switched only when the projectile is in the optimum position along the barrel

- Complex modeling and theoretical performance analysis
- Large induced voltages or back E.M.F's are produced

A.2 Methods of Operation

Although there are many different types of coilguns available each deffined by its method of operation, armature and stator coil construction, geometry and power supply all coilguns consist of a few common elements arranged in a similer circuit as shown in Figure 53 for a single stage launcher.

- Power supply
- Stator coil
- Armature or projectile
- Switching circuitry

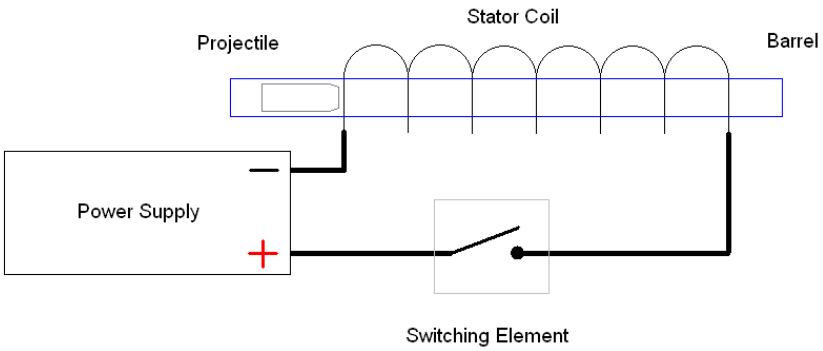

Figure 53: Basic circuit elements of a coilgun system.

This literature review will briefly review the 4 most popular (and well understood) types of launchers as listed below.

1. Reluctance launchers
2. Pulsed induction launchers
3. Travelling wave induction launchers
4. Helical (Brush Commuted) launchers

A.2.1 Reluctance Launchers

The simplest form of coilgun is the reluctance launcher operating as shown in Figure 54. The circuit used for is essentially the same as shown Figure in 53. The power supply is generally in the form of a capacitor while the projectile is in the form of a solid ferromagnetic cylinder. When the capacitor is fully charged or when the projectile reaches a suitable position in relation to the stator coil the switching element is closed thus discharging the capacitor into the stator coil. A large pulse current from the capacitor flows into the coil, creating a strong magnetic field which accelerates the ferromagnetic projectile into the coil. These devices operate on a single uni-polar current pulse supplied by polarized electrolytic capacitors. The aim is to choose a capacitor and stator coil with enough tank circuit resistance such that the LCR response is heavily damped, resulting in a uni-polar discharge pulse. Diodes are used in the circuit to prevent any oscillatory kickbacks which may still occur. If the current pulse is terminated before the projectile reaches the middle of the stator coil the projectile will exit the coil with a gain in velocity. However if the current pulse is not terminated by the time the projectile passes the middle of the stator coil, then the magnetic field will decelerate the coil, this phenomena is known as suck-back. The possibility of suck-back means that timing and the shape of the current pulse (over time) are the most important design considerations [6]. Furthermore these launchers are only capable of pulling ferromagnetic projectiles, if the projectile is a permanent magnet then it is possible that the projectile can be accelerated by pushing as well.

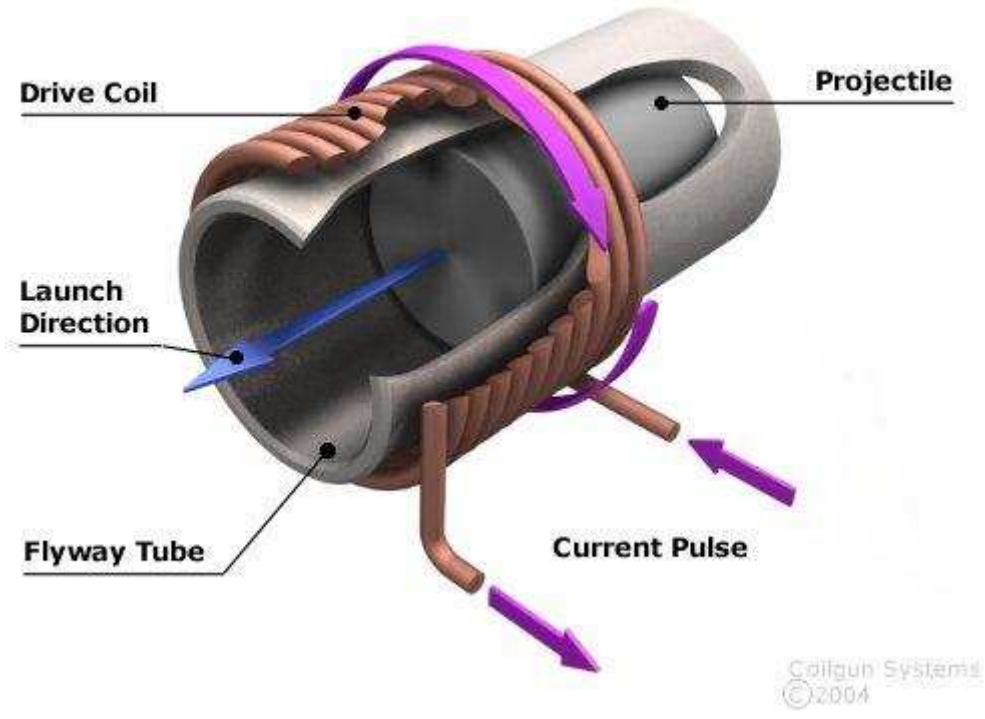

Figure 54: Illustrating the reluctance launchers operation [6].

The above explination however does not explain why it is called a reluctance gun, Figure 55 can give some insight into why this is so and shows a sectioned view through a solenoid stator coil carrying constant current (i.e. current is going into and out of page) with an iron projectile at different positions along its axis.

What happens is that the system (solenoid carrying current and the iron projectile) tries to minimize the reluctance of the path through which the lines of magnetic flux propagate. Now it is important to know that the reluctance of iron is far less than that of air, thus the mere presence of the iron projectile in the core of the solenoid decreases the reluctance experienced by the magnetic field. The field will thus pull the projectile to the center of the solenoid as shown [7].

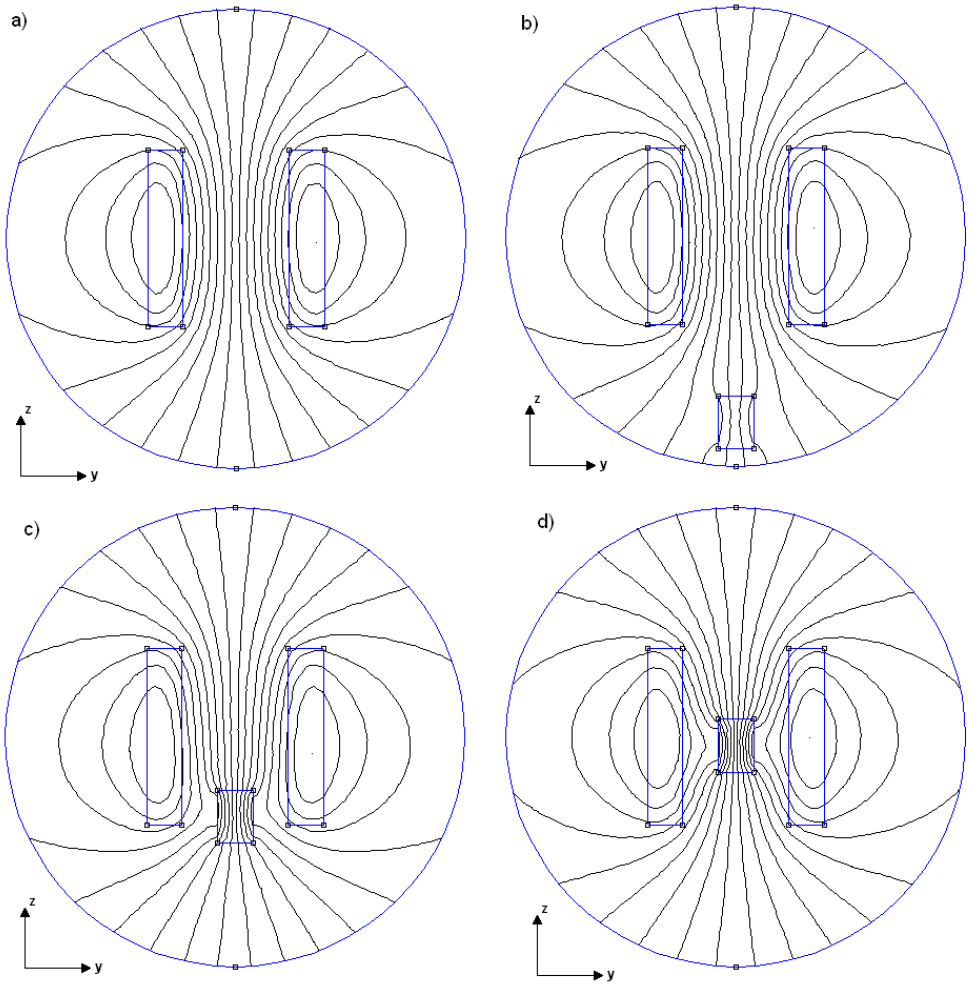

Figure 55: Section view of an air cored solenoid using FEMM software. a) No iron projectile near by; b,c,d) iron projectile moving progressively towards the center of the solenoid.

Although reluctance coilguns are the simplest type of coilgun available research on them suggests that to model them dynamically is very difficult. In addition the complexity involved in determining the force acting on a ferromagnetic projectile in a time varying magnetic field and the limiting effect of armature

saturation results in embellished use of ball park estimates in their design resulting in poor performance. Although there are many ways of optimizing the performance of these launchers through design and construction, they will always be are inherently inefficient as they operate on an over damped discharge current waveform meaning that by design much of the energy stored in the capacitor must be dissipated as heat. Never the less, the devices are very easily constructed.

A.2.2 Pulsed and Traveling Wave Induction Launchers

Induction launchers are the most promising form of coilgun technology available. Not only is their operation well understood but they also offer operating efficiencies well above 50%, this is perhaps the reason for most coilgun research using using this operation concept. Despite the research and understanding of these devices there is very little information on their synthesis or "step by step" design and development procedure.

> "Design clearly invovles highly complex trade-offs, as does the design of violins" [4].

The stator coils are typicaly in the form of wound coils, while the armatures are made of a conducting non magnetic material such as copper or aluminium, and can be in the form of either a wire would coil shorted on itself, single turn ring or even a solid cylinder. The tank circuit involved is similar to that shown in Figure 53 on page A-5, however the stator coils can be powered by either capacitors as described in Appendix A.2.2.1 on page A-12 or a 3 phase power supply as described in Appendix A.2.2.2 on page A-14. Both devices rely on two fundamental laws namely

- Faraday's Law of Induction

  States that the induced E.M.F in a closed current loop is proportional to the negative of the rate of change of magnetic flux through the loop [8]. When applied to an inductor coil the formula becomes

  $$\varepsilon = -N\frac{d\Phi}{dt}$$

  the negative in the above formula was first given by Lenz's Law. In the case of two coaxial coils as found in am induction based coilgun, the changing magnetic flux $\frac{d\Phi}{dt}$ is produced by the current waveform flowing in the stator coil and induces a voltage and thus a current flow in the shorted in the armature coil. This is known as *mutual inductance* and is the principle of operation found in a transformer.

- Lorentz Force Law

  The actual force responsible for accelerating the armature is a result of this law, which states that a charged particle moving in an electromagnetic field will experience a force proportional to amount

of charge on the particle, the strength of the electric and magnetic fields and the speed at which the particle moves. The force is perpendicular to both the direction of particle movement and direction of the magnetic field [9].This is illustrated in Figure 56 while the formula describing this law is given below

$$F = q\,(E + v \times B)$$

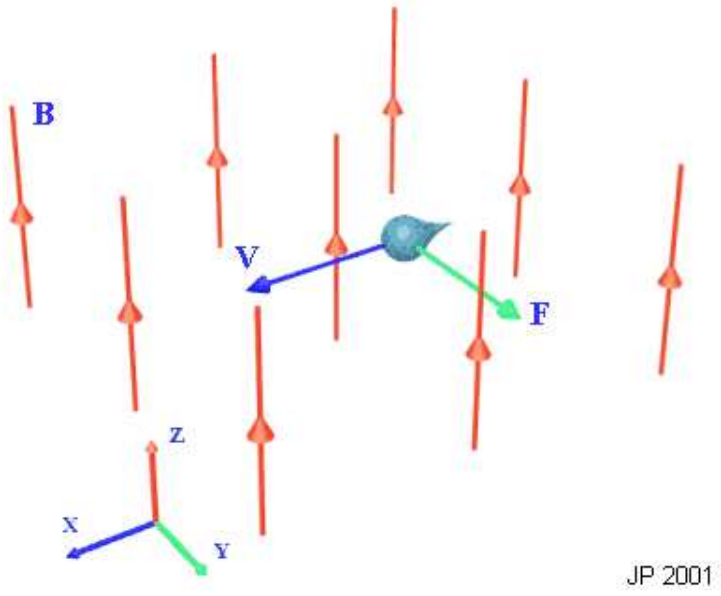

Figure 56: Figure illustrating the LORENZE FORCE LAW, it is important to note that this figure describes the force on a charged particle in the absence of an electric field E [10].

Combining these two laws the basic principle of operation of an induction launchers is easily understood. Figure 57 shows two coils, one connected to a power supply and one the other shorted on itself (representing the stator and armature coils respectively). The current waveform flowing in the stator coil creates a time varying radial and axial magnetic fields B_z and B_x or $B_y$respectively . The magnetic field B_z which has an associated magnetic flux going through the armature coil in turn induces a voltage in the armature coil as predicted by FARADAY'S LAW OF INDUCTION and thus current flow (since the armature is shorted) which is opposite in direction to the stator coil current. These opposing currents flowing in the stator and armature coils will result in the two coils repelling each other as predicted by the LORENTZ FORCE LAW specifically applied to current carrying conductors in nearby proximity. Conceptually this is also visualized as the interaction between the radial magnetic field in the stator and the tangential/circumferential current in the armature, creating a force perpendicular to both aforementioned quantities producing a forward acceleration on the armature.

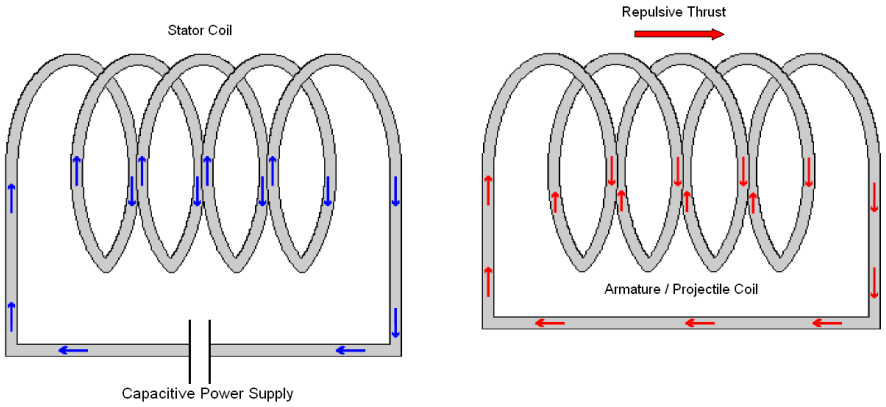

Figure 57: Illustrating the principle of operation of an induction based coilgun.

The design of the armatures used in these devices is crucial to their functioning. As mentioned earlier the armatures can be either simply a solid cylinder or ring made of a conducting material or better still a wire wound coil shorted on itself. The implications of using the above types are armature is discussed in more detail in Appendix on page A-32. Shown in Figure A-10 below is a section through an induction coilgun operating with a solid armature, the similarity between the induction launcher and reluctance launcher is clearly quite obvious.

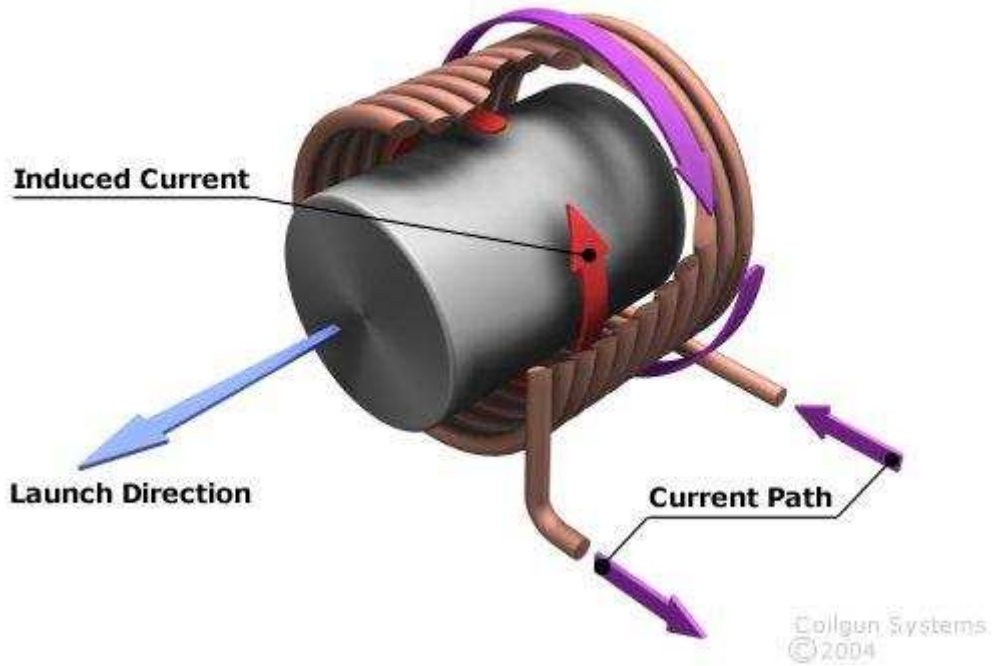

Figure 58: Illustrating the induction launchers operation [11].

A more exact analysis of operation for these guns can be found in Appendix on page A-17. These coil launcher types are highly complex machines but they do offer a much more accurate process of dynamic

performance analysis compared to modeling of reluctance launchers, taking into account the effect the two coils have on each other as they approach. This makes them a very attractive launcher type in addition to their higher operating efficiencies when compared conventional reluctance based coilguns.

A.2.2.1 Pulsed Induction Launchers

The defining attribute of these launchers is that they are driven by a decaying oscillatory current pulse in the stator coils. The source of such a current pulse is normally a capacitor discharging itself through the stator coil. These devices often consist of several stator coils, each one representing an acceleration stage. The coils are energized with a certain time sequence so as to generate a traveling electromagnetic wave that interacts with the currents induced in the in the armature and thus accelerating it [12]. A multistage capacitor driven induction launcher is schematically shown in Figure 59 below. The armature moving down the barrel an at increasing velocity after each passing stage means that the energy transferred to the armature in the latter stages must happen quicker than it did in the preceding stages.

It is also clearly observed that the capacitor and stator coil inductor in the tank circuit form a common LC circuit resulting in a typically oscillatory discharge current wave form during stator coil excitation. Manipulation of the tank circuit elements allows this waveforms frequency to be varied. With the optimum frequency of this waveform being related to the transit time of the armature between two alternate stator coils [13] and wire skin-effect considerations.

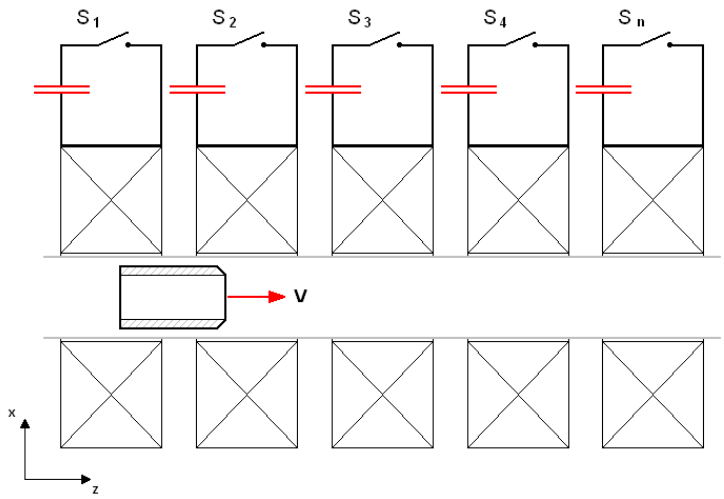

Figure 59: Simplified schematic of an n-stage induction launcher. S_1- S_n representing each individual stator coils "trigger switch" to be fired at specific intervals based on the projectiles passage through the barrel.

Noting that the capacitors store only a fraction of the energy transferred to the projectile, the ability to use the remaining energy in a prior stage capacitor to help the following stages capacitor drive its associated stator coil will make efficiencies above 90% very possible [4]. One such novel methode has already been described in the literature [13] and the schematic for this is shown in Figure 60 below.

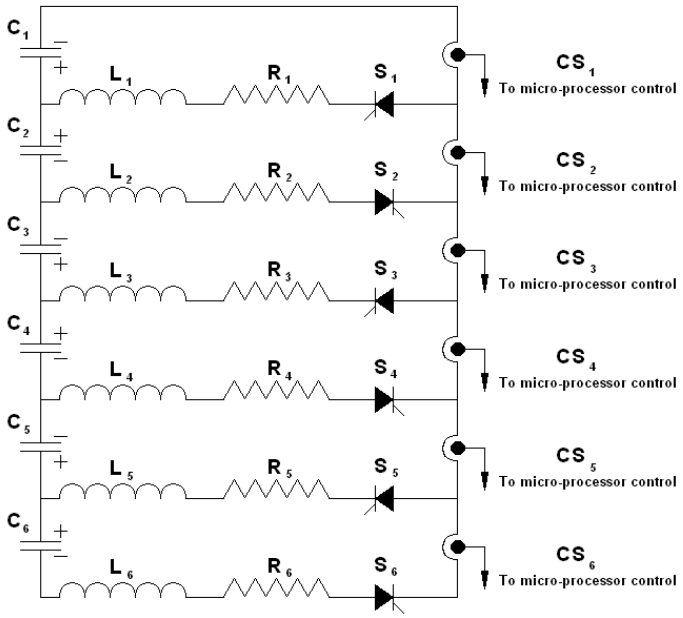

Figure 60: Schematic of a 6 Stage launcher circuit that allows "energy recovery" [13].

The inductances L_1-L_6 represent the equivalent barrel coils, while values for resistors R_1-R_6 are chosen such that the energy dissipated by each is equal to the sum of the kinetic energy and resistive losses of each section. S_1-S_6 and CS_1-CS_6 are trigger switches and HALL EFFECT current sensors respectively. All capacitors C_1-C_2 are charged to the same initial voltage, but cascade connected. Consider when $S_1$is closed at time t_0 an energy equivalent to the kinetic energy transferred to the armature is dissipated by resistor R_1, the left over energy in the inductor reverses the charge across the capacitor C_1 as shown in Figure 61 below.

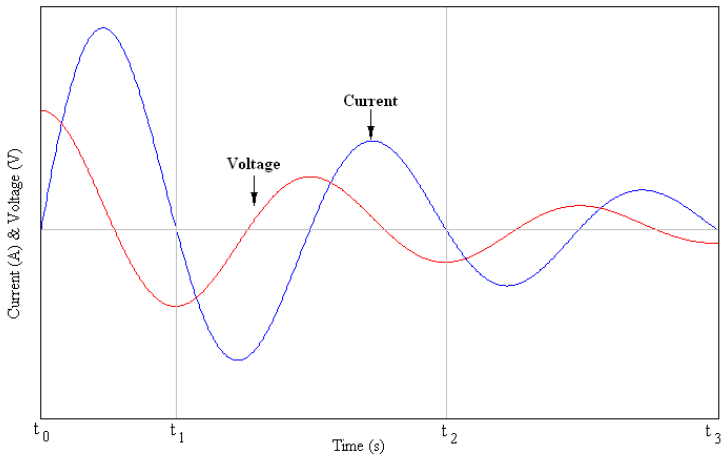

Figure 61: Typical oscillatory and voltage current waveforms in the stator coil circuit. Note the phase difference between the two.

At time = t_1 the instant of zero current crossing, switch S_1 opens and switch S_2 closes. This connects the two capacitors $C_1$and C_2 in series, generating a higher initial voltage for stage 2 and increasing the oscillation frequency (Capacitors in series decreases bank capacitance resulting in a higher tank circuit oscillation frequency). This switching process continues until all stator coils have been energized. The entire system can be controlled using a single microprocessor for both current measurement and circuit switching. Obviously in practice linear induction launchers require more than one current cycle to achieve for effective acceleration of the stator coil the microprocessor can easily be setup so that it only toggles switches S_1 & S_2 at a later 0 current crossings, for example at time = t_2 & time = t_3

This method can also be adapted to operate on Reluctance launchers and will also eliminate the problem of *suck-back* because each stage is turned off at the instant of zero current crossing.

A.2.2.2 Traveling Wave Induction Launchers

This type of induction launcher is very similar in its fundamental operation to the pulsed induction launcher described above it differs however in that the device operates with each of its stator coils driven by a continuous oscillating sinusoidal current. Similarly though like the pulsed induction launcher the latter stages operate with at higher frequency to compensate for the projectile moving faster. Like an A.C. induction motor, they can also be operated by poly-phase currents. The stator coils themselves are not single coils but rather multiple coils wound into one stator coil stage, this shown in Figure below 62 for a 3-phase (A, B,C) oscillating power supply. The oscillating 3 phase currents creates a sinusoidal varying magnetic field, one for each winding on the stator coil, which when summed results in a traveling magnetic wave moving in the z axis with velocity v_s, proportional to the power supply frequency f and the pole pitch Θ, given by

$$v_s = 2f\Theta$$

It is this magnetic field, that interacts with the armature coil inducing a current in the armature that is repelled by the current in the stator coil.

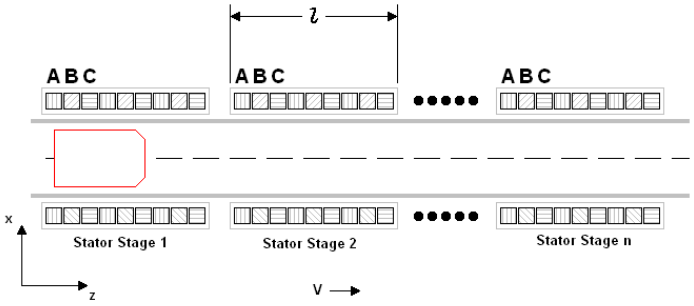

Figure 62: Modular n-stage 3 phase linear induction launcher coil configuration [13].

As long as there is a difference in speed between the traveling magnetic wave velocity v_s and the projectile velocity v_z an azimuthal current will be induced in the armature. This difference in speed is known as the slip velocity, and along as some slip velocity exists the armature will experience a time rate of change in magnetic flux through it, thus inducing the azimuthal current in the armature. Resulting in a force on the projectile as desribed at the start of this Section on page A-8. The projectile will thus try to follow the traveling magnetic wave, much similar to an asynchronous A.C. induction motor. If the slip speed was 0 $m.s^{-1}$and the armature was moving at the same speed as the magnetic field, the armature will then experience no change in flux over time and thus no azimuthal currents will be induced. The armature will cease accelerating and maintain a velocity very close to the traveling wave velocity.

The excitation currents may be generated by rotating generators or capacitors, where each stator coil must go through one or more cycles of voltage and current oscillations as the armature passes through it.

A.2.3 Helical (Brush Commuted) Launchers

These coilguns operate on common principle used in the induction type launchers, namely the Lorentz Force Law, they differ only in that the armature coils are not excited through induction, but rather through direct connection to a D.C supply source through contact brushes that are in sliding contact with two trailing feed wires of the armature coil, similar to what is shown in Figure 63.

It is also possible to excite both stator and armature coils with the same power supply provided that the armature coil is connected in serries with the stator coil through the brushes and that the armature coil be aranged so that the currents flowing through the armature and stator coil flow in opposite directions, thus producing a repulsive force [18]. An example of such a launcher is illustrated in Figure 63 below.

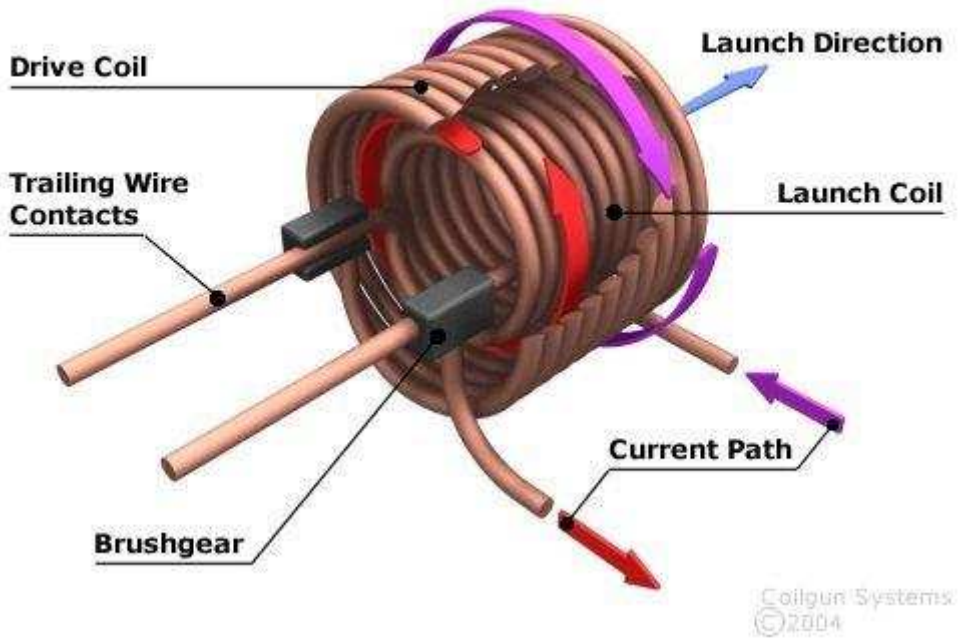

Figure 63: Illustrating the helical launchers operation [18].

Exciting the armature coil through sliding brushes has the great advantage in that it the launcher can both attract and repel the armature thus getting more acceleration for a given cycle or stator coil stage, but it also presents some interesting design and construction challenges for both the stator and armature coils and the entire launcher barrel. Furthermore in large scale applications, where very high velocities are obtained, the brushes fail due to mechanical wear [4].

A.3 Applications of Technology

The variety of advantages co-axial linear induction launchers offer over rail guns (Discussed A A.1) lends the technology to many various applications. Already many L.I.Ms outperform certain existing devices like steam catapults, heavy military artillery while also providing a practical means for scientists and engineers to accelerate materials to hyper velocity for mechanics research. Furthermore a unique advantage of co-axial L.I.M is the ability to accelerate a projectile located outside the drive coil or barrel, thus permitting the launching of large vehicles such as spacecraft which surround the drive [4]. In fact the most popular application of this technology is for Earth to Orbit launching of spacecraft and satellites, this is feasibly possible because of the increasing returns to performance the linear induction motors enjoy when their size is increased. In nearly all of the literature regarding the subject, the simulation codes successfully used to predict the performance of a laboratory scale launcher have been used to pinpoint concept designs for high efficiency, high velocity E.T.O launchers [33].

A recent application for the technology has been proposed, if it ever became apparent that catastrophic climate changes due global warming were inevitable and drastic emergency methods would be needed to cool the earth. The low E.T.O launching cost of this technology (estimated at 50 U.S Dollars per Kilogram) would be used to launch numerous small lightweight optical refracting screens with low reflectivity into space, in an attempt reduce the total amount heating energy the earth receives from the sun [34].

A.4 Theoretical Analysis and Modeling

The problem of designing a working and efficient or "optimized" coilgun is made difficult because of the high degree of interrelation between the variables involved. For example, the force acting on the projectile is a function of the currents flowing through the coils, which is (at least) a function of the mutual induction between the armature and stator coils. The mutual induction is a function of the axial distance/seperation between the coils, which is a function of the projectiles velocity which itself is a function of the acceleration of the armature which finally is proportional to the force acting on the armature, which is where this analogy began. To complicate matters further the systems dynamic nature means most of these variables are themselves time varying.

Despite all this, the basic operation is fairly well understood and there are many methods in the literature which provide engineers with simple equations that give good approximations to all the variables involved [14]. Using differential equations almost every variable of the system can be modeled and theoretically determined for a specified launcher system, time period, and initial conditions using a modern day desktop computer. The following Section will explain and outline a basic analysis method which can be used predict the performance of a pulsed linear induction motor. The computer simulation program which is used to develop the laboratory scale pulsed linear induction motor is be based on the theory presented here.

A.4.1 Lumped Parameter Circuit and the Current Fillament Method

The currents induced in the armature coil are assumed to flow in circumferential paths on the outer skin on the armature, this current flow and its distribution will for simplicity be assumed to be uniform although in practice with solid ring type armatures this is not true. The armature is thus conceptually (or physically) divided into a set of conducting rings, each with its own approximatly uniform current density and equivelend circuit similar to the stator coil [15].

The launcher shown in Figure 64 below can thus be modeled using the equivalent circuit shown in Figure 65 which follows.

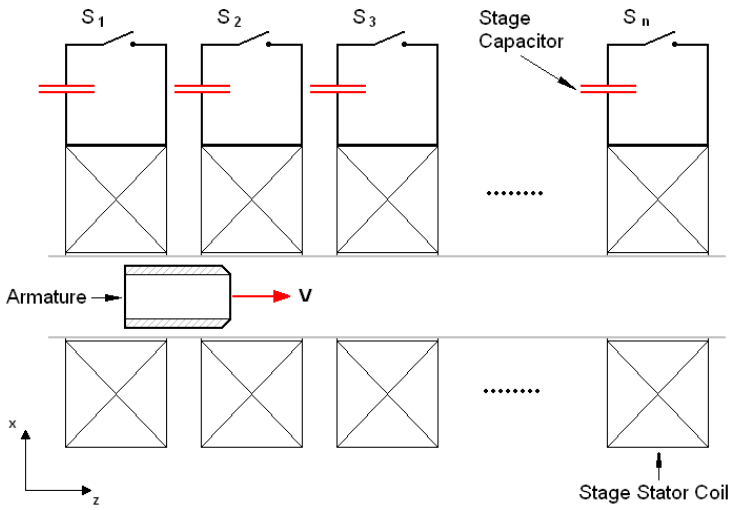

Figure 64: Generic multistage capacitor driven induction launcher.

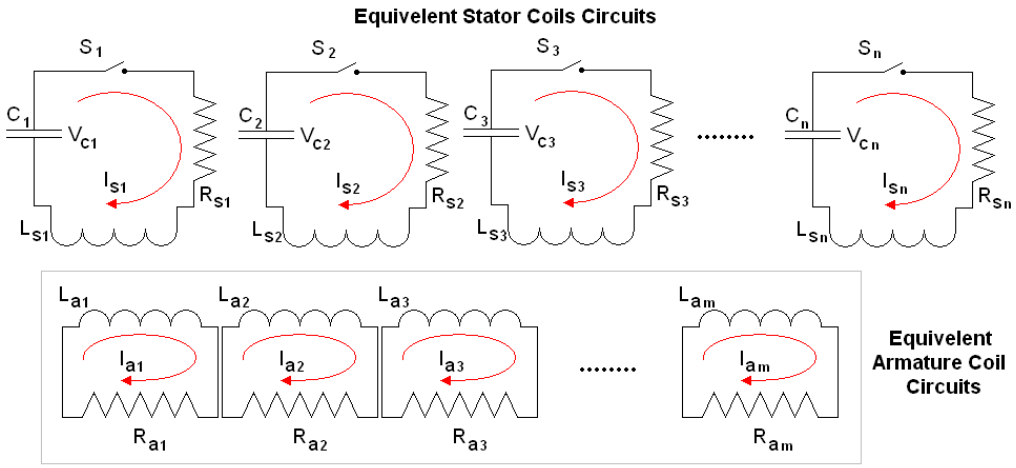

Figure 65: Equivalent Lumped Parameter circuit model of the capacitor driven coil launcher [12].

The number of stator coils in the equivalent circuit depends on the performance specifications (for example: muzzle velocity, weight of the projectile and barrel length), while the number of armature coils depends on accuracy required for the analysis in the case of a solid ring type armature where the current distribution is not uniform along the armatures length. For convention we denote n stator coil stages. Assuming a wound helical stator coil which forces the current distribution to be uniform, using KIRCHOFF'S VOLTAGE LAW applied to a single stator coil stage and armature coil we develop two coupled ordinary differential equations that govern the stator and armature currents [16].

$$V_s = I_s R_s + L_{ss}\frac{dI_s}{dt} + M_{sa}\frac{dI_a}{dt} + I_a\left(\frac{ds_z}{dt} \times \frac{dM_{sa}}{dz}\right)$$

$$0 = I_a R_a + L_{aa}\frac{dI_a}{dt} + M_{as}\frac{dI_s}{dt} + I_s\left(\frac{ds_z}{dt} \times \frac{dM_{as}}{dz}\right)$$

Where $\frac{ds_z}{dt}$ is the velocity v_s, of the armature coil relative to the stationary stator coil. If an additional armature coil division was use to model a non-uniform current distribution (Found in conducting solid or ring armatures.) then there would be an additional differential equation corresponding to that equivalent coil, thus greatly increasing computational complexity.

The magnetic energy stored in the system (stator and armature coils) is given as

$$E_{magnetic} = \frac{1}{2}L_{ss}I_{ss}^2 + \frac{1}{2}L_{aa}I_{aa}^2 + MI_{ss}I_{aa}$$

Note that the variable M represents the mutual inductance of the coil pair is a function of z or axial separation of the coils. The instantaneous force F_z on the armature required to cause a displacement dz in the z direction is therefore given as

$$F_z(t) = \frac{dE_{magnetic}}{dz} = I_a(t)\, I_s(t)\, \frac{dM}{dz}$$

NEWTON'S 3RD LAW then becomes the third differential equation relating the armatures velocity to the accelerating force F_z [17].

$$m_a\frac{dv_z}{dt} = F_z = I_s(t)\, I_a(t)\, \frac{dM}{dz}$$

Note that the voltage sum in armature coil is equal to zero because the armature is shorted on itself. The above coupled equations are somewhat readily solved using a suitable numerical method (Runge Kutta etc) subject to a voltage waveform and a set of initial conditions. All temperature rises are calculated assuming that the ohmic losses are dissipated adiabatically in the windings, which is true for micro second events [16].

Fortunatly the self inductances $L_{ss}$and L_{aa} are constant during the operation of the launcher unlike the mutual inductance M and the mutual inductance gradient $\frac{dM}{dz}$ which are functions of elliptic integrals and are readily calculated as functions of stator and armature coil geometry and separation. Their evalution is discussed in detail in Appendix A.4.2 on page A-20.

The above equations thus provide a rough estimation of the most important performance parameters over time (i.e. coil currents, acceleration, velocity, position and losses) which can be used to determine more

complex performance parameters such as the thermal and mechanical stresses in the stator and armature coils, which may or may not be important. The coil separation is easily determined by the numerical integration of acceleration with respect to time as shown below

$$s_z(t) = s_{z_0} + \int_{t_0}^{t} v_z \, dt$$

A.4.2 Self Inductance, Mutual Inductance and the Mutual Inductance Gradient

As shown in the section prior to this, the axial force F_z on the armature is greatly dependant on the mutual inductance gradient $\frac{dM}{dz}$ between armature and stator coils. Figure 66 below shows the mutual inductance and its gradient as a function of armature and stator coil seperation. The mutual inductance gradient has two humps, anti-symmetrical with respect to the drive coil reflecting the fact that the force on the armature will be reversed as the coil crosses the mid-plane of the stator coil, furthermore the implication of zero mutual inductance gradient at the mid-plane of the stator coils is that there will be zero force on the armature at this position. Also noted is that the mutual inductance is at its maximum when the two coils are co-planar, while the mutual inductance gradient has its maximum at the inflection point of the mutual inductance function. The distance from the center of the stator coil to axial positions where the mutual inductance gradient is at its maximum (or minimum) is called the induction length, which is always less than or equal to the stator coil radius [4]. The inductance length effects the optimum positioning and available axial length wherein which effective acceleration of the armature is achieved, for a given set of coils.

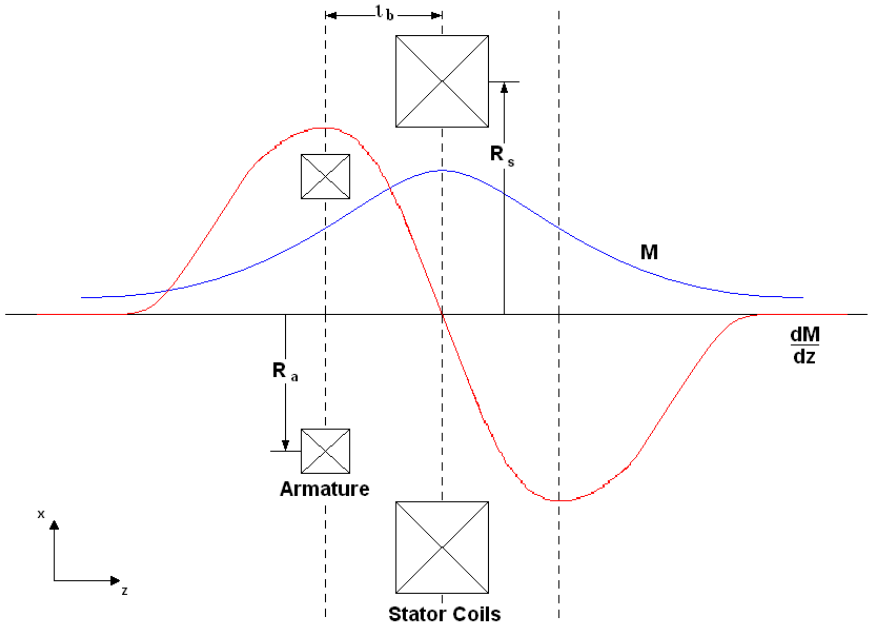

Figure 66: Showing the mutual inductance M, its gradient $\frac{dM}{dz}$and the inductance length as a function of coil separation [4].

Each coil self inductances L_{ss} and L_{aa} their mutual inductance M and its gradient G are readily calculated using an method where a given coil is divided into equivalent conducting hoops as shown in Figure 67 below. For two conducting hoops or *filaments* (as shown in Figure 68 below) the mutual inductance M and mutual inductance gradient $\frac{dM}{dz}$ are calculated as a function of coil separation z and coil radi r_i & r_j [15]. This elementary approach is better known as LYLE'S METHOD OF CALCULATING MUTUAL INDUCTANCE.

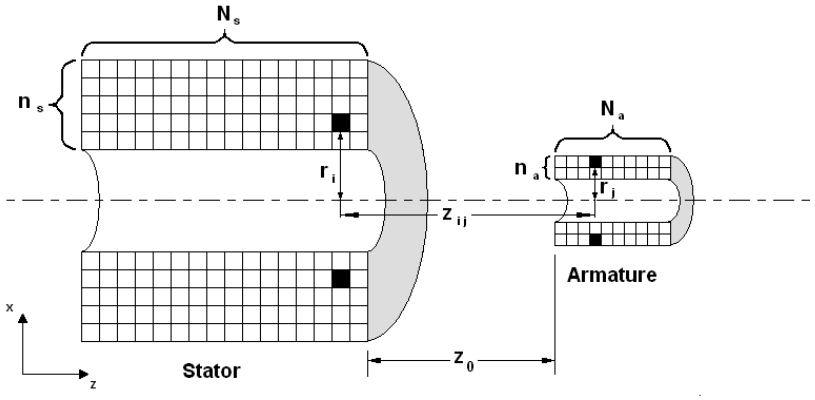

Figure 67: Division of real coils into an array of filamentary coils [15].

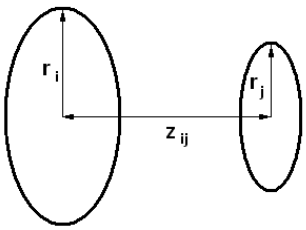

Figure 68: Diagram for filamentary inductance formula [15].

The mutual inductance for two coil filaments separated a distance z as shown above in Figure 68 is given by the relation below as derived by Silvester [43, 20].

$$m_{ij} = \mu_0 \sqrt{r_i r_j} \left\{ \left(\frac{2}{k} - k \right) K(k) - \frac{2}{k} E(k) \right\}$$

$$k = \sqrt{\frac{4 r_i r_j}{z^2 + (r_i + r_j)^2}}$$

where $K(k)$ and $E(k)$ are complete elliptic integrals of the first and second kind, the partial derivative of m, $\frac{\delta m}{\delta z}$ is readily taken to determine the gradient.

$$\frac{\delta m_{ij}}{\delta z} = \frac{\mu_0 k \times z}{4\left(1-k^2\right)\sqrt{r_i r_j}}\left\{2\left(1-k^2\right)K(k) - \left(2-k^2\right)E(k)\right\}$$

A.4.2.1 Mutual Inductance and Mutual Inductance Gradient

The above analysis readily allows the elemental inductance parameters for two elemental hoops to be calculated. However what is needed is the inductance parameters for the entire armature and stator coils, thus each elemental mutual inductance and mutual inductance gradient contribution must be summed up to determine the total mutual inductance and mutual inductance gradient for the two specified coils at a given axial separation.

Working with the general arrangement shown in Figure 69, where the stator and armature coils have N_s and N_a turns respectively. The cross sectional area of the coil is divided N_s and N_a axial elements and n_s and n_a radial elements as shown. The mutual inductance between an i$^{\text{th}}$ element in the stator and the j$^{\text{th}}$ element in the armature is given by

$$\Delta M_{sa} = \frac{N_s N_a}{(N_s \times n_s)(N_a \times n_a)} m_{ij}$$

The mutual inductance between the stator and armature is thus given by the average of the sum of all mutual inductances between all pairs of filamentary coils multiplied by the turns product as shown below.

$$M_{sa} = \sum_{i=1}^{N_s \times n_s} \sum_{j=1}^{N_a \times n_a} \Delta M_{sa} = \frac{N_S N_a}{(Ns \times n_1)(Ns \times n_2)} \sum_{i=1}^{N_s \times n_s} \sum_{j=1}^{N_a \times n_a} m_{ij}$$

Similarly the inductance gradient is given as

$$\frac{dM_{sa}}{dz} = \sum_{i=1}^{N_s \times n_s} \sum_{j=1}^{N_a \times n_a} \Delta M_{sa} = \frac{N_S N_a}{(Ns \times n_s)(Ns \times n_a)} \sum_{i=1}^{N_s \times n_s} \sum_{j=1}^{N_a \times n_a} \frac{\delta m_{ij}}{\delta z}$$

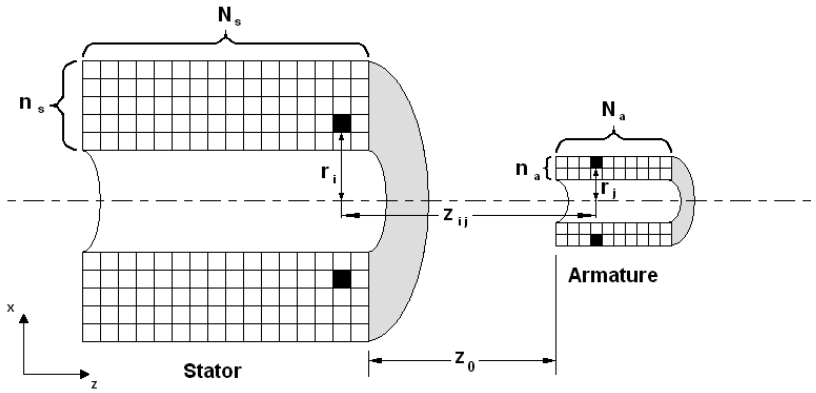

Figure 69: Section through coils illustrating the division of real coils into of filamentry elements or coils [15].

A.4.2.2 Self Inductances

Continuing with the general arrangement shown in Figure 69 the self inductance of each coil is calculated using Grover's expression for the inductance of a single turn circular coil of square cross section given below for the stator coil, calculation of the armature coil self inductance is done in a similar manner [15, 20].

$$L_{ss} = \left(\frac{N_S}{N_s \times n_s}\right)^2 \left\{ 2 \sum_{i=1}^{(N_s \times n_s - 1)} \sum_{i=1}^{n_s} m_{ij} + \sum_{i=1}^{n_s} l_i \right\}$$

where according to Grover

$$l_i = \frac{\mu_0}{2} \left\{ \left(1 + \frac{\zeta_i}{6}\right) \ln \frac{8}{\zeta_i} + 0.2041\zeta_i - 0.84834\zeta_i \right\}$$

with $\zeta_i = \left(\frac{c_i}{2a_i}\right)$ where c_i and a_i are the mean diameter and side length respectively for the i$^{\text{th}}$element.

As shown in Appendix A.4.1 on page A-17 the operation of an induction launcher is greatly dependant on these inductance values and how they change over time and axial displacement. The above method presents a useful and powerful tool which is most necessary in determining a given launchers theoretical performance. The inductance values can be can be pre-calculated and stored into an array for interpolation during the numerical simulation which is discussed in more detail in the section following.

A.4.3 Time Step Numerical Solution and Computer Simulation

The equations discussed in Appendix A.4.1 on page A-17 are differential equations and to have any practical meaning must be solved using a suitable numerical method to provide the designer with detailed theoretical information regarding a specified launchers operation. These calculations and the aforementioned inductance analysis discussed in Section A.4.2 on page A-20 require numerous calculations to be made for each step in coil position and time. Doing this by hand to any degree of accuracy is highly improbable. The availability of modern day desktop computers however gives the designer a powerful tool capable of carrying out the necessary inductance calculations and simulations.

It is should be noted that in the following equations the mutual inductance $[M]$ and its gradient $[G]$ are functions of armature and stator separation and not time. These parameters are however a function of coil geometries alone (e.g. median coil diameters, diameter ratio, coil separation and winding lengths etc..) and for a given launcher simulation design must be pre-calculated for all possible armature positions

before the the time step simulation can executed (based on the equations of Appendix A.4.1 on page A-17) to determine a given launchers performance.

The differential equations of Appendix A.4.1 on page A-17, arranged into a matrix form allow for convenient expression and manipulation when solving the time step numerical problem and is shown below [17].

$$[V] = [L] \cdot [\dot{I}] - [M] \cdot [\dot{I}] + [R] \cdot [I] - v \times [G] \cdot [I]$$

where

$[V] = \begin{bmatrix} V_s \\ 0 \end{bmatrix}$ Coil Voltage Matrix

$[L] = \begin{bmatrix} L_{ss} & 0 \\ 0 & L_{aa} \end{bmatrix}$ Self Inductance Matrix

$[M] = \begin{bmatrix} 0 & M_{sa} \\ M_{as} & 0 \end{bmatrix}$ Mutual Inductance Matrix

$[G] = \begin{bmatrix} 0 & \frac{dM_{sa}}{dz} \\ \frac{dM_{as}}{dz} & 0 \end{bmatrix}$ Mutual Inductance Gradient Matrix

$[R] = \begin{bmatrix} R_{ss} & 0 \\ 0 & R_{aa} \end{bmatrix}$ Resistance Matrix

$[I] = \begin{bmatrix} I_s \\ I_a \end{bmatrix}$ Coil Current Matrix

$[\dot{I}] = \begin{bmatrix} \dot{I}_s \\ \dot{I}_a \end{bmatrix}$ Rate of Coil Current Change Matrix

Placing all the differential terms on the left hand side and solving for the differential current matrix (through the inverse of the $[[L] - [M]]$matrix) we find

$$[[L] + [M]]\,[\dot{I}] = [V] - [R] \cdot [I] - v_z \times [G] \cdot [I]$$

$$[\dot{I}] = [[L] + [M]]^{-1} \cdot [[V] - [R] \cdot [I] - v_z \times [G] \cdot [I]]$$

Using a subscript notation for a time step procedure

$$\dot{[I]}_{t+1} = [[L]_t + [M]_t]^{-1} \cdot [[V]_t - [R] \cdot [I]_t - v_{zt} \times [G]_t \cdot [I]_t]$$

With the initial condition given by setting $[I]_0 = 0$, $[V]_0 = \begin{bmatrix} V_{initial} \\ 0 \end{bmatrix}$ and $v_{z0} = 0$

$$[\dot{I}]_0 = [[L]_0 - [M]_0]^{-1} \cdot [V]_0$$

Thus $[I]_1 = [I]_0 + \triangle t \cdot [\dot{I}]_0 = \triangle t \cdot [\dot{I}]_0$, thereafter the solution for the current matrix is generally given as

$$[I]_{t+1} = [I]_t + \triangle t \cdot_t [\dot{I}]$$

Solving the stator and armature coils currents is important because the force acting on the armature (and thus the acceleration) is greatly dependant of the product of these currents as shown in Appendix A.4.1 on page A-17.

The force acting on the armature at a given time t is thus given as

$$F_{z\,@\,(t+1)} = Transpose([I]_{t+1}) \cdot [G]_{t+1} \cdot [I]_{t+1}$$

The armature acceleration is obtained directly by diving by the armature mass

$$a_{z\,@\,(t+1)} = \frac{F_{z\,@\,(t+1)}}{m_a}$$

The armature velocity v_z and displacement s_z is then determined through a numerical integration of the acelleration and velocity respectively, hence the need to only solve for the coil currents. The accuracy of this solution is obviously governed by the magnitude of the time step $\triangle t$ used and the positional accuracy to which the mutual inductance $[M]$ and its gradient $[G]$ matrices are solved.

$$v_{z\,@\,(t+1)} = v_t + \triangle t \cdot a_{z\,@\,(t+1)}$$

$$s_{z\,@\,(t+1)} = s_{z\,@\,(t+1)} + \triangle t \cdot v_{z\,@\,(t+1)}$$

The time step simulation for an induction launcher thus reduces to the following algorithm [17].

1. Specify coil geometries.

2. Calculate all inductance parameters for the launcher.

   Namely the self inductance $[L]$, mutual inductance $[M]$ and its gradient $[G]$.

3. Specify or calculate all initial values involved.

   E.g. Initial voltage, current, velocity and armature position etc...

4. Begin time step simulation.

5. Calculate both coil currents using the equivalent circuit model.

6. Calculate new acceleration, velocity and displacement.

7. Store instantaneous results.

8. Interpolate new inductance parameters from data simulation in Step 2 (Change in coil separation results in a change in $[M]$ and $[G]$).

9. Return to Step 5, incrementing the problem time by $\triangle t$.

10. Continue the simulation for desired problem time.

It would seem remarkable that the many dynamic variables of such a complex system are so easily solved. While providing a powerful and useful design analysis tool, the above simulations will only yield a result as good as defined by how closely the input system parameters match those for an "optimum" solution. The design problem now becomes one of optimization and finding a set of input variables that will result in a launcher design that meets a given specification which may be based on operating efficiency, length, physical size or even thermal limits of the material used to wind the coils themselves.

A.4.4 Energy Balance

To critically asses the performance of a launcher system it is necessary to consider the energy balance of the device determine to better understand how it uses the initial energy provided by the capacitor over time. This will help to achieve more successful launcher designs. The energy balance typically includes the following terms

- Electric energy stored in the capacitor bank
- Magnetic energy stored in the coils
- The kinetic energy gained by the projectile
- Ohmic losses due to the stator and armature coil resistances

The goal being to ensure that the maximum amount of electric energy stored in the capacitor is transferred to the armature as kinetic energy thus maximizing system efficiency. Multiplying the matrix voltage equations of Section A.4.3 on page A-23 by the current $[I]^T$ the power balance of the system is derived.

$$[I]^T [\cdot V] = [I]^T \cdot [[L] - [M]] \cdot [\dot{I}] + [I]^T \cdot [R] \cdot [I] - [I]^T \cdot v_z \times [G] \cdot [I]$$

The instantaneous energy balance is derived through integration of the terms in the power balance with respect to time [12] to obtain the relationship below

$$E(t)_{capcitor} = E(t)_{magnetic} + E(t)_{ohm} + E(t)_{work}$$

where the instantaneous system energies are given as

$E(t)_{capacitor} = \frac{1}{2} C V_{initial}^2 - \int_0^t [I]^T [\cdot V]\, dt$

$E(t)_{magnetic} = \frac{1}{2} \int_0^t [I]^T \cdot [[L] + [M]] \cdot [\dot{I}] dt = \frac{1}{2} [I]^T \cdot [[L] + [M]] \cdot [I]$

$E(t)_{ohm} = \int_0^t [I]^T \cdot [R] \cdot [I]\, dt$

$E(t)_{work} = \frac{1}{2} \int_0^t [I]^T \cdot v \cdot [G] \cdot [I]\, dt = \frac{1}{2} \int_0^l [I]^T \cdot [G] \cdot [I]\, dx$

A.4.5 Armature/Stator Heating and Ohmic Loss

The total ohmic loss of the system E_{ohm} is the sum of the ohmic losses in the stator coil, armature coil and to some extent (but not discussed here) the heating of the capacitor (ESR) losses as shown below.

$$E_{ohm} = E_{ohmstator} + E_{ohmarmature}$$

where

$$E_{ohmstator} = \int_0^{t_f} R_{ss} \cdot I_s^2 dt$$

$$E_{ohmarmature} = \int_0^{t_f} R_{aa} \cdot I_a^2 dt$$

Where R_{ss} and R_{aa} are the stator and armature coil resistances whos calculation is based on the specified coil geometry and wire resistivity. The calculation of R_{ss} and R_{aa} can be found in Appendix B.3.4 on page B-11

For short millisecond events the heating processes can be assumed to be adiabatic, in that all the heat energy lost is directly absorbed into the armature and stator coils thus raising their temperature as given below for both armature and stator coils [16, 12], asuming enameled copper winding wire is used.

$$\triangle T_{stator} = \frac{E_{ohmstator}}{c_{p;Copper} \cdot m_s}$$

$$\triangle T_{armature} = \frac{E_{ohmarmature}}{c_{p;Copper} \cdot m_a}$$

A.4.6 Mechanical Stress

During operation the armature and stator coils of a co-axial linear induction motor (operating in push mode) will experience a crushing and expanding pressure respectively. This pressure is a result of the current in each coil's windings interacting with the net axial magnetic field B_z resulting in a radial force acting on the armature or stator coils as predicted by LORENTZ FORCE LAW. If the induction motor were operating in a pull mode the opposite will be true and the stator coil experience a compressive radial force while the armature will experience the expansive force [1]. This section considers push mode operation only.

For a given coil carrying a current I of N turns and length l, its axial magnetic field strength can be approximated as $B_z \approx \mu_0 \frac{NI}{l}$. The crushing or expansion force can now be approximated as a magnetic pressure $p_{magnetic} = \frac{B_z^2}{2 \cdot \mu_0}$ [16, 23]. If an annular internal support structure is to be used for the armature then the maximum compressive hoop stress in the support structure will occur at the structures inner radius and is modeled using Roark Table 31, case 1c [1, 24] as shown below.

$$\sigma_{haa} = \frac{-2 \cdot b^2 \cdot p_{magnetic}}{b^2 - d^2}$$

Where b and d are the armature coil inner radius and the coil form inner radius respectively. However for the stator coil where the support structure is external (preventing expansion of stator windings) the maximum expansive hoop stress in the stator support structure is one again found at its inner radius and can be predicted using Roarks Table 32, case 1a [1, 24].

$$\sigma_{hss} = p_{magnetic} \frac{c^2 + a^2}{c^2 - a^2}$$

Where a and c are the support structures inner radius (stator coil outer radius) and the support structure outer radius. If however it is not necessary to use an external stator coil support structure (and thus relaying on the stator coil itself for structural support) then we the hoop stress in the coil is approximately given as

$$\sigma_{hss} = p_{magnetic} \frac{r_{si}}{(r_{so} - r_{si})}$$

The coil and armature support structures for a low energy L.I.M are typically very thin, for this reason we can approximate them to behave as thin walled cylinders and taking only the hoop stresses into account, using the Tresca Theory of Failure we can estimate that failure will occur when the hoop stress (in the stator coil windings and the armature coil form) exceeds the respective materials tesnsile yeild strength, as shown below [25].

$$\sigma_h \leq \sigma_y$$

An important note is that when calculating the magnitude of the axial magnetic field strength B_z we could add the field contributions of both the stator coil and the armature coil, but because in a L.I.M the respective coil currents will be anti-parallel the sum of magnetic fields will infact be a difference, and the hoop stresses on the coils will in fact be lower while the armature is inside the stator coil [4]. In view of this, the maximum axial magnetic field is taken as that created only by the peak current flowing in the stator coil and is assumed to be constant when it actually is'nt because the current is oscillatory , thus providing a very conservative estimation of the forces on the armature and stator coils.

A.5 Design considerations and Launcher Synthesis

While theory and understanding of a linear induction launcher is well understood and easily modeled, there exists no fixed or formal design process which one can follow to design a launcher that optimally meets a given set of requirements and specifications [21]. Design would usually proceed by making certain assumptions that will give an indication of the inductance and therefore size and shape of the stator and armature coils. Certain combinations can then be tested with a simulation with various initial input conditions as discussed in Appendix A.4.3 on page A-23, but this iterative process soon becomes tedious and impractical as stages are added to the launcher system and often results in launchers with low operating efficiencies [22].

This part of the literature review will present all the important design concepts, considerations and operating parameters of specific relevance to a capacitor driven pulsed induction launcher found in the extensive published literature available. This section includes numerous topics ranging from stator and armature coil design to selection criteria for the tank circuit capacitor and switching elements. Thus providing an effective starting point for specifying many of the launchers systems.

A.5.1 Stator Coil

The operation of any electromagnetic co-axial linear launcher is largely dependant design of the stator coil in terms of how well it is matched to a given power supply and the armature which it must drive. In

capacitor driven linear induction motor, the frequency of the LC oscillatory current wave in the stator coils is related to the stator coils inductance and the tank circuit capacitor as illustrated by the equations below.

$$\omega_0 = \frac{1}{\sqrt{L_{ss}C}}$$

and

$$\omega_d = \sqrt{\omega_0^2 - \alpha^2}$$

where $\alpha = \frac{R}{2L}$. Since the tank circuit resistance is very small the damped frequency of oscillation is very much close to the resonant frequency of the system. This is an important relationship if the capacitance of the proposed test launcher has already been specified by specifying the operation voltage and energy initial storage as part of the systems performance requirement specifications. The stator coil inductance must be chosen to keep the frequency of oscillation with tolerable limits to avoid phenomena such as corona discharge and the skin-effect.

Using a computer analysis methode very similar to that discussed in Appendix A.4, scientists and engineers have created computer optimization routines which seeks out the best design for a given set of parameter ranges. The results of extensive launcher research based on these optimization routines has revealed some interesting insights, especially regarding the geometries of the two coils. For example, the comparison between optimum designs of different launcher bores has revealed that launcher efficiency greatly improves as the bore size increases reflected by the results shown in 11. Furthermore it was determined that long thin stator and armature coils pairs yielded the best results [2].

Table 11: Results of launcher bore investigation [2].

Bore Diameter (mm)	Stage Efficiency (%)	Entrance Velocity ($m.s^{-1}$)	Temperature Rise (K)	Projectile Mass (g)
30	25.6	1.414	14	100
45	48.2	1.414	8	337.5
60	55.5	1.414	4	800

Discussed in Appendix A.4.3 on page A-23 was the fact that force F_z acting on the armature is proportional to the mutual inductance gradient between two coils. This gradient is also closely related to the radius ratio $\frac{r_a}{r_s}$ of the two coils as is the available induction length l_b of a given coil pair. These tradeoffs are shown graphically in Figure 70 below, note that at close to unity radius ratio, the inductance gradient

approaches infinity. What we learn from Figure 70 is that, a longer inductance length is achieved through a small radius ratio, while a higher radius ratio will provide a higher inductance gradient.

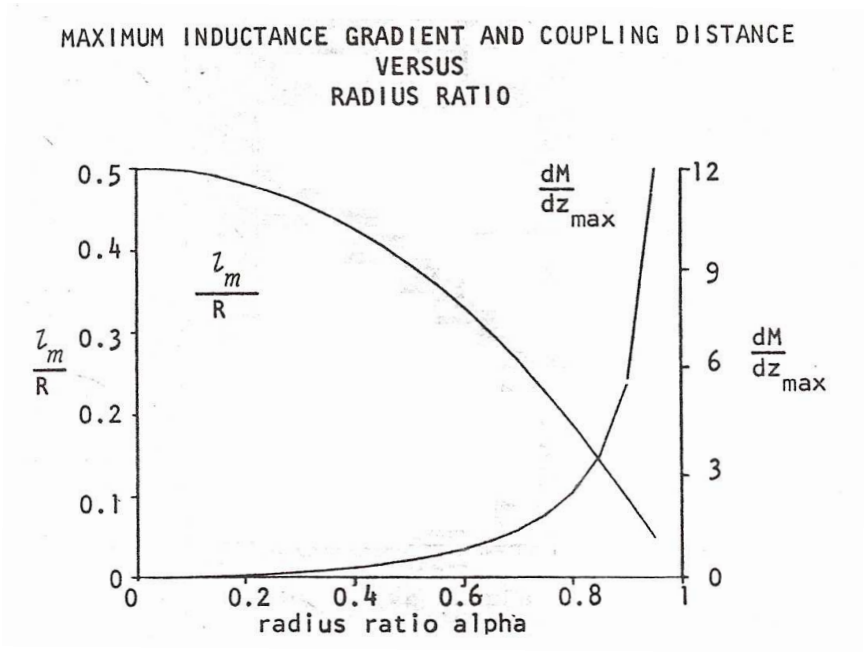

Figure 70: Inductance gradient & normalized induction length as a function of the radius ratio $\frac{r_a}{r_s}$ [4].

During operation the interaction between the axial magnetic field B_z (generated by the time varying currents in the stator & armature coils) and the induced currents flowing in the stator coil, result in the stator coil being expanded radialy outwards, while the armature is compressed radially inward. This is a significant point, because the coil form onto which the stator coil is wound, need not be very strong or rigid, resulting in a thinner coil form, decreasing the space between armature and stator windings increasing the radius ratio $\frac{r_a}{r_s}$ improving efficiency of the launcher [1]. This expanding internal pressure on the stator and armature windings is discussed in more detail in Appendix A.4.6 on page A-28

The performance of the stator coil is almost entirely related to its geometry and that of its corresponding armature. However also of great importance is the resistance of the stator coil and its thermal limitations. Good efficiency requires that the both stator and armature coils are of a low resistance [14]. The oscillatory currents flowing in the armature are in the order of 10^3 Amps, and thus some consideration must be given to its current handling capability especially at very high energy and voltage levels, see Appendix A.4.5 on page A-27 for further detail. It should be noted in this respect however that the heating of the stator coil is much less of a problem than in the armature because of the very short operating time involved the stator coils temperature rise is tolerable while the armature will have many induced current pulses (one for each stage) thus rising the armature coils temperature considerably higher than the stator coil temperatures. [12].

A.5.2 Armature

The armature of a given linear induction launcher must be suited to the stator coils driving it not only in terms of its inductance, geometry but also and most importantly its weight. Great attention to detail must be taken when designing the armature coil because it will be the component of the linear induction motor that undergoes the most abuse, especially at high voltages and energies. In a similar way that the stator coil is expended radially outwards as (discused in Section A.5.1 on page A-29) the armature is compressed radially inwards. Furthermore the desire for high muzzle velocities with a fixed amount of stored energy implies that the armatures mass must be minimized [1].

Initial studies involved single turned monolithic conducting rings made of aluminium or copper [16] as shown in Figure 71. For the purposes of modeling, the rings were notionally divided into a number of separate conducting rings which interacted with the changing magnetic field created by the oscillatory currents flowing in the stator coil. Simulation and experiments showed that the induced currents tended to concentrate at the back of the armature (i.e the end trailing motion), resulting in excessive heating and high stresses in this region of the armature in addition to limiting opperating efficiencies to 15% or less [16].

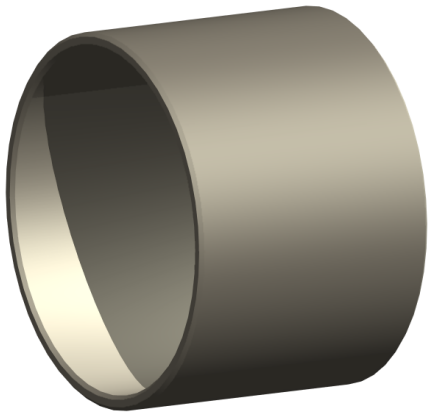

Figure 71: Single turn monolithic aluminium armature.

Another armature alternative is realized when the armature is made up of a wire wound coil shorted on its ends. This configuration forces a uniform axial distribution of the induced currents along the armature coils length and the temperature rise can be reduced by over an order of magnitude while allowing the realization of efficiencies above 40%. Two types of wire wound armature coils are shown below in Figure 72. The requirement that they be shorted at the ends (allowing current to flow) thus poses some interesting design and manufacturing challenges, never the less the gains realized from doing so are significant [16].

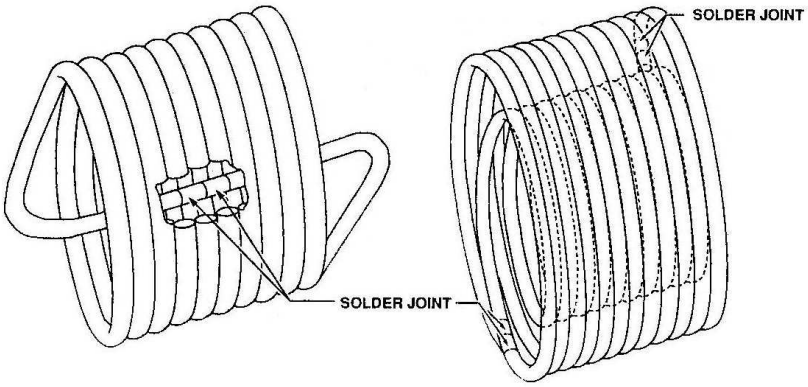

Figure 72: Two types of multiturn armatures from left to right: Shorted internaly and a Multilayer Armature shorted on its winding surface [16].

As mentioned, in addition to the large axial acceleration forces, the armature will also experience crushing radial forces that are a result of the interaction axial magnetic field B_z and the circumferential currents in the armature, discussed in more detail on Appendix A.4.6 on page A-28. There are two armature design philosophies to manage crushing of the armature windings. One is two wind the coils such that their winding serves as a support structure. The second option is to provide the armature with its own internal non-conducting support structure, which may be annular or solid. It should noted that in the case on a annular support structure the hoop stress σ_h to which the support structure is subjected will effectively be double that experienced by a solid cylinder [1].

A.5.3 Barrel

The launcher barrel is the sum off the stator coils wound directly onto a suitable form with a suitable mounting system. The only requirement is that the coilform itself is made of a non conducting material. This is because the magnetic field created by the stator coil must only be allowed to induce currents in the armature, the use of metal coil form will result in heating due to the eddy currents being induced in the in the conducting coilform and reducing overall efficiency of the induction motor. Similarly in high energy linear launchers ($>$ 2MJ) it maybe required that the coil form material selection also be able to handle the temperature rise of the stator coil as well.

Assuming a push mode operating, the stator coils themselves will also experience a similar magnetic pressure as discussed at the end of Section A.5.2 on page A-32, causing the stator coils to expand during operation. This means the coil form will not experience any compressive radial forces and as such the coil forms wall thickness need not be very thick. Thinner walls of the coil form allow for increased coupling between the driving stator and armature coils greatly improving efficiency, as previously illustrated in Figure 70 on page A-31 [1].

Although in theory the radial Lorentz Forces acting simultaniously around the full circumference of the armature would resolve to an equilibrium serving to axially locate the amature about the z axis of the slightly oversized launching tube, however in practice it is noted that stator coils are wound onto Paxoline, Lexan or coilforms while in addition making use of P.T.F.E liners to greatly reduce friction between coil form and armature windings [15, 5].

As previously discussed, the performance of a L.I.L stage is greatly dependant on the initial position of the armature relative to the stator when the power is applied to the stator winding. When designing a multistage device great consideration must be made as to how each stage is "switched" or "turned-on" and that switching indeed occurs when the passing armature coil reaches its optimum position (for maximum stage efficiency) relative to the stage stator coil. The implication of this is that the position of the armature in the launcher barrel must be tracked as the projectile is accelerated from each stator to the next. There are obviously a number of ways of achieving this and the method chosen should be determined by the armature velocity, size and launcher geometry. Available methods are of example

- Accelerometers and transmitters on the armature coil, wirelessly streaming real-time data regarding armature acceleration (from which velocity and position data can be determined)
- Measuring the ultrasonic phase-shift between an ultrasound signal received from the armature and the known signal it transmits.
- Physical switch commutation actuated by the passing armature.

There is one reliable method of detecting armature position for stage switching control in particular which uses optical methods and is similar to physical switch commutation, in that it relies passing of the armature that physically interrupt a beam of light that crosses the diameter of the barrel form thus occluding the light beams path to a phototransistor or photodiode. This method has repetitively proven itself in small laboratory experiments [5] and can be implemented as shown in Figure 73 below.

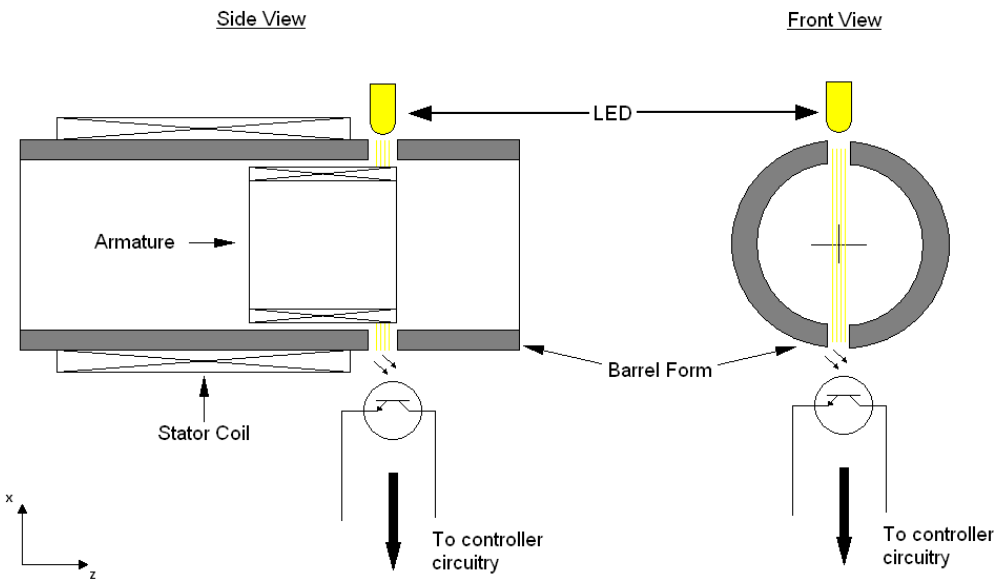

Figure 73: Sectioned view through stator coil support tube, showing diametrically spaced holes allowing light beam to cross the armatures acceleration path.

The use of such a method does come with the design cost that the geometry of the stator and armature coil pairs must be such that when the armature is in its optimum positioning for the stator coil to be fired, part of the armature must already be sticking out of the stator coil in order for it to be detected in the first place, this is better understood in terms of the sectioned view of the launcher, provided in Figure 73 above.

A.5.4 Capacitor Power Supply

There are a number of different ways to power a linear induction motor, largely depending on its operation principle as discussed in Appendix A.2 on page A-5. Of specific interest however is the capacitor driven linear induction motor and hence the implications regarding the use of capacitors as the systems power supply. When the capacitor is discharged into the stator coil inductor the resulting oscillatory (alternating about 0 Volts) current that flows within the system produces the time varying current needed by the stator coil to induce a voltage in the armature, this will require non polarized capacitors and thus immediately ruling out the use of polarized electrolytic capacitors, limiting the choice of capacitor type to those summarized in Table 12 below.

Table 12: Non-polorized capacitor comparison [27].

	Ceramic	Polyester	Polyethylene	Polystyrene	Polypropylene
ESR	Medium	Low	Low	Very Low	Very Low
ESL	Low	High	High	Low	Medium
Typical Capacitance	0.1 pF - 100 pF	0.1 nF - 160 μF	1 nF - 4.7 μF	22 pF -2μF	68 pF-22 μF
Typical Voltage Ratings	6.3 V-50 kV	50 V-1 kV	16 V-400 V	50 V-630 V	50 V-3 kV
Size	Small	Medium-Large	Large	Large	Large
Cost	High	Low	Medium	Low	Medium

Some of the more important capacitor specifications to consider when selecting the correct capacitor include [28, 30].

Rated Capacitance C

This specifies the amount of charge the capacitor is capable of storing and is measured in Farads. The amount of energy stored in a capacitor is closely related to its capacitance and the voltage to which it is charged, a relationship commonly expressed as $E_{cap} = \frac{1}{2}CV^2$.

Rated Voltage U_s

This is the maximum voltage with which the capacitor can operate continuously without breaking down the dielectric resulting in failure of the device. For A.C applications it can be quoted as an effective R.M.S and as a peak non-repetitive rating as described below.

Peak Non-repetitive Voltage U_{pk}

This represents the maximum peak non-repetitive voltage rating the capacitor can tolerate without dielectric failure, it is normally specified as a maximum voltage value (Which is greater than the rated voltage U_s) which lasts for a specified time period, further more it is quite common to specify the maximum allowable number of cycles where the maximum peak voltage is exceeded before failure occurs.

Maximum Operating Current I_{rms}

This value specifies the maximum allowable R.M.S current which can flow through the continuously operating capacitor without resulting in failure of the device due to excessive heating. Values

quoted in data sheets are often related to the capacitors power dissipation or the current carrying limits of its connection terminals

Peak Repetitive Current I_{pkr}

This value specifies the maximum peak allowable current that the capacitor can withstand repetitively without resulting in failure of the device and is given as

$$I_{pkr} = C \cdot \frac{dV}{dt}$$

where term $\frac{dV}{dt}$is the maximum allowable rate of voltage rise for the capacitor, another specification discussed later.

Peak Non-repetitive Current I_{pk}

This value, similarly to the peak non-repetitive voltage rating specifies the maximum current the capacitor can tolerate briefly during a fault/failure. It is normally a current rating over a specific period, sometimes the number of allowable periods where the current is close to the I_{pk} is also specified.

Maximum permissible rate of voltage rise $\frac{dV}{dt}$

This is the maximum allowable rate at which the capacitors voltage can rise or fall (with respect to time), repetitively and as discussed earlier is related to the capacitors peak repetitive current rating I_{pkr}.

Equivalent Series Resistance $E.S.R$

The actual capacitor used in life does not behave as the idealized device, instead we can expect a capacitor have some internal resistance associated with it. This is treated as a resistor connected in series with the capacitor as shown in Figure 74below. The heat dissipation of a capacitor is strongly related to this equivalent resistance, which is a dependant largely on the capacitors dielectric, conducting materials and construction.

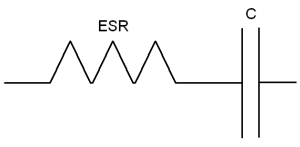

Figure 74: Non-ideal capacitor showing its E.S.R.

Equivalent Serries Inductance *E.S.L*

Similarly to the E.S.R we can also expect the capacitor to have some small internal inductance associated with it as shown below in Figure 75. In the case of an A.C as used by the L.I.M this series inductance may well result in reactive power losses, this happens when the operating frequency is high enough for the impedance associated with the E.S.L to be significant.

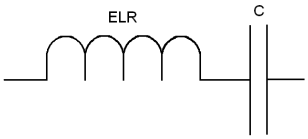

Figure 75: Non ideal capacitor showing its E.S.L.

Power Dissaption $\tan\delta$

When a capacitor has pulsed or oscillatory wave forms applied to it, the amount of power it can dissipate is not only related to the frequency, voltage and currents of the applied wave form, but it is the sum of these aforementioned components for each harmonic waveform which together make up the applied waveform. Furthermore, the power dissipated for each waveform is a function of a power dissipation factor $\tan\delta$, using subscript $_i$ to denote the relevant harmonic and for n significant harmonics the power dissipated is given as below [30].

$$P = \sum_{1}^{n} (V_{irms})^2 \cdot 2\pi f_i C \tan\delta$$

The capacitors in a L.I.M are expected to handle high frequency (+ 1 kHz) alternating currents while storing a significant amount of energy (> 20 Joules). Due to the low *dielectric loss* of polypropylene, metallized polypropylene capacitors are a good choice for this application. These dielectric losses are proportional to the square of the operating voltage and frequency, now since the voltage is proportional to the current and inversely proportional to frequency, the dielectric power loss is proportional to the square of the current and inversely proportional to the frequency, thus (for a given operating temp) current handling capability increases with frequency [31], furthermore these metallized polypropylene capacitors also have typically low E.S.Rs and E.S.Ls thus lending them favorably to L.I.M use, again their more typical specifications can be seen in Table 12. An example of such a capacitors datasheet can be found in Figure 76 below.

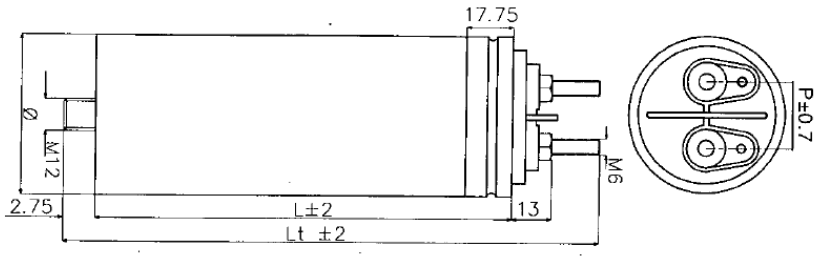

ELECTRICAL SPECIFICATION

Part no.	C µ F	Urms	Tgδ MAX	ESR mΩ	du/dt V/µs	Irms A	Lpkr A
01-05-0128	50	440V	0.0033	10	20	16	1000

MECHANICAL SPECIFICATION

Part no.	C µ F	Termination		P	L	Lt	Ø
		Screw	Nut				
01-05-0128	50	6 x 30HEX	M6X5HEX	24	150	192.75	60

Technical data	
Temperature range (case):	-25°C to +70°C
Capacitance tolerance:	±5%
Test voltage terminal to terminal:	1.5 x rated voltage
Test voltage terminal to case:	1.5 KV 50 Hz 60S
Permissible relative humidity:	Annual average < 95% on 30 days/year, continuously
	100%, on other days occasionally 100%
	Dewing not admissible
Life expectancy:	≥ 30 000 hours at Un

Figure 76: Afcap metallized polypropylene capacitor data [35].

In looking at the above capacitor data sheet one can appreciate the large difference (almost 60 times greater) between the continuous operating current I_{rms} and the max peak repetitive current I_{pkr} which the capacitor can provide. This peak repetitive current can also easily be increased by adding capacitors in parallel, thus creating a bank capacitor with a high total capacitance and thus the peak repetitive current of the bank is much greater than that of any single capacitor, in accordance with $I_{pkr} = C \cdot \frac{dV}{dt}$. Further interesting details are the low E.S.R, over voltage test data and operating temperature range. One of these capacitors on their own can store around 4 Joules of energy, which may not sound like much, but can still be quite lethal because these capacitors can release all of that energy in a one millisecond event, they are therefore well suited to high power applications.

A.5.5 Switching Elements

The switching element is a needed for precise control of when the energy stored in the capacitor is discharged into the stator coil. This can also be done in a number of ways, in view of the published literature describing typical L.I.M's operating on a voltage well above 2 kV, the common use of triggered

spark gaps is well documented to achieve precise triggering of each stage coil. The high operating currents and typically voltages of over 400 V renders the use of physical contact switches impractical and unsafe. Thus aside from spark gap technology, power semiconductors are the only other reliable means of switching the heavy voltages and currents need for the L.I.M's operation. Such semiconductor options include (but are not limited to); Silicon Controlled Rectifiers (S.C.R's), TRIAC's and IGBT's. This section will discuss in detail the design considerations and implications of using only the IGBT switching solution, however Figure 77 best illustrates a general overview of the operating capabilities for most available power semiconductors in terms of voltage, current and frequency.

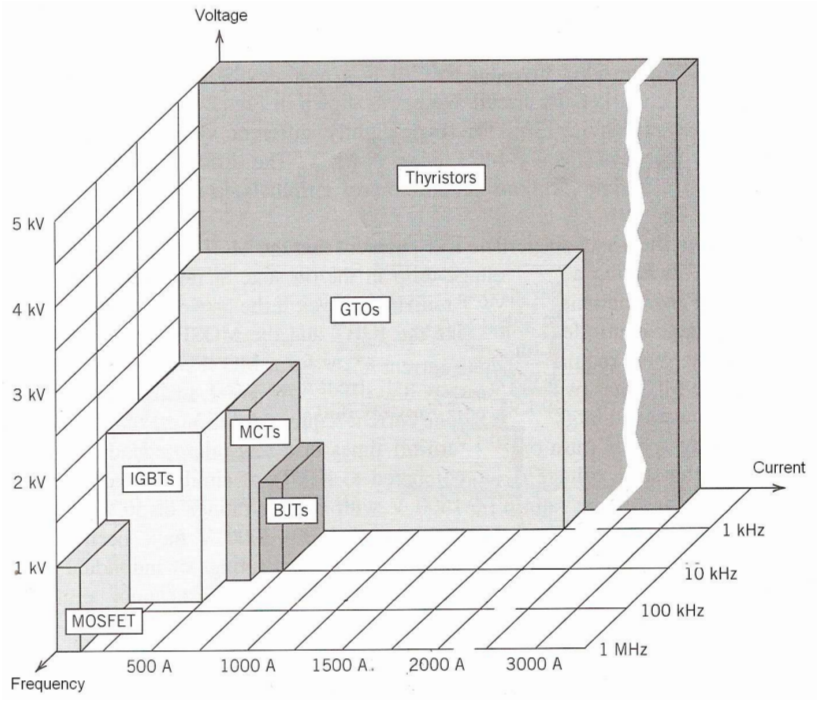

Figure 77: Typical continuous operating capabilities for various semiconductor devices [39].

IGBT technology has been greatly improved upon since the Figure 77 was first printed and IGBT's current ratings are now much higher and feature many desirable properties in general and specific to P.L.I.M applications. They use a M.O.S input gate and have a low on state collector emitter voltages V_{CE} (1.7 V - 2.8 V), high switching speeds and high current handling capabilities up to 1000 A with 600 V - 1700 V being typical voltage ratings. Further more their widespread availability has reduced their cost and thus making many previously uneconomically applications/projects possible [36]. The IGBT can be thought of as a MOSFET and a Bipolar Junction Transistor, and thus is switched on when a voltage is applied to the gate with only a small (insignificant) current drawn through the gate. The IGBT will be damaged if a reverse voltage is applied across its collector and emitter. Thus manufacturers very often include an anti-parallel protection diode that conducts any reverse voltage applied to the IGBT. The typical circuit symbol for an IGBT is shown in Figure 78 which also shows an IGBT with an anti-parallel

diode across its collector and emitter.

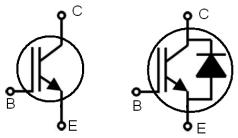

Figure 78: Circuit symbols for IGBT's with and without the anti-parallel diode.

The operation of a L.I.M will require a bipolar current flowing in the tank circuit. Thus the diode is useful in that it allows the bipolar current to be switched without damaging the IGBT. As mentioned IGBTs with this anti-parallel diode are readily available in discrete packages, an example of which is shown in Figure 79 below.

Figure 79: Mitsubish Power IGBT module (inc. anti-parallel diode) rated for continuous operation at 600V & 600A [37].

Datasheets regarding these IGBT modules are far more extensive than that of the capacitor shown in Figure 76 on page A-39, and hence a full example data sheet is not shown here in its entirety. These datasheets are rightfully very extensive as there are many considerations that must be taken into account when using semiconductors in any kind of power circuitry. Discussed here however are the most important device ratings found in the typical IGBT datasheet and their consequential circuit considerations relating to P.L.I.M applications. Also when looking at the datasheet for an IGBT incl. an anti-parcel diode, two sets of data are often presented on for the IGBT itself and the diode. For reference this datasheet will be discussed in terms of the Mitsubish Power IGBT & anti-parallel diode shown above in Figure 79 [37], and thus the symbolic naming standard for each of the ratings is the same as that used by Mitsubishi Electric [38].

A.5.5.1 Absolute Maximum Ratings These ratings are the most important ratings of IGBTs operation. A maximum rating is a value which establishes either a limiting capability or limiting condition, and is determined for specific environments and operating conditions (normally temperature). It is very common for a IGBT to operate beyond these maximum ratings for short time periode. The most important ratings are thus are discussed below making mention as to whether or note the rating can be exceeded.

A.5.5.1.1 IGBT & Diode

IGBT Collector Emitter Voltage V_{CES}

This is the maximum voltage that the IGBT can block across its collector and emitter terminals when it is in its off state (no voltage applied to its gate) without causing permanent breakdown of the semiconductor material.

Diode Collector Emitter Voltage V_{GES}

This rating specifies the maximum reverse voltage that can be applied to the diode with out causing failure.

Continuous IGBT & Diode Collector Current I_C

This rating specifies the maximum continuous D.C or A.C R.M.S current that can flow through the IGBT & diode. It is very often based on the junction temperature limitation of the device.

Repetitive Pulse IGBT & Diode Collector Current I_{CM}

This rating specifies the maximum peak pulse D.C A.C RMS current which can be conducted through the IGBT & diode for short time durations without causing failure of either device. Very often short time operation allows for significantly higher currents to be conducted through the devices than indicated by the datasheets for continuous current rating I_C and can often be up to 6 times larger, provided that the maximum junction temperature rating is not exceeded. The value is thus normally specified in terms of a current magnitude, frequency duty cycle [40]. This is a very important and relevant to L.I.M applications and is discussed in more detail in the following section.e

Junction Temperature T_{jmax}

During the operation of semiconductor devices heat is generated, this heat flows in all directions in the device but flows particularly well along the thermally conductive connectors. Thus the junction at which the metal terminals meet the semiconductor material (specific to the IGBT) tend to experience a large temperature rise [41]. This rise of temperature is an important limiting factor to the all semiconductor devices since components operating at higher junction temperatures can be expected to have shorter lifespans, and a general rule of thumb is that the failure probability of a semiconducting device doubles for every 10^{o}C - 15^{o}C above 50^{o}C [41, 42]. A thermal photograph allows us to visualise temperature rise in a semiconductor device, for example on such thermal photograph is shown in Figure 80 below. The maximum junction temperature thus represents maximum permissible temperature the devices junction can reach during continuous operation. It has already been mentioned that the peak pulse current capability of a semiconductor device is limited by this rating thus a good understanding of the junction temperature and how it is raised

is required when choosing to use a given IGBT beyond this continuous current rating, this topic is thus discussed in more detail in Appendix A.5.5.2 on page A-44.

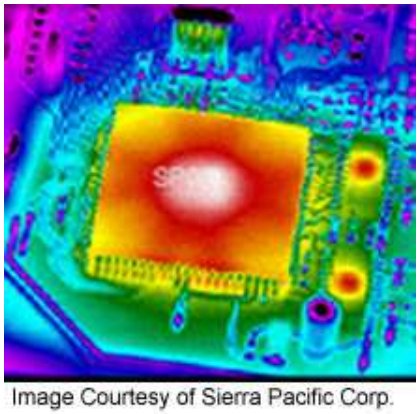

Figure 80: Thermal photograph of a computer chip in operation [41].

A.5.5.1.2 Specific to IGBT

IGBT Forward Collector Emitter Voltage Drop V_{CEsat}

When the IGBT is in its on state, its contribution to the total tank circuit resistance is expected to be very small and the power loss associated with it to be insignificant. However semiconductors often have some small voltage drop across themselves and in the case of IGBT's used in this project this can range anywhere from 1.7 V-2.8 V [37]. This rating specifies typical values for V_{CEsat} under various operating conditions. This small voltage drop is relevant as it affects the $V \cdot I$ power dissipation in the IGBT and thus is an important factor in determining junction temperature rise.

Gate Emiter Threshhold Voltage $V_{GE(th)}$

This value specifies the minimum voltage that must be applied to the MOS gate in order to turn the IGBT on. However, operating at lower voltages can result in high losses, this point is illustrated when looking at typical IGBTs I_C vs. V_{CE} family of curves (for various gate drive voltages) as shown in Figure 81 below. Exceeding this voltage may also damage the gate and MOS layer separating the gate from the emitter.

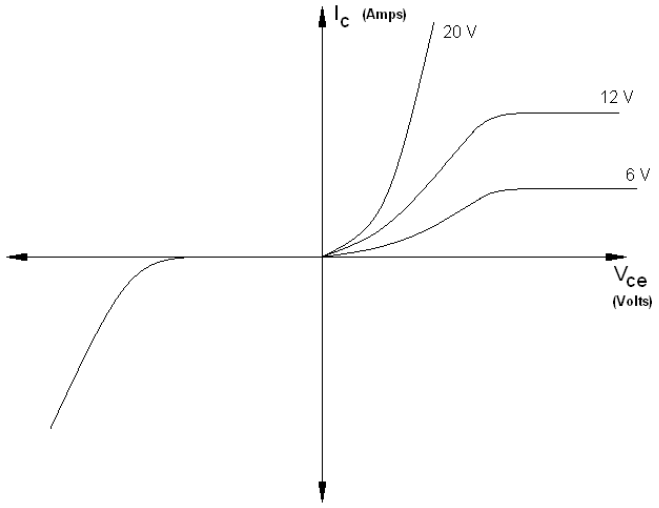

Figure 81: Typical IGBT I_C vs. V_{CE} family of curves for various gate drive voltages.

Figure 81 shows that increasing the collector emitter current at lower gate voltages tends to increase the IGBT's collector emitter saturation voltage, this is undesirable as power dissipated by the IGBT is directly proportional to this voltage. Furthermore, the conduction current plateaus shown in Figure 81 limit the maximum current the device can conduct at low gate voltages, in contrast operating at higher gate voltages there is a linear relationship between current I_c and collector emitter saturation voltage V_{CE} which is kept considerably lower as the conduction current is increased.

A.5.5.1.3 Specific to Anti Parralel Diode

Diode Forward Collector Emitter Voltage Drop V_{ECsat}

Like the IGBT forward collector emitter voltage drop, the diode also has a small voltage drop across its collector and emitter and the power dissipation through the diode alone is equal to the product of the forward current through the diode and this voltage.

A.5.5.2 Conduction Losses & Junction Temperature

It is clearly evident from the discussion above on the devices important ratings, the one rating which most others are related is the devices maximum allowable junction temperature. To properly explain the dynamics of heat transfer in a semiconductor is a vast subject and is obviously beyond the scope of this project. However when choosing an IGBT for a L.I.M switching application it is imperative to estimate whether the junction temperature will ever be exceeded during the operation period. In a L.I.M the IGBT & diode will be subjected to decaying oscillatory current waveform over a very short

time duration, in such an operating condition the current conducted by the device may greatly exceed it's continuous current rating, calculation of temperature rise under these conditions is based on the transient thermal impedance of the device or Z_{th}. Which is similar to a devices thermal resistance, but is a dynamic variable taking into account changes in the semiconductor material over the short time period. Data sheets will very often provide Z_{th} data for the IGBT and the anti-parallel diode in terms of pulse frequency and duty cycle as shown in Figure 82 below.

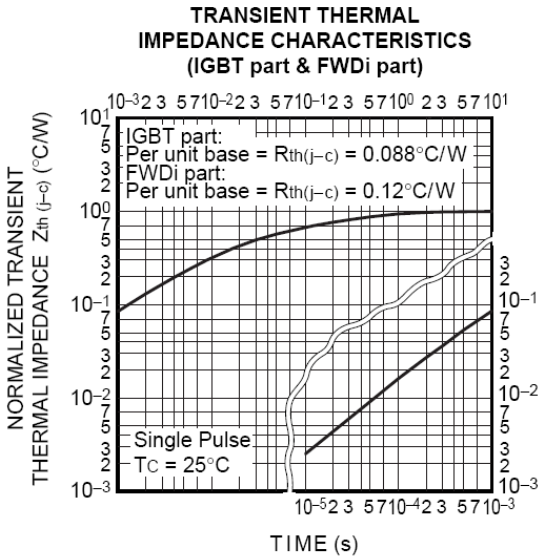

Figure 82: Typical transient thermal impedance Log graph. This one in particular quotes both diode and IGBT Z_{th}values as equal, thus presenting only a single curve. [37].

The Z_{th} is useful because provided power dissipation over time is known it allows estimation of the instantaneous junction temperature as shown below [42].

$$T_j(t) = P(t) \cdot Z_{th} + T_{jinit}$$

where the the instantaneos power is given as the product between the emiter collector coltage and the current being conducted as shown below for both diode and IGBT.

$$P_{diode}(t) = V_{CEsat}(t) \cdot I_s(t)$$

$$P_{IGBT}(t) = V_{ECsat}(t) \cdot I_s(t)$$

It is also important to realize that because the current in a L.I.M uses a bipolar current it assumed that the IGBT will conduct the positive half cycle and the diode will conduct the negative half cycle as

illustrated in Figure 83 below.

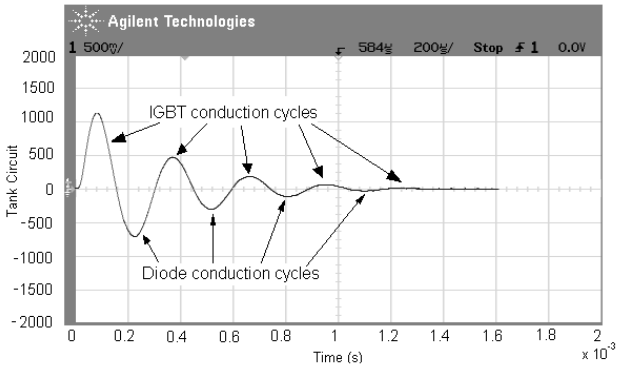

Figure 83: Illustrating how the oscillatory discharge currents are conducted between the tank circuit capacitor and the stator coil inductance.

The total junction temperature rise is the sum of the contributions from the diode and IGBT and thus (assuming the transient thermal impedance of the Diode and IGBT and equal, which may often be the case).

$$T_j(t) = T_{jdiode} + T_{jIGBT} + T_{jinit}$$

$$= P_{diode} \cdot Z_{th} + P_{IGBT} \cdot Z_{th} + T_{jinit}$$

Thus operation of the device will be safe so long as $T_j < T_{jmax}$, it should be stressed that this is only a basic approximation to the actual junction temperature, which may be considered conservative as it does not take into account any heat that may be dissipated through the heat sink onto which the IGBT module will be mounted.

A.6 Conclusions

This literature review is indeed broad and extensive; however the challenge of designing a pulsed linear induction motor is itself of such a nature and requires a broad range of knowledge from the designer. This literature review therefore has aimed to equip a designer with all the important knowledge and pertinent information regarding L.I.M design by covering topics such a theoretical modeling, capacitor & IGBT selection while in addition providing details on all critical mechanical and electrical design considerations. Much of the information presented above is discussed in terms of cumulative findings, assumptions and topics of interest which were revealed not only throughout research process but through the development and design of the test launcher constructed in this project. It thus serves as an excellent reference source

which was thoroughly researched and well referenced for increased credibility and to greatly facilitate any further research in light of this work.

B Supporting Simulations, Calculations and Operation Hypothesis

Contents

Figures

Tables

B.1 Introduction

This section will detail the actual analysis and calculations used to develop the pulsed linear induction launcher test rig. Much of the required theory, matrix math and numerical analysis has already been described in great detail in Appendix A.4 and is not included here for the sake of brevity, it is therefore highly recommended that the reader first study Appendix A.4 on page A-17 before attempting to jump straight into much of what is presented here. Furthermore it would be useful to note that all of the simulation results presented here are in context of Input Conditions to which the test rig was designed and form part of the devices specifications (unless otherwise states). A detailed list of test rig specifications can be found in Appendix C on page C-1. The reasonably powerful computation ability of a typical desktop computer was used extensively to compute and calculate all design data and specifications including (and to be discussed in this order) coil inductance simulation, the numerical time step simulation of all electrical and mechanical parameters over time and finally feasibility testing of components e.g. IGBT junction temperature rise and coil mechanical stress. All computation work was done using MATHWORKS MATLAB.

B.2 A Brief Discussion on Input Data.

Many of the operating variables of for a P.L.I.M remain variable even once the device is constructed for example operating voltage, capacitance and armature starting position. However when designing a test launcher system, the coil geometries which cannot be changed once the device is constructed therefore coil lengths, number of turns and radius ratio of stator and armature are thus fixed variables which are the most important because they largely determine the range of the variable operating parameters such as voltage. It is for this reason that the information presented here is given mainly in terms of geometries on which test launchers coils have been built as summarized in Table 13 below.

Table 13: Important non-variable parameters for P.L.I.M test rig.

Stator Coil Inner Diameter	mm	50
Stator Coil Length	mm	37
No. of Stator Coil Turns	n/a	16
Stator Coil Wire ϕ	mm	2.3
Stator Coil Resistance	mΩ	11
Armature Coil Inner Diameter	mm	40
Armature Coil Length	mm	27.4
No. of Armature Coil Turns	n/a	15
Armature Coil Wire ϕ	mm	1.8
Armature Coil Resistance	mΩ	13.6
Armature Coil Total Mass	grams	58
Radius Ratio $\frac{r_a}{r_s}$	n/a	0.838

B.3 Coil Pair Inductance and Resistance Calculation

As discussed in Section A.4, the first step in simulating L.I.L's operation is to determine the inductance parameters for the two coils in terms of self inductances L_{ss}, L_{aa} and the mutual inductance in addition to the mutual inductancegradient M_{sa} and G_{sa} respectively. Again the method for doing this has been discussed in great detail in Appendix A.4.2 on page A-20.

In all inductance simulations the coils were notionally divided up into N_s and N_a longitudinal sections in both cases these values were set equal to the number of coils in each corresponding stator/armature coil winding layer. In addition the radial divisions n_s and n_a were varied until suitable convergence of the inductance values were achieved. Figure 84 below illustrates this notional division for both coils.

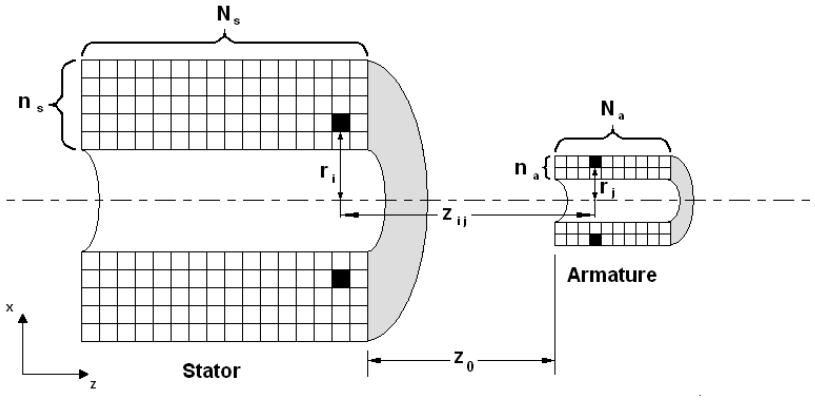

Figure 84: Section through coils illustrating the division of real coils into filamentary elements or coils [15].

Obviously, having written a computer simulation to determine coil inductance one needs to compare the output results to results from elsewhere in order to verify the simulation is in fact correct before any

development of the numerical simulation can be attempted. On one occasion this was done by comparing the measured self inductance of a coil to that predicted by the simulation, this however turned out to be quite tedious, fortunately many inductance calculators can be found online, one in particular was most useful and its method was well referenced and most importantly different to that used in this project [44].

As mentioned determination of these inductance values requires the evaluation of elliptic integrals, it should be be noted that errors in the results were encountered when using Matlabs built in elliptic integral evaluation function. However when evaluating the elliptic integrals using a function based on a method outlined by [15, 45], the errors would be corrected and the simulation results would converge on a values suitably close to that predicted by [44].

B.3.1 Self Inductances

Figures 85 & 86 show plots of the simulation stator and armature coils inductance and their error when compared to results predicted by [44], for the coil geometries specified in Table 13 on page B-4.

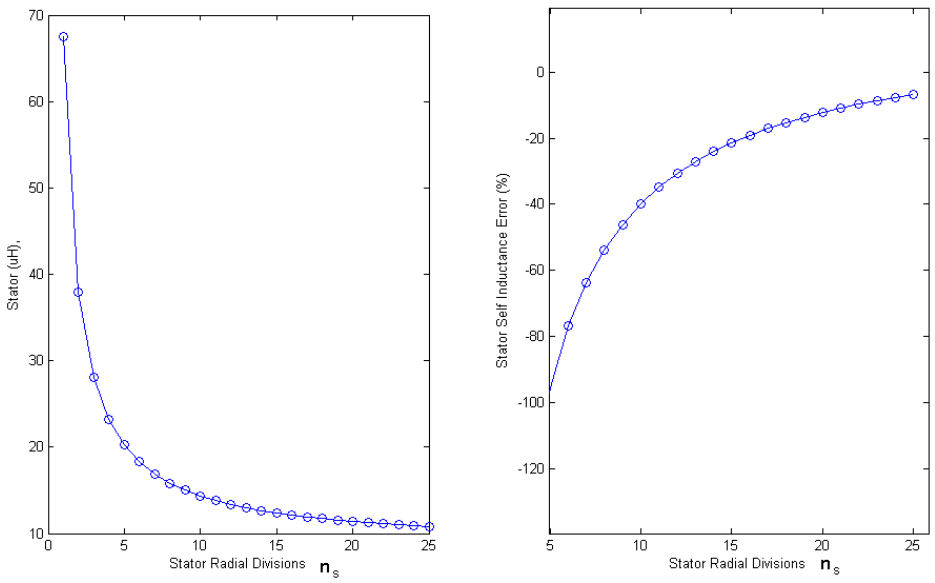

Figure 85: Stator coil self inductance L_{ss} as a function of n_s. Note rapid convergence of results and also the low error percentage at n_s =25.

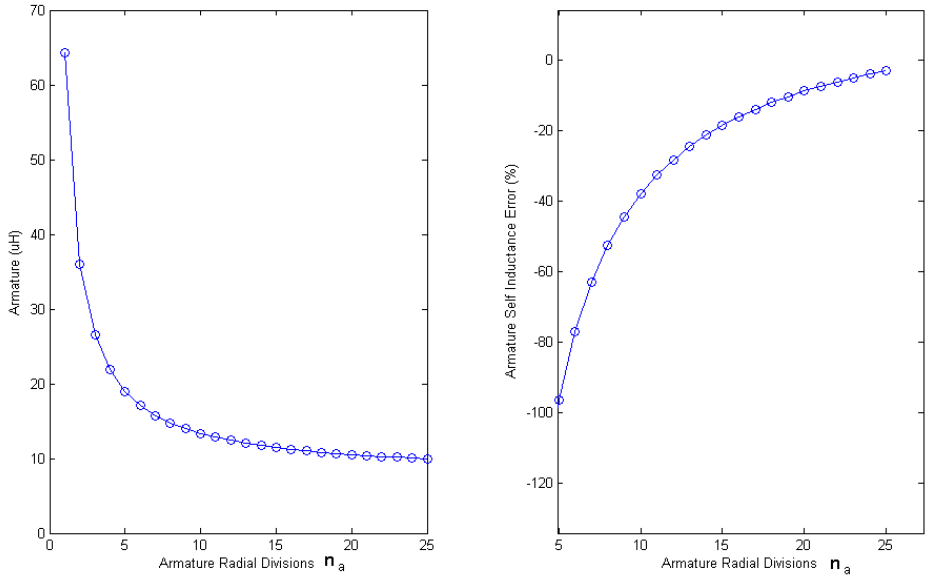

Figure 86: Armature coil self inductance L_{aa} as a function of n_a. Again note rapid convergence of results and also the low error percentage at n_a =25.

These values are thus used to form the co-efficient matrix $[L]$, which is a constant for given coil geometries, and does not change as the relative position of the coils changes unlike the mutual inductance and its gradient which does change as the coils move closer/further apart.

Thus for all inductance simulations (self, mutual and mutual inductance gradient) a subdivision of $n_s = n_a = 25$ was used, while N_s and $N_a$would simply be set eqaul to the number of turns per winding layer of the respective coil. The results of the self inductance simulation are summarized in Table 14 below.

Table 14: Summary of important coil self inductance simulation for armature and stator coils. Also shown for comparison was the self inductance calculated by another inductance calculator [44].

	n	N	$L_{sim}(\mu\text{H})$	L_{ref} (μH) [44]
Stator Coil	25	16	11.42	10.70
Armature Coil	25	15	9.96	9.67

B.3.2 Mutual Inductance and Mutual Inductance Gradient

Again, using the approach outlined in Appendix A.4.2 on page A-20 the mutual inductance and its gradient (with respect to axial position of the coils) was also determined. For test verification purposes the coil separation was set such that the armature coils were centrally located within each other. This was chosen as a test reference position because it is known (as shown by Figure 66 on page A-21) that the mutual inductance gradient of the two coils in that position will be zero. Figure 87 on page B-8 illustrates

the extremly rapid convergance of the simulation result when the mutual inductance between two coils is calculated for various coil divisions n_s and n_a , furthermore it illustrates that the result is very accurate even for coarse coil divisions (i.e at low values of n_s and n_a). The mutual inductances calcululated by the simulator were again compared to those determined from another inductance calculator [44] for the same inputs.

Unfortunately the calculator used to compare inductance results did not calculate a mutual inductance gradient value, however as mentioned because of the specific coil position to be tested we can expect the mutual inductance gradient to be very close to 0 H/m and this is indeed what the simulation has predicted and is reflected in Figure 88 on page B-9. With maximum mutual inductance of the between the two coils occouring when when they are co-axially located (axial seperation of 0 m), the comparative results of these analyses are shown in Table 15 below.

Table 15: Mutual inductance and mutual inductance gradient values for the specified armature & stator coil geometries (axially located within each other i.e. zero seperation between coil centers).

	n	N	$M_{sim}(\mu\text{H})$	M_{ref} (μH)	$G_{sim}(\mu\text{H/m})$	G_{ref} $(\mu\text{H/m})$
Stator Coil	25	15	8.57	8.49	0	0

These inductance values are then used to construct co-efficient matrices M and G.

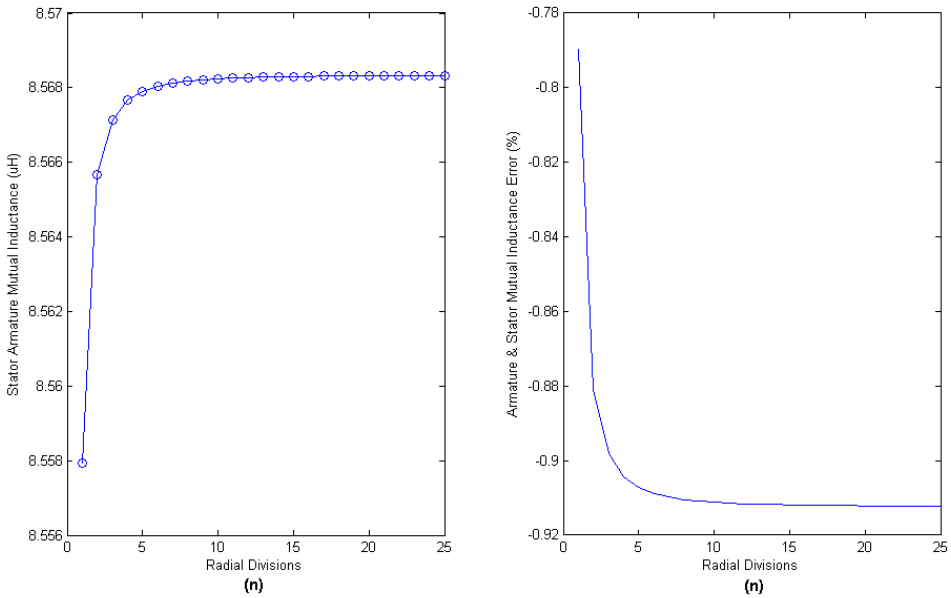

Figure 87: Armature and stator coil mutual inductance M_{sa} or M_{as} (for specified coil separation). Also of interest is that the error value is less than 1%.

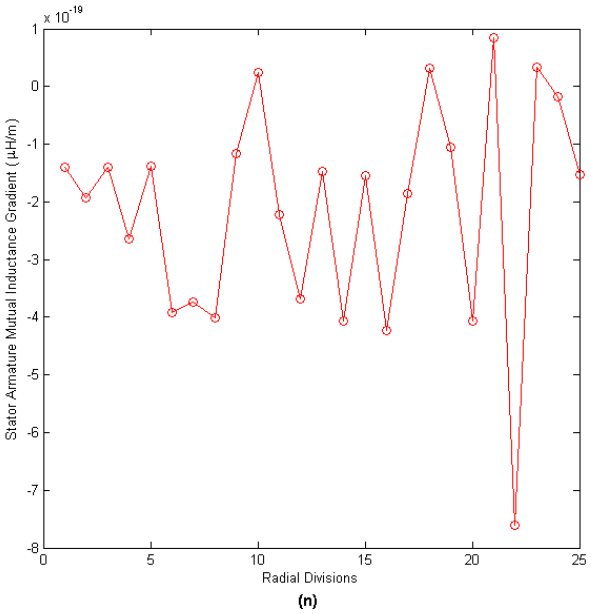

Figure 88: Mutual inductance gradient (as a function of radial coil division) for the two coils when the armature coil is centrally located within the stator coil, Although the graph might seem very peaky/noisy the value of this inductance gradient is in the order of $10^{-19}\mu$H/m, and thus is deemed sufficiently close to 0 H/m.

B.3.3 Complete Inductance Parameters of Launcher System

Since mutual inductance and its gradient change as the coils separation changes this necessitating that the coefficient matrices M and G must be evaluated for a specified range of armature and stator separation before the numerical time step simulation is executed. This was implemented in Matlab where code was written to calculate and plot M_{sa} and G_{sa}as function of coil position. The resulting curves for M_{sa} and G_{sa} vs. coil position are shown in Figure 89 below. These curves matched those predicted by the literature (See Figure 66 on page A-21) thus verifying this analysis to some extent

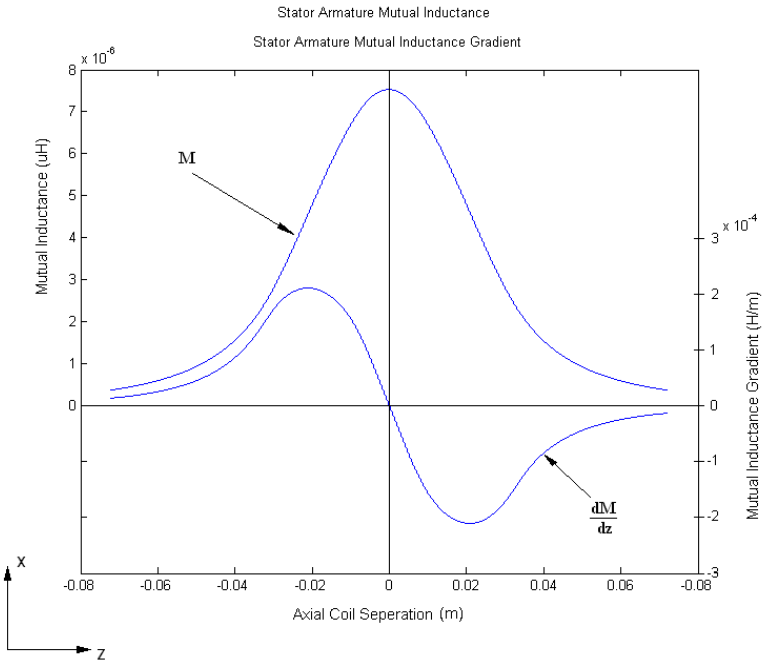

Figure 89: Curves for $M_{sa}$and G_{sa}vs. axial coil separation clearly reflecting the fact fact that $G_{sa} = \frac{d}{dz} M_{sa}$.

Again re-emphasizing that both L_{ss} and L_{aa} effectively remain constant throughout the event, unlike M_{sa} and G_{sa}, there values only need to be calculated once. The accuracy of this data is thus subject to the number of places at which M_{sa} and G_{sa} are evaluated. During the numerical simulation this inductance data will be interpolated at each time step and the relevant M_{sa} and G_{sa} corresponding to coil position $s_z(t)$ will be used to construct the correct co-efficient matrices for the given instant of the time simulation. Since Matlabs default interpolation is linear, a sufficiently high number of coil positions must be evaluated to ensure that the input data of the numerical launchers is of a "good" quality. Figure 89 reflects data for which a high number of positions were evaluted, more specific details regarding the results of Figure 89 are provided in Table 16 below.

Table 16: Details of inductance simulation shown in Figure 89.

Position Range	m	-0.0721 to 0.0721
Position Step	mm	0.01
Number of data points	n/a	14430
Evulation Time	Hours	≈14
n_s	n/a	25
n_a	n/a	25

B.3.4 Coil Resistances

The coil resistances are also calculated in the Matlab simulation, based on user defined coil inputs such as number of turns and copper wire resistivity as shown in table below

Table 17: Input data used to determine armature and stator coil resistances [3].

No of turns on stator coil	n/a	16
Stator coil wire resistivity	mΩ/meter	4.1328
Length of stator coil wire	m	2.63
Stator Coil Resitivity	mΩ	10.9
No of turns on armature coil	n/a	15
Armature coil wire resistivity	mΩ/meter	6.5698
Length of armature coil wire	m	2.06
Armature Coil Resitivity	mΩ	13.37

It was assumed that both coils would be wound as single layers coils and that each turn was approximately equal to the circumference defined by the mean radius of the wound coil, and so the coils length is given as a the product of the circumference of one coil turn and the number of turns, as such the coil resistance was estimated for both armature and stator coils

$$R = \sum_{k=1}^{l} n(2\pi r_l) \cdot \rho$$

where l, n, r_l and ρ are the number of winding layers, number of turns per layer, winding layer radius and wire resitivity respectively.

B.4 Numerical Launcher Simulation.

Based on the results of Appendix B.3 on page B-5 and some specifications in Appendix C on page C-1 there is enough data to simulate the entire operation event of a P.L.I.M. Matlab was used to numerically solve the lumped parameter circuit differential equations described in Appendix A.4.1 on page A-17 and thus almost every time varying quantity of the devices operation can be determined including coil currents, voltage in the capacitor, IGBT Junction temperature rise, armature position, aceleration and velocity. Using a numerical solution to solve for quantities over time, it is important that a sufficiently small time step or Δt is chosen to ensure that no numerical errors propagate which would result in incorrect data, more so after the data is manipulated to derive other performance variables. An example

of a numerical error is discussed in Appendix B.11 on page B-26. The details of the numerical solution used for all analysis to follow is thus provided in Table 18 below.

Table 18: Details of numerical simulation used common to all the results that follow.

Time Period	μsec	0 - 4000
Time Step	μsec	0.1
Points evaluated	n/a	40001

B.4.1 A Brief Discussion on Input Data

Clearly the most important input data for the numerical simulation is the inductance parameters for all possible coil positions. Above that there is also the energy initially stored in the capacitor, initial capacitor voltage, initial coil separation and of course, armature mass. Considering only a single stage of the launcher system all of the following graphs in this Appendix correspond to the given input details shown in Table 19 below, unless otherwise stated.

Table 19: Single stage initial operating parameters.

Stage Energy	J	25
Initial Voltage	V	440
Stage Capacitance	μF	315
Initial Coil Seperation	mm	16

B.5 Electrical Parameters

The differential equations allow plots of instantaneous current over time to be made, these are necessary because the product of the two coil currents $I(t)_{ss}$ and $I(t)_{aa}$ are needed to calculate the instantaneous force $F(t)_z$ acting on the armature coil and all other mechanical and electrical parameters of interest. The voltage across the capacitor over time is also of interest in that it is proportional to the energy stored in the capacitor at any given instant. The algorithm described in Appendix A.4.3 on page A-23 was implemented in Matlab, allowing all of the launchers performance parameters to be quantified over time. This section will present and discuss the current and voltage waveforms for a single stage of the test launcher based on the aforementioned input parameters.

Starting with the stator coil Figure 90 shows the resulting current and voltage waveforms over the prescribed time domain, reflecting the highly oscillatory behavior of both current and voltage across the capacitor and through stator coil inductance. In addition Figure 91 below also illustrates that a similar

current waveform is induced in the armature coil over the given time periode. Comparison of the currents wave forms in Figures 90 & 91 show that at any given instant the armature current is the opposite polarity to that of the stator coils current. An expected consequence of LENZ'S LAW again serving to validate the simulation.

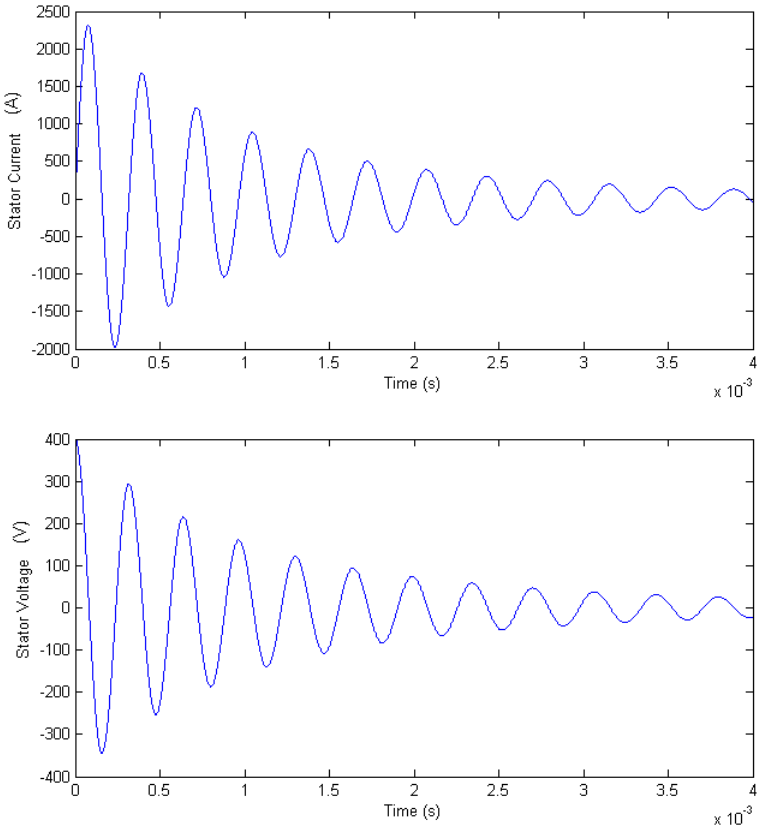

Figure 90: Graphs of stator current and voltage over the specified time domain.

Figure 91 does not show the armature coil voltage, the reason for this is that the armature coil is shorted on itself and thus the voltage across it is always 0 V (or close to 0 V, depending on the quality of the solder joint).

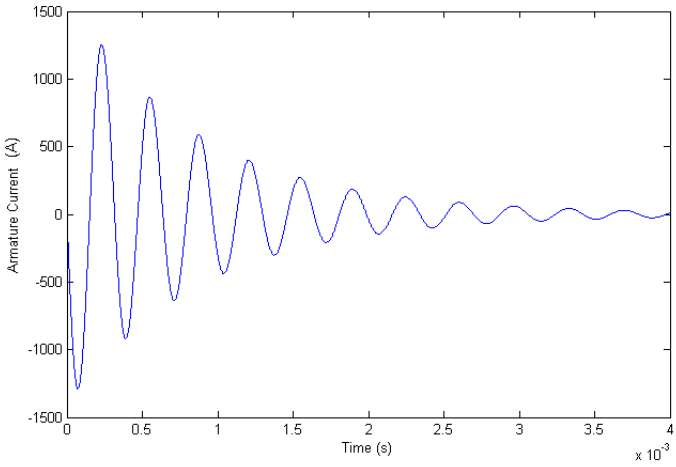

Figure 91: Induced current waveform of the armature coil.

These results are very important in that they are used to derive many of the P.L.I.M's operation specifications, which the capacitors and switch gear components must be able to tolerate. As such the useful data extrapolated from this analysis is tabulated in Table 20 below.

Table 20: Important theoretical specifications regarding coil current and voltage.

Maximum Stator Coil Current	A	2260.5
Stator Coil R.M.S Current	A	599.76
Maximum Stator Coil $\frac{dI}{dt}$	A/μs	29.12
Maximum Capacitor $\frac{dV}{dt}$	V/μs	5.04
Maximum half-wave periode	μs	158.8
Maximum Armature Coil Current	A	1164

B.6 Mechanical Parameters

Based on the theory outlined in Appendix A.4.1 on page A-17, the instantaneous force acting on the armature coil is readily calculated provided the instantaneous current and inductance data is provided. The numerical simulation algorithm implemented in Maltab provided acceleration profiles for the armature coil over the specified time period. Numerically integrating this acceleration profile over the specified

time period made calculation of the instantaneous armature velocity and displacement possible. For the specified coil geometries and inputs of Tables 13, 20, 19, Figures 92 and 93 below show the resulting plots of amature coil acceleration, velocity and position over time.

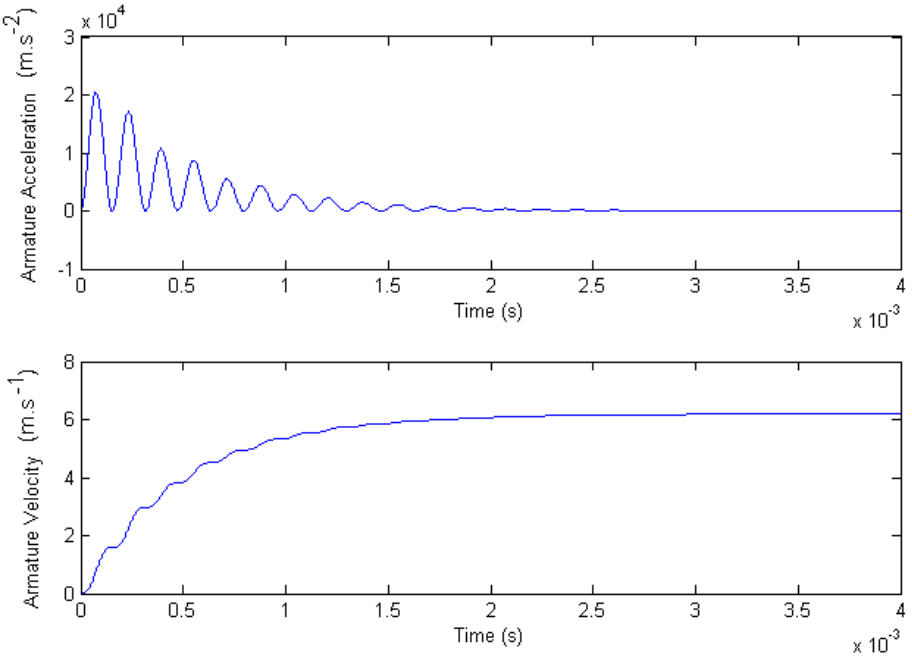

Figure 92: Instantaneous plots of armature coil acceleration and velocity.

This analysis reveals that the armature coils is subjected to an extremely high acceleration which is in the order of 1500 G's. This acceleration being proportional to the product of the armature and stator coil currents is not constant or linear; instead it is a series of pulses which decay in magnitude in a manner similar to the coil currents and capacitor voltage. The rather "bumpy" velocity profile also shown in Figure 92 reflects this pulsating acceleration profile. These results also predict an appreciable gain in armature kinetic energy over a very short time period and displacement. The armature coil displacement profile is shown in Figure 93 below.

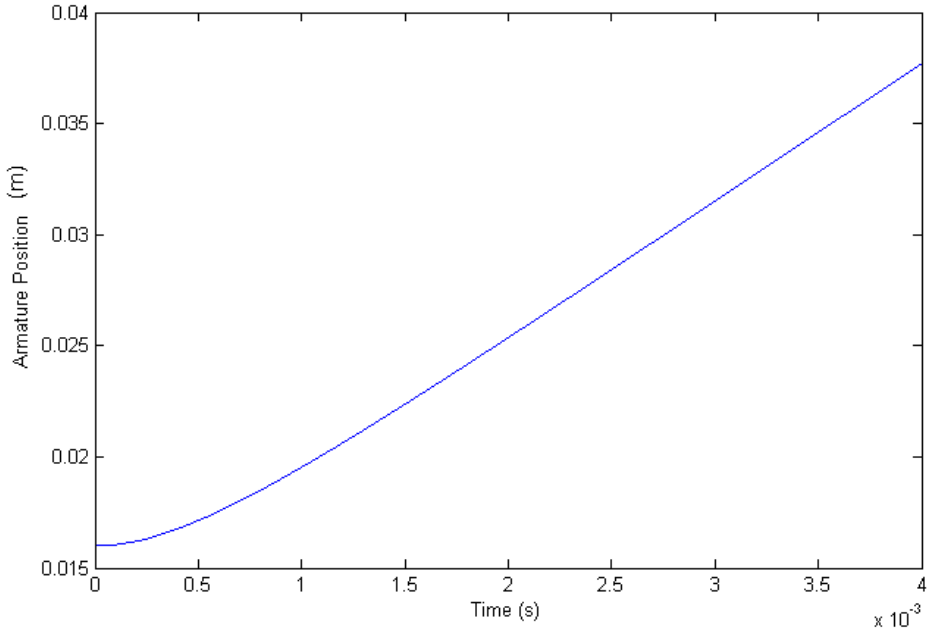

Figure 93: Instantaneous plot of armature coil position over time (ignoring friction), note the initial offset. This measurement is based on the distance between each coils center.

At this point it is important to discuss a major simplifying assumption of this simulation. The analysis described in Appendix A.4.3 on page A-23 represents the idealized operation of a P.L.I.M and does not take into account the mechanical losses from friction between the armature coil and stator coil form. This is reflected in that even though the coil currents and accelerations decays to 0 as shown in Figures 92 & 93 above, the velocity and displacement profiles continue unimpeded . In practice this is not true and despite the centralizing radial force acting on the armature coil which axially locates it preventing contact between the stator coil form and armature coil windings, friction some friction is still anticipated, resulting in armature positions and velocity profiles which look different particularly towards the end of the specified time period.

The mechanical data thus forms the P.L.I.M's predictive performance specifications, the important quantities of this analysis are summarized in Table 21 below.

Table 21: Predicted mechanical performance of a single stage test P.L.I.M.

Max Armature Velocity	$m.s^{-1}$	6.25
Max Armature Kinetic Energy	J	1.13
Max Armature Acceleration	G	1910
Stage Efficiency	%	4.54

Efficiency of the test launcher was taken in as the final armature kinetic energy over the initial electric energy stored in the capacitor before discharge. This might not seem like much, however it does exceed the initial performance specifcation of 3.5%. Also simulations carried out on the same single stage launcher show that if the projectile does not start off from rest, the efficiency is increased therefore the gain in armature kinetic energy is increased. Thus if a multiple stage launcher were built with the same coil geometry a higher overall efficiency can be achieved. This idea discussed in more fully in Appendix B.13 on page B-30.

B.7 Coil Heating

Using the heating analysis and assumptions outlined in Section A.4.5 on page A-27, the instantaneous plots of coil current can be used to calculate heating of the armature and stator coils based on the I^2R power losses. Although the coil currents are high, the pulsating nature and short time period would intuitively result in a small temperature rise in the coils. Simultaneously executing this analysis within the numerical simulation allows for instantaneous temperature of the coils to be calculated (based on the assumption of adiabatic heating) and thus the total temperature rise. The results of this simulation are summarized in Table 22 below.

Table 22: Temperature rise of stator and armature coils.

Initial Stator Coil Temperature	^{o}C	25
Stator Coil ΔT	^{o}C	0.4857
Initial Armature Coil Temperature	^{o}C	25
Armature Coil ΔT	^{o}C	0.3198

Even though the most of the energy initially stored in the capacitor dissipated as heat in the coils it is immediately evident that using such a low input energy (25J) results in an almost insignificant temperature rise as initally expected.

B.8 Stator and Armature Mechanical Stress

During the operation of the linear induction launcher, the stator and armature coils experience a radial expansive and compressive pressure respectively. These pressures and their theoretical modeling are discussed in more detail in Appendix A.4.6 on page A-28, presented here is a basic stress analysis performed to ensure that the armatures coil form is not crushed or that the copper stator coil will not "burst". Starting with the stator coil, it was assumed that this coil would not have an external support structure, and that the coil itself would form its own support structure. That said the hoop stress developed in

the coil due to the magnetic pressure is compared directly to the yield strength of copper (which is a conservative assumption because the copper wire is finely extruded and coated in enamel making its yield strength somewhat higher). The hoop stress in the stator coil is given as

$$\sigma_{hss} = p_{magnetic} \frac{r_{si}}{(r_{so} - r_{si})}$$

$$= \frac{B_z^2}{2 \cdot \mu_0} \cdot \frac{r_{si}}{(r_{so} - r_{si})} = \frac{\left(\mu_0 \frac{N_s I_{ss}}{l_s}\right)^2}{2 \cdot \mu_0} \cdot \frac{r_{si}}{(r_{so} - r_{si})}$$

$$= \frac{\mu_0 \left(N_s I_{ss}\right)^2}{2 l_s^2} \cdot \frac{r_{si}}{(r_{so} - r_{si})} = 6.76\,\text{Mpa}$$

The typical yield stress of copper (70 Mpa) greatly exceeds the maximum hoop stress that will be developed in the copper coils with a safety factor close to 10. Furthermore, as discussed in Appendix A.4.6 on page A-28 this is a very conservative design estimate as it assumes a constant peak current which is obviously not the case as the current is a decaying oscillatory waveform and it also does not take into account the reduction of the axial magnetic field B_z when the armature is near the stator coil. As such it is expected that the actual stress to which the stator is exposed is somewhat less than the above estimate.

The armature coil however is wound on a polypropylene coilform support structure shown in Figure 94 below, the wall thickness of this form is aprroximatly 2.5 mm.

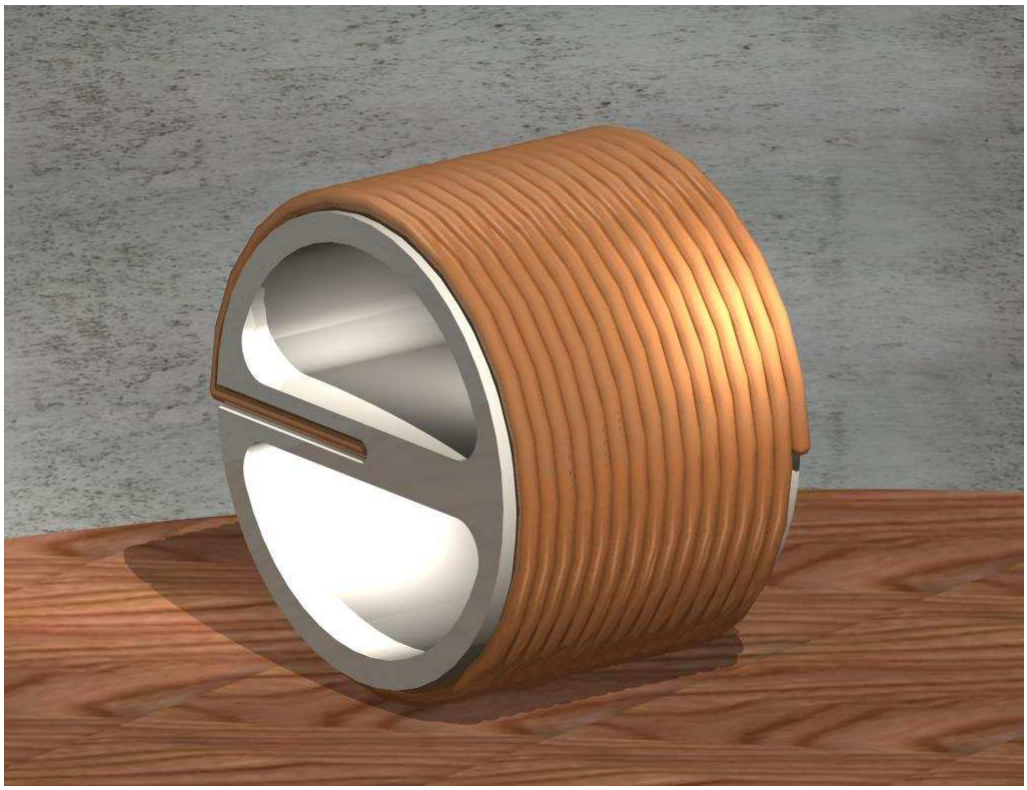

Figure 94: Conceptual 3D rendering of what the armature coil will look like.

During its passage through the active stator coil, it will experience a compressive force acting circumferentially around the armature winding surface. This is a result of the interaction of circumferential coil current and axial magnetic field B_z. As described in Appendix A.4.6 on page A-28 The hoop stress in the armature coil form is given as

$$\sigma_{haa} = \frac{-2 \cdot b^2 \cdot p_{magnetic}}{b^2 - d^2}$$

$$= \frac{\mu_0 \left(N_s I_{ss}\right)^2}{2 l_s^2} \cdot \frac{-2 \cdot b^2}{b^2 - d^2} = 2.65\,\text{Mpa}$$

The yield stress of polypropylene is in the order or 12 Mpa which exceeds the hoop stress developed in the support structure by a safety factor greater than 4. Again similarly to the stator coil analysis, this analysis is rather conservative in that it also assumes a uniform peak stator coil current and also does not account for the reduction of axial magnetic field B_z due to the armatures passing through the stator coil. It should also be noted that the central diametrical support structure of the armature form needed for routing the wire thought the coils central axis to short the single layer coil effectively will serve to strengthen the armature support structure, also not taken into account is the actual structural support of the armature coil itself and its contribution to the armatures total structural rigidity.

Clearly evident from this analysis is that the radial or expansive forces to which the armature and stator coils are subjected are not of great concern at the specified operating voltages and energies.

B.9 Capacitor Selection

The important considerations regarding capacitor selection and capacitor bank design were mainly the current handling capability and ohmic heating of the device in addition to the more obvious operating voltage limitation. In the operation of the launcher the oscillatory currents flowing in the capacitor are of a very high magnitude which greatly exceeds many capacitors continuous R.M.S rating. However this rating can be exceeded for very short m.sec events provided the capacitor is not heated excessively or subjected to voltages exceeding its rating. As such this section will present the basic calculations (which were implemented in Matlab for simplicity and completeness of the simulation code) done to verify the suitability of the chosen capacitor used in the tank circuit capacitor bank. Apart from device limits, many of the variables needed for these calculations were determined by the device manufacturer and are presented in the device's data sheet.

Figure 95 below shows the data sheet of the metalized polypropylene capacitor which is used tank circuit capacitor of the single stage test launcher.

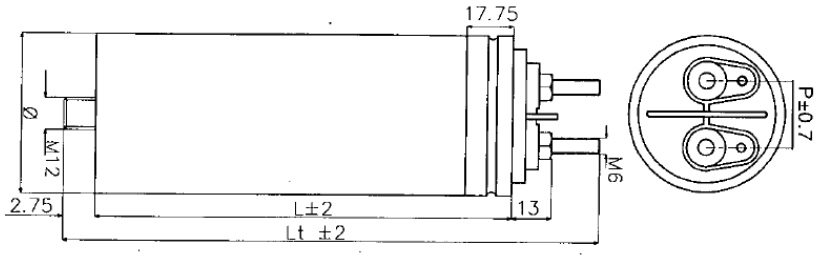

ELECTRICAL SPECIFICATION

Part no.	C µ F	Urms	Tgδ MAX	ESR mΩ	du/dt V/µs	Irms A	Lpkr A
01-05-0128	50	440V	0.0033	10	20	16	1000

MECHANICAL SPECIFICATION

Part no.	C µ F	Termination		P	L	Lt	∅
		Screw	Nut				
01-05-0128	50	6 x 30HEX	M6X5HEX	24	150	192.75	60

Technical data	
Temperature range (case):	-25°C to +70°C
Capacitance tolerance:	±5%
Test voltage terminal to terminal:	1.5 x rated voltage
Test voltage terminal to case:	1.5 KV 50 Hz 60S
Permissible relative humidity:	Annual average < 95% on 30 days/year, continuously
	100%, on other days occasionally 100%
	Dewing not admissible
Life expectancy:	≥ 30 000 hours at Un

Figure 95: Afcap metalized poloypropelyne capacitor data [35].

The specifications which the capacitor had to meet were determined using the launcher's numerical simulation results to be discussed in the sections that follow.

B.9.1 Current Handling

As shown by this devices datasheet, a single capacitor is capable up supplying a peak repetitive pulse current of 1000 A. If however 6 of these capacitors are connected in parallel as shown schematically and physically in Figure 96 below.

Figure 96: Actual capacitor bank used in laboratory test launcher (Left) and schematic representation of this bank(Right).

Not only is the total bank capacitance raised to 300 μF (assumed close enough to the origional input parameter and specification of 315 μf) but the peak repetitive pulse current capability of the bank is also raised to 6000 A. The peak repetitive pulse current for the launcher is given as system is given as

$$I_{pkr} = C \cdot \frac{dV}{dt}$$

Where C is the bank capacitance and $\frac{dV}{dt}$ is conservativly set to the maximum rate of voltage rise in the capacitor and is calculated from the simulation results for the instantaneous capacitor voltage over time V_s as shown in Figure 97 below.

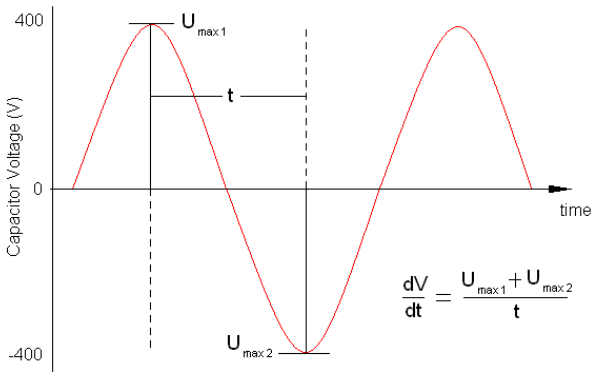

Figure 97: Illustrating how $\frac{dV}{dt}$ is calculated for a given voltage waveform.

Table 23 below effectively compares the specifications of the capacitor bank (of 6 capacitors) to the operating specifications set by the launchers simulation. It is immediately clear that the peak repetitive

pulse current rating of the bank greatly exceeds the operating currents it will be subjected to during the launchers operation.

Table 23: Important performance specifications of the single stage launcher capacitor bank.

	Simulation Requirement Specification	Capacitor Bank Specification
Peak Repative Pulse Current	1574 A	6000 A
Max $\frac{dV}{dt}$	5.04 V/μsec	20 V/μsec

B.9.2 Heating Energy Loss

In practice the capacitor is not an ideal device, having a small series resistance which resulting in the capacitor dissipating some energy as heat. More advantageously though is that when using 6 capacitors in parallel the total equivalent series resistance of the bank will be 6 times less (resistors in parallel) and so energy lost to heating the capacitor is given as

$$E_{capheat} = \frac{1}{6}\int_0^{t_f} I_{ss}^2 \cdot ESR\, dt = 0.27\,\text{mJ}$$

This was numerically integrated while running the time step numerical launcher simulation and the results revealed that the energy dissipation was small enough to be considered insignificant hence neglecting its inclusion in the energy audit of Appendix B.11 on page B-26. It was also assumed that such a small amount of energy dissipation would result in a neglegable temperature rise in the capacitor.

B.10 Switch Gear Selection

Since it was decided early in the project to use IGBTs for switching the high voltage and currents from the capacitor into the stator coil, the important considerations were studied carefully. The major concerns have already been identified and discussed at great length in Appendix A.5.5 on page A-39. Presented here is the thermal analysis and its results used to determine the suitability of the chosen IGBT module. All of the following results and graphs are based on the same 25 J single stage launcher as discussed throughout this section. Figure 98 belows is a summary of the datasheet for the chosen IGBT device which includes the anti parallel diode.

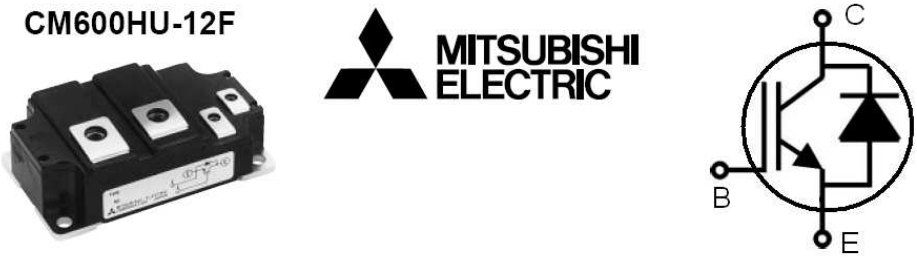

MAXIMUM RATINGS (T_j = 25°C)

Symbol	Parameter	Conditions	Ratings	Unit
V_{CES}	Collector-emitter voltage	G-E Short	600	V
V_{GES}	Gate-emitter voltage	C-E Short	±20	V
I_C	Collector current	T_C = 25°C	600	A
I_{CM}		Pulse (Note 2)	1200	
I_E (Note 1)	Emitter current	T_C = 25°C	600	A
I_{EM} (Note 1)		Pulse (Note 2)	1200	
P_C (Note 3)	Maximum collector dissipation	T_C = 25°C	1420	W
T_j	Junction temperature		–40 ~ +150	°C
T_j	Junction temperature		–40 ~ +150	°C

ELECTRICAL CHARACTERISTICS (T_j = 25°C)

Symbol	Parameter	Test conditions	Limits			Unit
			Min.	Typ.	Max.	
$V_{GE(th)}$	Gate-emitter threshold voltage	I_C = 60mA, V_{CE} = 10V	5	6	7	V
I_{GES}	Gate leakage current	V_{GE} = V_{CES}, V_{CE} = 0V	—	—	80	µA
$V_{CE(sat)}$	Collector-emitter saturation voltage	T_j = 25°C, I_C = 600A, V_{GE} = 15V	—	1.6	2.2	V
		T_j = 125°C, I_C = 600A, V_{GE} = 15V	—	1.6	—	
$t_{d(on)}$	Turn-on delay time	V_{CC} = 300V, I_C = 600A, V_{GE1} = V_{GE2} = 15V, R_G = 3.1Ω, Inductive load switching operation, I_E = 600A	—	—	600	ns
t_r	Turn-on rise time		—	—	400	
$t_{d(off)}$	Turn-off delay time		—	—	900	
t_f	Turn-off fall time		—	—	250	
t_{rr} (Note 1)	Reverse recovery time		—	—	300	ns
Q_{rr} (Note 1)	Reverse recovery charge		—	11.7	—	µC
V_{EC} (Note 1)	Emitter-collector voltage	I_E = 600A, V_{GE} = 0V	—	—	2.6	V

Note 1. I_E, V_{EC}, t_{rr}, Q_{rr}, die/dt represent characteristics of the anti-parallel, emitter to collector free-wheel diode. (FWDi).
2. Pulse width and repetition rate should be such that the device junction temp. (T_j) does not exceed T_{jmax} rating.
3. Junction temperature (T_j) should not increase beyond 150°C.

Figure 98: Data sheet summary of the important parameters for the IGBT (Mitsubishi CM600HU-12F) used to switch the test launchers tank circuit [37].

This depth of analysis for the component is required because during the operation of the linear induction motor, the IGBT & diode will be subjected to currents way beyond that of its rated continuous operating current. As discussed the limiting factor of the IGBT current capability is its junction temperature. Therefore the current can exceed the devices continuous current ratings provided that that the junction temperature does not exceed the devices absolute maximum rating. Figure 99 below shows this "pulsating" power dissipation through the IGBT and the diode over the same time period. Furthermore these power pulses are alternating, reflecting the fact that the IGBT conducts for the positive half cycle while the diode conducts for the negative half cycle. Also shown is the average power dissipation of the aforementioned power curves, which was used in calculating the maximum temperature rise of the junction for each power pulse as given below. Thus giving the total operational temperature rise as the summation of temperature increases for all IGBT and Diode power pulses where each temperature rise is estimated as the product of the average power and the transient thermal impedance of the conducting device as shown [40].

$$\triangle T_{IGBT} = P_{avgIGBT} \cdot Z_{thIGBT}$$

$$\triangle T_{Diode} = P_{avgIGBT} \cdot Z_{thIGBT}$$

$$T_j = \sum \triangle T_{IGBT} + \sum \triangle T_{Diode} + T_{jinitial}$$

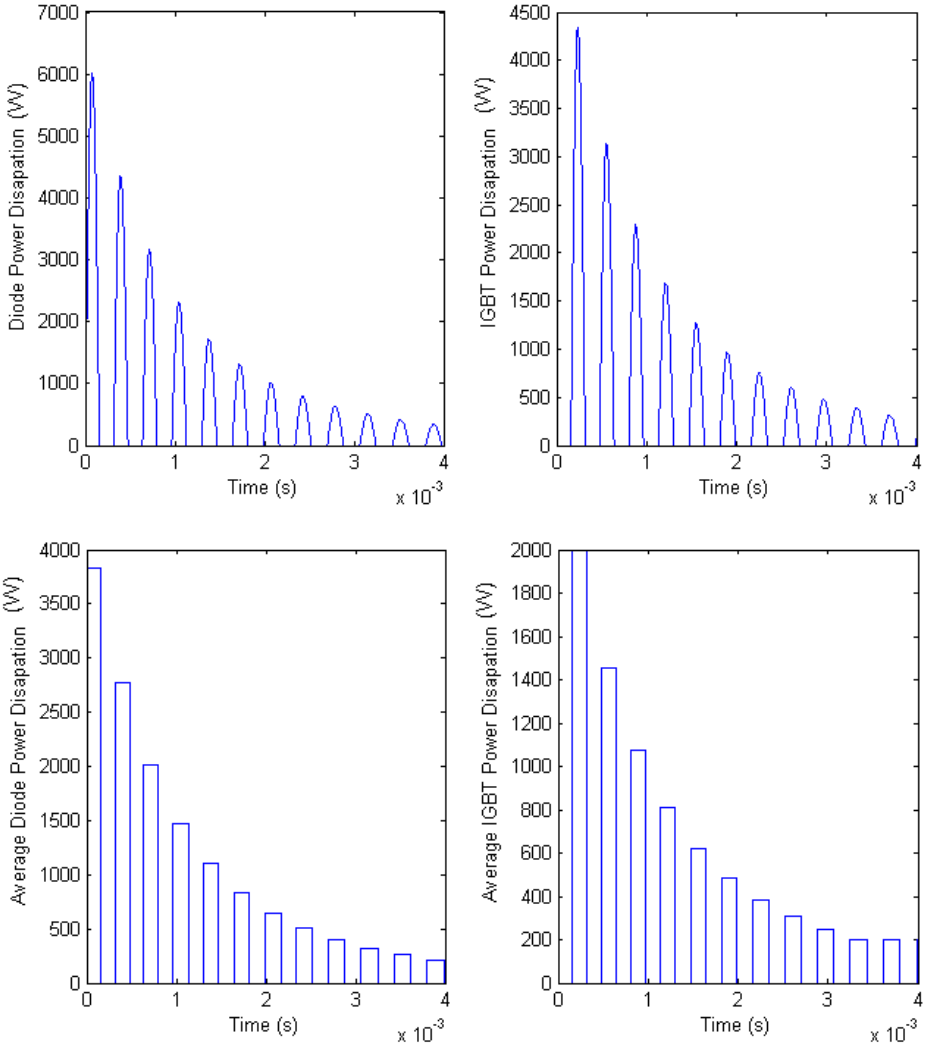

Figure 99: Actual and avergage power dissipation through IGBT and diode for a single launching event.

The values of Z_{th} are dependant on the length or period of the given power pulse and are provided in the devices data sheet, in the form of the log graph shown in Figure 100 below.

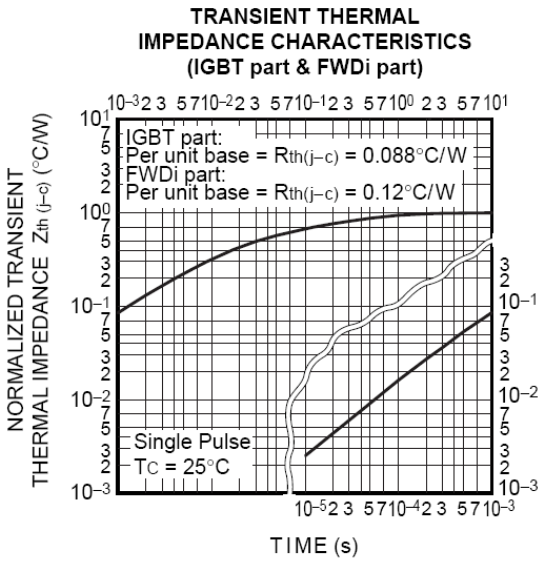

Figure 100: Transient thermal impeadance graph of the Mitsubish CM600HU-12F used to switch the tank circuit of the laboratory test launcher [37].

Using the transient thermal impedance value corresponding to the pulse periode of the power (period = 20μ.sec) as shown in Figure 100. The results of this thermal analysis are summarized below in Table 24, assuming an initial junction temperature to be that of room temperature (25^{o}C). Furthermore this analysis can be considered some what conservative as it does not take into account the heatsink to which the device is mounted.

Table 24: Peak and Average power dissipation through switching device and estimated junction temperature at the end of one launch.

Peak Power (IGBT)	W	4343
Peak Power (Diode)	W	6012.5
Max Average Power (IGBT)	W	2761
Max Average Power (Diode)	W	3825
IGBT Z_{th}	^{o}C/W	0.0035
Diode Z_{th}	^{o}C/W	0.0035
Device Juntion Temp	^{o}C	118

This thermal analysis reveals the junction temperature of the IGBT with anti-parallel diode will not exceed the maximum limit of 150^{o}C for a single armature launch operation and is in fact within the safe operating limit of 125^{o}C as quoted by the device data sheet.

B.11 Energy Balance

Again using the approach outlined in Appendix A.4.4 on page A-26 a full instantaneous energy audit was performed at each time interval during the numerical simulation to confirm the energy balance equation presented below.

$$E_{capinitial} - E_{capacitor} - E_{magnetic} - E_{heat} - E_{kinetic} = 0$$

Noting that all analysis and performance quantities are based purely on the differential equations described in Appendix A.4.1 on page A-17, testing the simulation in terms of an energy balance will verify its correctness to a great extent. As mentioned however, this was one particular part of the analysis which was vulnerable to the pitfalls of the numerical method. Figures 101 & 102 are both for the exact same simulation inputs and conditions, however Figure 101 uses a much larger (1000 times greater) time step or Δt than Figure 102 resulting in a much quicker simulation which is however plagued by the rounding errors reflected by the oscillatory energy balance that decays to a negative number, suggesting that more energy has been used in the system than was originally provided by the capacitor. This is obviously an incorrect result and running the same simulation with a much smaller Δt resulted a much longer simulation time but it did however completely eliminate the rounding errors in the energy balance. This is illustrated in Figure 102 where the energy balance is 0 J at all times throughout time period of interest.

All the values used in quantifying system energies are determined through solving the differential equations for the lumped parameter circuit discribed in Appendix A.4.1 on page A-17, this energy balance is thus indeed a profound verification of the model since it has correctly predicted the Law of Conservation of Energy. This serves as excellent evidence that the simulation is at least correct in an ideal sense (ignoring of course mechanical friction and circuit wiring resistances). Both simulations of Figures 101 & 102 are of the same time period, the time step of both simulations however was different as tabulated in Table 22 below.

Table 25: Time step data for Figures 101 & 102.

Large Δt simulation (Figure 101)	μsec	10
Small Δt simulation (Figure 102)	n sec	10

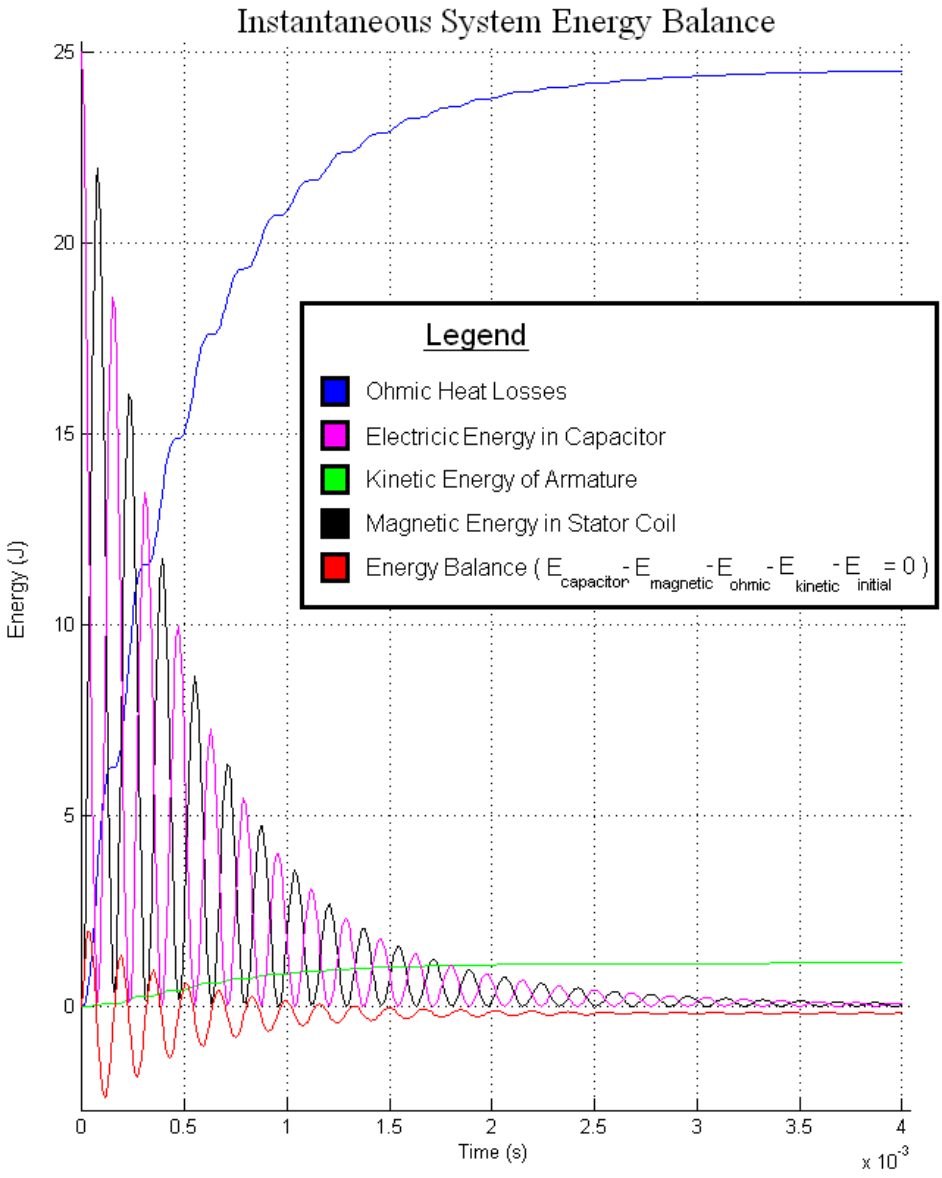

Figure 101: Instantaneous energy balance of a single stage 25J Stage using a high Δt reflecting the only numerical error encountered in the launchers analysis.

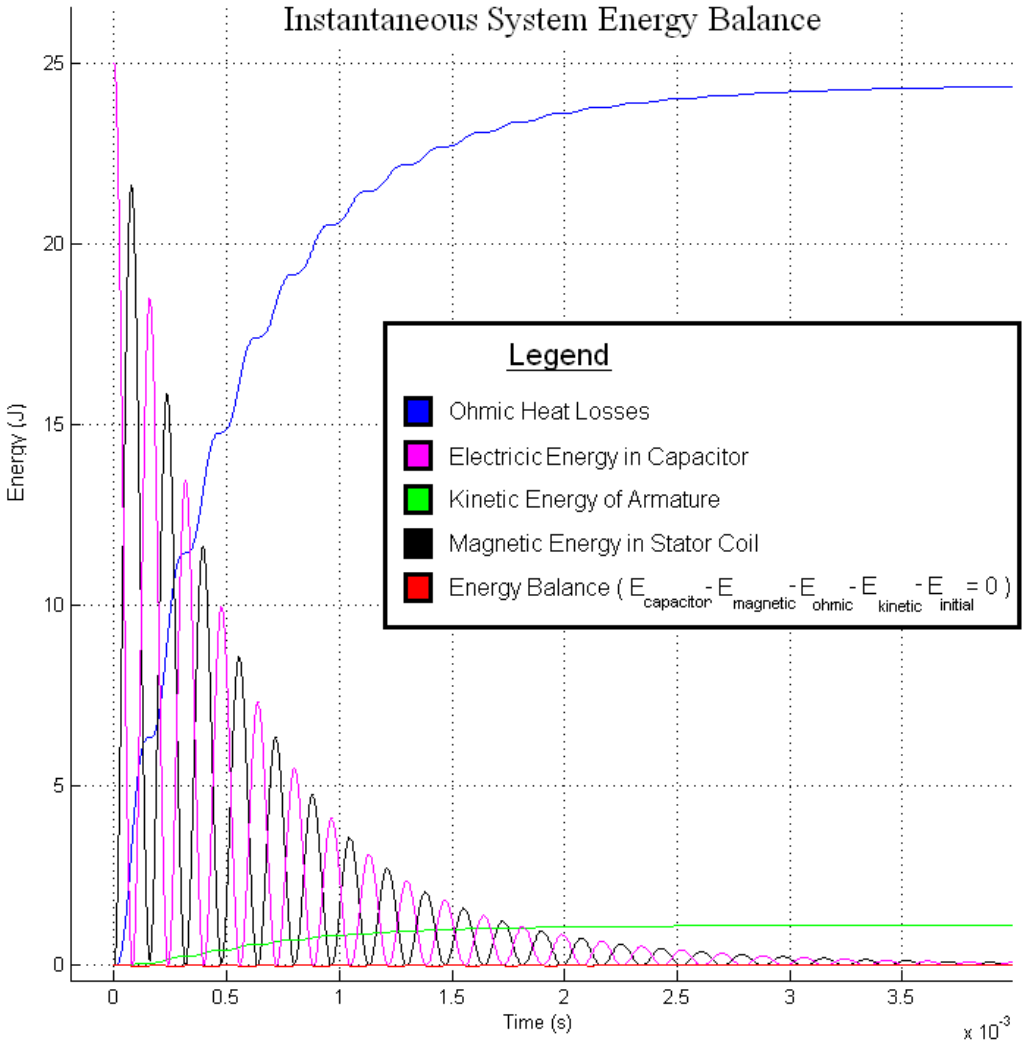

Figure 102: A similar instantaneous energy balance of the same single stage 25J launcher but with a much smaller Δt. Notice that the oscillatory anomaly of the energy balance found in Figure 101 has been eleminated.

Further analysis of the system energies illustrated in Figure 102 above also reveals that the oscillatory sharing of energy between a capacitor and inductor, which decays in magnitude as the systems energy is dissipated as heat in the coils (and of course a gain in armature kinetic energy). The rate at which the energy in capacitor and inductor decays is obviously related to the circuit resistance. The simulation reflects the relationship between system energies and resistive losses in that the heating curve has a similar (but inverse) appearance to that of the capacitor and inductor energy curves (because total heat dissipated increases as capacitor and inductor energy decreases). This analysis gives invaluable insight into where the systems energy is at any point in time during the launchers operation and illustrates that most of the losses are due heat dissipation.

This energy analysis also reveals that rate at which armature kinetic energy increases after t=1.75 msec is very small (largely due to the armature coil being outside of the induction length l_b), at this point

there is still a small but significant amount of energy which can be recovered and used in the proceeding stages as opposed to being dissipated as heat. One possible implementation for such an energy recovery system has already be described in Appendix A.2.2.1 on page A-12

B.12 Armature Initial Position Investigation

As discussed in Section A.4.2 on page A-20 on page it is clear that the operation and performance of a given launcher stage is greatly dependant on the coil separation when power is applied to the stator coil. To determine the variation on luancher performance with coil seperation, the simulation code was used to test various initial positions and plot the variation of performance in terms of final final velocity and stage efficiency. The results of this investigation are shown graphically in Figure 103 below, with more details regarding the positions tested and results of analysis shown in Table 26 following.

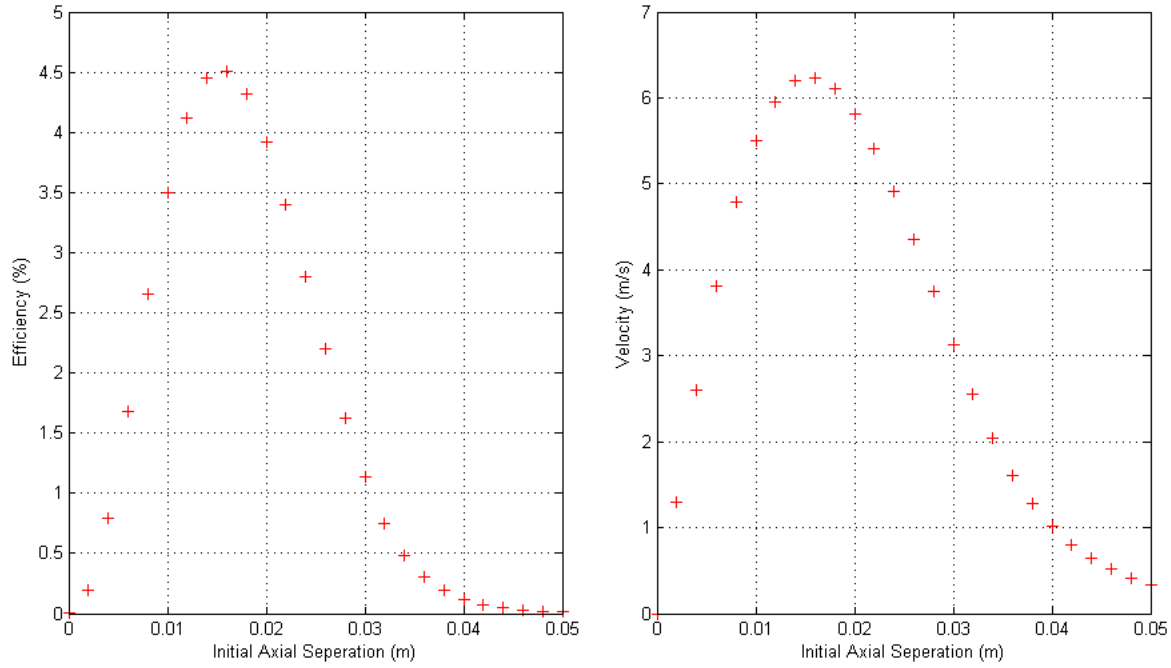

Figure 103: Plots of the single stage launchers efficiency and velocity for various initial armature and stator coil separations.

This analysis correctly illustrates that at when the axial separation of the coils is 0 mm (i.e. the coils are axially located with the armature coil centrally located within the stator coil) the armature does not accelerate in either direction since the mutual inductance gradient G and thus the accelerating force F_z is zero. The resulting efficiency is 0 %, however as coil separation is increased the stage efficiency increases resulting in higher armature velocities. This performance gain in acceleration increases until it hits its peak after which performance begins to drop as separation is increased, reflecting the fact the armature is to far outside of the induction length l_b for efficient energy transfer to take place.

Table 26: Information regarding the armature position analysis implemented in Matlab.

Range of Position tests	m	0 - 0.05
Distance between each position	mm	0.002
Total positions evaluated	no.	26
Position yielding highest performance	mm	0.016

B.13 Multiple Stage Investigation

A complete six stage launcher was also modeled to determine if efficiency of the launcher would increase as additional acceleration stages were added. The coil geometries and initial conditions are identical to those shown in Table 13 on page B-4 & Table 19 on page B-12 while all numerical simulations were carried out with the specified time step shown in Table 18 on page B-12. The results of this analysis are illustrated in Figure 104 below.

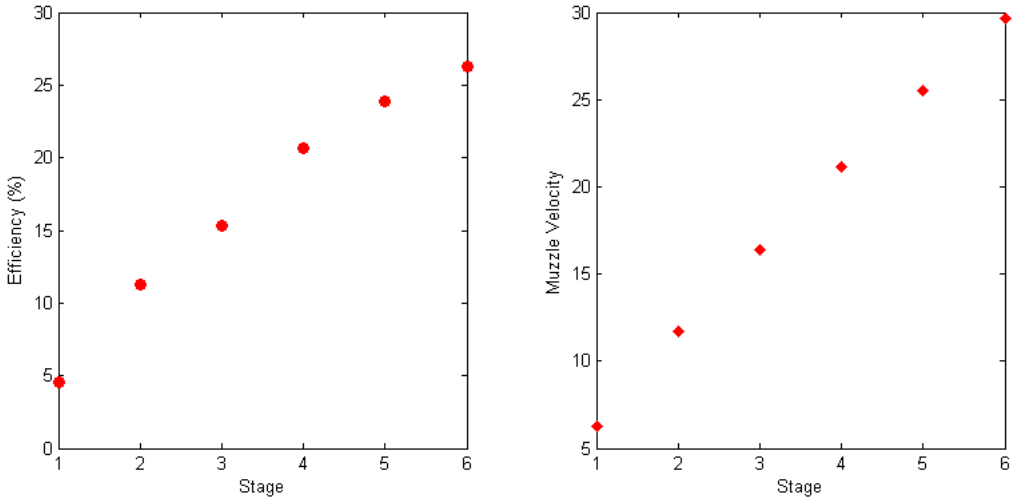

Figure 104: Graphic representation of the proposed 6 Stage P.L.I.M theoretical stage efficiencies and velocities.

This analysis has revealed that each proceeding stage operates at a higher efficiency than its preceding stage. This is a result that has been well noted in the literature and is largely due to the fact that any given launcher will perform better if the armatures initial velocity is increased, however the gains from this do approach a limit and is reflected by the decreasing gradient of the efficiency curve in Figure 104. The gains will decrease because the armature eventually reaches a velocity where it passes the induction length to quickly for effective energy transfer to take place. To compensate for this effect, the initial separation of the coils for the final 3 stages is slightly closer than the preceding 3 stages. Also shown is

the final velocity reached at the end of each acceleration stage showing that this launcher can theoretically and ideally achieve an armature velocity just below of 30 $m.s^{-1}$, a more detailed overall summary of the proposed 6 stage linear induction launchers performance is provided in Table 27 below.

Table 27: Proposed 6 Stage P.L.I.M theoretical performance results.

Stage	Efficiency (%)	Velocity ($m.s^{-1}$)	Armature Kinetic Energy (J)	Initial Coil Seperation (mm)
1	4.5	6.25	1.1	16
2	11.3	11.67	4.0	16
3	15.2	16.36	7.8	16
4	20.6	21.10	12.9	10
5	23.5	25.45	18.9	10
6	25.8	29.50	25.2	10

B.14 Summary

This appendix has covered the complete analysis used in developing the single stage launcher and conceptual multi-stage system based around this single stage device. These calculations have thus show that the launcher meets many of the initial Performance Specification Requirements as listed Table 1 on page 5 in addition to providing new specifications for the systems and components whose selection/construction and integration will form the comple linear induction launcher system. These calculations are however based on a few simplifying assumptions as listed below.

1. Tank circuit resistance is assumed to be negligible and only the estimated stator coil resistance is considered.
2. The associated voltage drop across the IGBT and diode have an insignificant effect on the tank circuits behavior.
3. The on-state resistance of the IGBT and diode is insignificant.
4. The system is assumed to be mechanically ideal and as such friction is neglected.

These calculations do more than just specify systems performance they also form the theoretical hypothesis of the systems behavior which will be critically compared, with insight to the actual performance of the system in practice.

C List of Specifications

Contents

Tables

C.1 Introduction

This Appendix outlines with justification, the performance specifications for the laboratory test launcher. These specifications fall into two main categories as discussed below.

- Performance Requirement Specifications

  These detail the main operating specifications which the launcher system must achieve in order to view the completed systems as a success. These specifications were drawn up very early in the projects development and many formed part of the original project proposal.

- Other Specifications

  These are the specifications which the many systems that form the linear induction motor must meet in order for their integration to result in a complete and operating linear induction launcher system. They are typically developed as stages of the system's design are completed. They also include dates for project deliverables, cost and saftey specifications.

Wherever possible the following specifications detail the required performance of the device and or its systems and not the device itself. However in some cases it was necessary to specify items relating to system as they form an important aspect of the expect systems performance. The actual parameters achieved in practice are also listed for convenient comparison.

C.2 Performance Specifications List

NOTE:

D = Demand

W = Wish

TBC = To Be Confirmed

Table 28: Complete specifications of the concept 6 stage linear induction launcher and the single stage test linear induction launcher.

D/W	Requirement	Desired	Actual	Rev	Location
1. Performance Specification					C.3.1
1.1 Main Performance Requirements Specification					C.3.1.1
D	Modular construction	Yes	Yes	0	C.3.1.1.1
D	Operating energy	150 J	144 J	0	C.3.1.1.2
D	Stage energy	25 J	24 J	0	C.3.1.1.3
D	Stage efficiency	3.5 %	TBC	0	C.3.1.1.4
W	Operating voltage	<500 V	400 V	0	C.3.1.1.5
W	Total length	< 1 m	500 mm	0	C.3.1.1.6
D	Robust and sturdy test rig	Yes	Yes	0	C.3.1.1.7
1.2 Launcher Barrel Form Specification					C.3.1.2
W	Made of a non-conducting material	Yes	Yes	0	C.3.1.2.1
W	Length	<500 mm	500 mm	0	C.3.1.2.2
D	Outer diameter	50 mm	50 mm	0	C.3.1.2.3
W	Wall thickness	<5 mm	2 mm	0	C.3.1.2.4
1.3 Stage Capacitor Bank Specification					C.3.1.3
W	Voltage rating	400 V	440 V	0	C.3.1.3.1
W	Bank capacitance	312.5 μF	300 μF	0	C.3.1.3.2
W	Peak repatative current	2300 A	6000 A	0	C.3.1.3.3
W	E.S.R	<10 mΩ	1.67 mΩ	0	C.3.1.3.4
D	Non-polarized polypropylene dielectric	Yes	Yes	0	C.3.1.3.5
D	Low E.S.L	Yes	Yes	0	C.3.1.3.6
1.4 Single Stator Coil Specification					C.3.1.4
W	Stator coil inner diameter	50 mm	50 mm	0	C.3.1.4.1
W	No. of stator coil turns	16	16	0	C.3.1.4.2
W	Stator coil wire wire	2.3 mm	2.3 mm	0	C.3.1.4.3
W	Stator coil length	37 mm	38 mm	0	C.3.1.4.4
W	Stator coil resistance	11 mΩ	6 mΩ	0	C.3.1.4.5
D	Sturdy mounting/securing of coil to barrel form	Yes	Yes	0	C.3.1.4.6
1.5 Armature Coil Specification					C.3.1.5
D	Armature mass	58 g	68 g	0	C.3.1.5.1

D/W	Requirement	Desired	Actual	Rev	Location
W	Armature coil inner diameter	40 mm	40 mm	0	C.3.1.5.2
W	No. of armature coil turns	15	14.5	0	C.3.1.5.3
W	Armature coil wire diameter	1.8 mm	1.8 mm	0	C.3.1.5.4
W	Armature coil length	27.4 mm	30 mm	0	C.3.1.5.5
D	Initial stator and armature coil offset	16mm	16mm	0	C.3.1.5.6
W	Armature coil resistance	13.6 mΩ	TBC	0	C.3.1.5.7
D	Armature coil form	Yes	Yes	0	C.3.1.5.8
D	Sturdy mounting/securing of coils to form	Yes	Yes	0	C.3.1.5.9
1.6 IGBT Device Specification					C.3.1.6
D	Tolerable junction temperature rise	$>$ 118^{o}C	150^{o}C	0	C.3.1.6.1
D	Voltage rating	450 V	600 V	0	C.3.1.6.2
W	Peak repetitive pulse current	2300 A	2300 A	0	C.3.1.6.3
W	Gate drive voltage	4.5 V -20 V	16 V	0	C.3.1.6.4
D	Anti-parallel diode	Yes	Yes	0	C.3.1.6.5
1.7 Control Circuitry					C.3.1.7
D	Use GT16 mMicroprocessor	Yes	Yes	0	C.3.1.7.1
D	Drive on voltage (Output high)	16 V	16 V	0	C.3.1.7.2
D	Drive off voltage (Output Low)	$<$ 4.5V	0.5 V	0	C.3.1.7.3
W	Pulse period	8 msec	2 sec	0	C.3.1.7.4
2. Experimental Measurements					C.3.2
D	Stator current	Yes	Yes	0	C.3.2.1
W	Capacitor voltage	Yes	No	0	C.3.2.2
W	Armature velocity tracked with optical sensors	Yes	No	0	C.3.2.3
3. Safety					C.3.3
D	Device must be properly grounded	Yes	Yes	0	C.3.3.1
D	Control circuity for IGBT optically isollated	Yes	Yes	0	C.3.3.2
D	IGBT properly mounted to heat sink	Yes	Yes	0	C.3.3.3
4. Cost					C.3.4
	Total cost	$<$ R 1500.00	$>$ R 2500.00	0	C.3.4.1
5. Dates for deliverables					C.3.5
D	Parts drawings submissions	Before 07/09/2007	22/08/2007	0	C.3.5.1
D	Final report submission	31/10/2007	31/10/2006	0	C.3.5.2
D	Presentation	20/11/2007	20/11/2007	0	C.3.5.3

C.3 Specification Justification

C.3.1 Performance Specifications

C.3.1.1 Main Performance Requirement Specification

C.3.1.1.1 Modular construction It was required from the onset that the test rig should be designed in such away that its construction would be modular, allowing for this project to conduct small scale test research on the technology first before any further investment is committed to its expansion and development. Additional benefits for building a multistage pulsed linear induction launcher include improved overall efficiency and stage capacitor energy recycling capability. This report must investigate the feasibility of the technology and compare the theoretical and practical performance of a single stage launcher which will ultimately form part of a 6 stage modular linear induction launcher.

C.3.1.1.2 Operating energy The initial energy input specification of 150 J (stored in capacitors) was quoted for a complete 6 stage linear induction launcher. This projects scope will only allow for a single stages construction and testing. If its performance is satisfactory and if time allows the construction additional stages may be included in the projects scope.

C.3.1.1.3 Stage energy The specification of a 6 stage launcher operating on an initial energy of 150 J implies that each stage be operated on 25 J, thus the test launcher has been designed to operate with a maximum initial stage energy input of 25 J.

C.3.1.1.4 Stage efficiency This specification was set very early in the launchers development and was initially set as a bench mark based on the performance of reluctance launchers, which at the time was thought to be the best way of making a coil gun. However in light of an extensive literary review it was determined that a coil gun operating on the principle of induction would allow for overall and stage efficiencies far exceeding the specified 3.5 %.

C.3.1.1.5 Operating voltage The typical operating voltages seen in the literature are in the order of 10^3 V, presumably this is because the ohmic losses due to resistance in the coils is decreased by reducing pulsed current, however to keep power the same a higher voltage is required. Operating a device at high voltage has its obvious benefits, however when only dealing with such a small stage energy it becomes impractical and extremely expensive. As such, the launcher must be designed to operate on a voltage less than 500 V, while maintaining stage energy of 25 J.

C.3.1.1.6 Total length This refers to the total allowable length of the complete 6 stage linear induction launcher (defined as the longest side of the devices foot print) and is specified to be less than 1m. This specification has been made purely for the sake of miniaturization and also reflects the impressive acceleration capabilities of a linear induction motor.

C.3.1.1.7 Robust and sturdy test rig The test rig must be a quality device worthy of further research into the subject. A robust and sturdy design will go a long to make this will happen. Also because it is an electrical device the design must also strive for stability, rigidity requiring careful assembly and quality wirework to ensure no unfortunate accidents occur.

C.3.1.2 Launcher Barrel Form Specification

C.3.1.2.1 Made of a non-conducting material This specification relates to the most important material property required of the launcher barrel form. It is important that the form be made of a non conducting material to avoid the induction of eddy currents in the form itself, which would result in significant losses that would manifest in the heating of the coil form.

C.3.1.2.2 Length This specification relates to the actual length of barrel required for a full 6 stage linear induction launcher and is specified to be less than 500 mm again purely for miniaturization of the device.

C.3.1.2.3 Outer diameter Research on the subject, as discussed in the literature review reveals that for a given input power, the launchers performance will improve as its barrel bore was increased. Of course the improvements gained from increasing stator coil diameter eventually become less significant and (to borrow a phrase from economics) the marginal utility in doing so becomes negative. For this reason a typical diameter of 50 mm has been specified as the outer diameter onto which the stator coil will be wound directly.

C.3.1.2.4 Wall thickness To improve inductive coupling (and thus performance) of the launcher, the armature stator coil radius ratio $\frac{r_a}{r_s}$ must be as practically close to 1 as possible. To achieve this, the wall thickness of the stator coil form must be as thin as possible and thus a preliminary wall thickness has been specified to be less than 5 mm.

C.3.1.3 Stage Capacitor Bank Specification

C.3.1.3.1 Voltage rating This specification is set to in order to meet one of the projects primary objectives; that being to construct a pulsed linear induction launcher capable of operating on practical power and energy sources. This is an advantageous design objective in that it is a lot easier and cheaper to acquire low voltage power electrical components and devices. As such this projects initial operating voltage which is the voltage the capacitor must be able to tolerate is specified as 400 V, a voltage readily available in laboratory conditions.

C.3.1.3.2 Bank capacitance Since the energy stored in a capacitor is proportional to its capacitance and the voltage to which the capacitor is charged, having specified the initial system energy input of 25 J and the operating voltage the stage capacitance is implicitly specified as well. The above relationship is expressed as

$$E_{cap} = \frac{1}{2}CV^2$$

Solving for C in the above equation and substituting the specified voltage and input energy the stage capacitance is specified as 312.5μF, rounding this figure to the closest 100 μF, the bank capacitance is specified as 300μF.

C.3.1.3.3 Peak repatative current The desired peak repetitive current is a calculated in the numerical launcher simulation and represents the peak current achieved by the oscillatory current discharge waveform produced when the capacitor is discharged into the stator coil. Assuming this peak current does not decay and setting it to the max possible value determined in the simulation a capacitor chosen to meet this requirement will be a very conservative choice. Determined by calculation the capacitor bank (comprising of 6 identical capacitors connected in parallel) has a peak repetitive current rating of 6000 A greatly exceeding the required 2300 A specification determined by the launchers theoretical model.

C.3.1.3.4 E.S.R During the operation of a the linear induction launcher large currents will flow in and out of the capacitor, therefore the capacitor must ideally have a low equivalent series resistance to reduce $I^2 \cdot ESR$ heating losses in the capacitor which would result in a reduced efficiency and possible damage to the capacitor. Since the max operating currents of the launcher are in the order of 10^3 A, a series resistance which is less than 10 mΩ will result in a power dissipation of less than 10 W. Further advantages of using capacitors in parallel is that the bank resistance will be only 1.67 mΩ thus greatly reducing the heating of each capacitor within in the bank.

C.3.1.3.5 Non-polarized polypropylene dielectric The operation of a pulsed linear induction motor involves a bipolar oscillatory current in the tank circuit. As such the capacitors must thus be non-polarized in order to tolerate the reverse voltages and currents applied to it. A.C capacitors options were well researched and the findings are presented in the literature review. Polypropylene capacitors must be used as these showed to be the most attractive in that they have relatively large capacitances, high operating voltage ratings, low cost, great availability, low E.S.R and E.S.L.

C.3.1.3.6 Low E.S.L The literature review revealed that the frequency of oscillation of the launchers current and voltage would be in the order of 5 kHz; as such any additional series inductance in the tank circuit would result in an appreciable reactance in the tank circuit which may adversely effect the launchers operation. The capacitor used must therefore feature this design attribute.

C.3.1.4 Stator Coil Specification

C.3.1.4.1 Stator coil inner diameter In light of the extensive literature on the subject it was clear that maximizing the stator coils diameter would greatly improve a launchers performance. A reasonable diameter was estimated to be around 50 mm. This was a practical diameter for which a coil form could be readily bought of the shelf. Since the stator will be wound directly onto the barrel form its inner diameter is specified to be equal to the outer diameter of the barrel form (which is 50mm).

C.3.1.4.2 No. of stator coil turns The capacitor being completely specified, the value of the stator coil inductance must be chosen such that the peak current is limited to a value below 2500 A and operating frequency of operation below 3 kHz. This limitation is mainly to ensure that a reasonably priced semiconductor switching device can easily be easilyand to reduce the possibility of the skin effect occurring in the stator coil. All these variables are related to the peak current in the circuit as shown [13].

$$I_{max} = \frac{V_s}{L_{ss} \cdot \omega}$$

This relates to the number of turns in the the number of turns on the stator coil greatly determines its self inductance. This initial estimate showed that a stator coil self inductance in the order of 10 μH would be suitable. In practice additional stator turns increases the stator coils resistively which greatly increases damping, decreasing launcher performance. Since it is expected that both coils would have a similar length, the number of turns on the stator must not be great as this would result in a heavier armature. Comparative launcher simulation tests wherein which the armature, capacitance and initial voltage were fixed, show that a 50 mm stator coil with 16 turns of 2.3 mm enameled copper wire would operate with efficiency beyond the specification of 3.5% and the peak discharge current to less than 2500 A.

C.3.1.4.3 Stator coil wire diameter The choice of stator coil wire diameter choice was one of fabrication practicality and electrical suitability. Too thick a wire would be incredibly difficult to wind uniformly. While it is true that using thicker wire would reduce overall circuit resistance, however this is only strictly true for D.C current and when oscillatory or A.C currents are considered the skin effect must also be taken into account. With the size of the tank circuit capacitor specified and an the stator coil inductance known an approximate frequency of operation can be estimated to be in the order of 3kHz using the formula below

$$f = \frac{1}{2\pi\sqrt{L_{ss} \cdot C}}$$

The skin effect will result in the current flowing through the stator coil to flow on the outer surface of the wire. This reduces the effective current carrying area of the wire resulting in losses. This skin effect is worsened by increasing frequency or increasing wire diameter. The wire diameter chosen is the largest diameter practically possible (to minimize resistance while being easy to wind) which could operate at a frequency close to 3 kHz [3]. The chosen wire diamter is thus 2.3mm.

C.3.1.4.4 Stator coil length The length of the stator coil is a value derived from previous specifications. It is important that this length is not more than 50 mm or else completing a 6 stage launcher based on the stator coil design would exceed the overall specified length of 500mm (allowing for mounting and stage spacing). The final stator coil length is the product of the number of coil turns and the coil wire diameter, yielding a stator coil length of 37 mm.

C.3.1.4.5 Stator coil resistance Since this value is in the order of 10^{-3} Ω measuring the actual value cannot be done with a standard ohmeter. The coil resistance used in launcher modeling was infact calculated in the simulation code (as shown in Appendix B.3.4 on page B-11) as 11 mΩ. When measured with a Galvanic ohmeter the stator coil resistance was approximatly 6 mΩ, far less than that predicted by the simulation, thus giving more allowance for tank circuit wiring resistance.

C.3.1.4.6 Sturdy mounting/securing of coil to barrel form The stator coil will conduct thousands of Amps and therefore must be securely mounted to the barrel form to avoid accidental movement or distortion of the windings which may occur because the current flowing in each turn is effectively anti-parallel to the same current in the turns adjacent. The stator coil is thus held in place using varnish and clear tape at its ends.

C.3.1.5 Armature Coil Specification

C.3.1.5.1 Armature mass Minimization of armature mass is of great importance if high accelerations are hoped to be achieved. This was considered throughout the armatures design most specifically when selecting the correct number of turns for the coil. Weight was also reduced by removing material on the polypropelene coilform as shown in. The armature weight was determined using ProEngineer using specified material densities shown in Table 29 below, yeilding a design weight specification of 58 g.

Table 29: Densities used in armature and stator coil mass calculations [47, 48].

Density of Copper	8.96 g.cm^{-3}
Density of Polypropylene	0.95 g.cm^{-3}

The final armature weight of 68 g was only slightly heavier than expected, largely due to the additional weight of the varnish used to protect and secure the coil to the form.

C.3.1.5.2 Armature coil inner diameter The stator coil form is purchased off the shelf having an inner diameter of 46 mm. The armature coil form diameter was chosen such that radius ratio of the armature and stator coils is maximised. Therefore for a a clearance of 1 mm between the armature coil and the stator coil form and assuming an initial armature coil wire diameter of 2 mm the coil form is constrained to a maximum diameter of 40 mm.

C.3.1.5.3 No. of armature coil turns Assuming an initial wire diameter of 2 mm the number of armature turns was chosen such that the armature coils length would be similar to that of the specified stator coil. To achieve this around 18 turns are required. However it was revealed by extensive simulation that the weight of this many turns would severely limit performance and choosing a number slightly less would greatly improved the coil pair's performance. As such the specified number of turns is 15.

C.3.1.5.4 Armature coil wire diameter Initial simulations were conducted with an armature wire diameter of 2 mm. In practice 1.8 mm enameled copper wire is used. The slightly increased coil resistance, however the performance gains from weight minimizations more than made up for this. Furthermore it would increase the spacing between armature coil and the stator coil form to 1.8 mm enough to be certain there would be no interference, even after varnish is applied to the armature windings.

C.3.1.5.5 Armature coil length Similarly to the stator coil, the armature coil length is a specification derived from the number of coil turns and widning wire diameter specifications. The final armature coil length is therefore 27.4 mm, approximately 9 mm shorter than the stator coil.

C.3.1.5.6 Initial stator and armature coil offset The armature and stator coil pair must have lengths such that when the armature is in its optimum position (for the corresponding stage stator coil to be energized), part of the armature must be outside of the stator coil in order for the optical position detection of the armature to take place. Since both armature and stator coil geometries are now completely specified it was determined through the computer simulation that the optimum armature/stator coil axial separation would be 16mm. At this position the requirement that the armature coil be outside of the stator coil is achieved, enabling optical triggering to be used on the device if any stage expansion research is conducted.

C.3.1.5.7 Armature coil resistance Since this value is in the order of 10^{-3} Ω measuring the actual resistance cannot be done with a standard ohmeter. Furthermore the armature coil would be shorted on istelf and thus measuring the actual resistance of the final coil is very difficult indeed. The coil resistance used in simulation was infact calculated in the simulation code as 13.6 mΩ.

C.3.1.5.8 Polypropelyne armature coil form A polypropylene coilform must be used as this is the lightest commercially available plastic. It also has excellent mechanical properties, meaning that more material can be removed (reducing weight) leaving the coil form walls thinner still but strong enough for the armature coils to be wound onto them and to resist any compressive stresses which may be experienced during the launching operation.

C.3.1.5.9 Sturdy mounting/securing of coils to form Like the stator coil, the induced current flowing in the armature coil could cause distortion of the windings. For this reason the armature windings are secured to the form by coating the coil windings in varnish. A total of 6 coats of varnish have been applied to all armature coils which neatly secures the windings in place. This increased the armatures total weight by approximately 10 g.

C.3.1.6 IGBT Device Specification

C.3.1.6.1 Tolerable junction temperature rise To be sure that the IGBT device may be operated beyond its specified continuous current capability for short time durations it must be determined whether or not its junction temperature will exceed the specified maximum limit of the device. Since most semiconductor devices have a maximum allowable junction temperature of 150 ^{o}C selecting the device was a simple matter of find a device with a suitable on state voltage rating and a transient thermal impedance (both used to calculate junction temperature rise) which would maintain the junction temperature below 150^oC.

Based on the junction temperature rise simulations (discussed and calculated in Appendices A.5.5 on page A-39 & B.10 on page B-22) the chosen IGBT module's junction would reach a maximum temperature of 118 ^{o}C which is suitably lower than the devices maximum limit of 150 ^{o}C [37].

C.3.1.6.2 Voltage rating Since the maximum voltage to be applied to the stator coil during the capacitors discharge is already specified as to be 400 V, an IGBT module (with anti-parallel protection diode) must be chosen such that its switching voltage or maximum voltage which it can block during its off state than this. The chosen device (Mitsubish CM600HU-12F) had a voltage rating of 600V providing an overload safety factor of 1.5.

C.3.1.6.3 Peak repetitive pulse current The peak repatative pulse current is the maximum current magnitude seen by the device during its operation. The theoretical value was determined by theoretical modeling taking the maximum peak current in the oscilatory waveform which occours when the capacitor is discharged into the stator coil. This waveform obviously decays, and thus quoting the maximum value can be considered as a very conservative assumption.

C.3.1.6.4 Gate drive voltage This is a very important specification which must be taken into account when designing the devices drive circuitry. The value in the chosen IGBT module's data sheet the maximum gate emitter voltage or drive voltage as seen. The drive circuitry which provides the output drive pulse for the IGBT's gate cannot exceed this maximum value as it may result in permanent damage of the device. However if the gate voltage is far to low it will result in an increased saturation voltage across the collector and emitter during the IGBT's conduction cycles, severely limiting the current which is conducted.

C.3.1.6.5 Anti-parallel diode The chosen IGBT module must also have a built in anti-parallel protection diode across its collector and emitter. This is to ensure conduction of positive and negative cycles of the oscillatory tank circuit current.

C.3.1.7 Control Circuitry

C.3.1.7.1 Use GT16 Microprocessor Since the single stage test linear induction launcher was originally developed to operate as part of a 6 stage launcher it is important that the devices control circuitry is built to allow for convenient implementation of a GT16 Microprocessor control. As such the control circuit must have to lines, (Ground and +5 V) which can be connected directly to a microprocessor kit. The launcher must be triggered by pulling the +5 V to ground, the ground line is to reference the microprocessors control circuitry.

C.3.1.7.2 Drive on state voltage (Output High) The magnitude of the drive voltage was chosen such that it would be high enough for the device to operate in its linear region (thus minimizing the collector emitter voltage across the IGBT) without being to close to the absolute maximum limit. The drive voltage used is 16 V, typical for most IGBT applications.

C.3.1.7.3 Drive off state voltage (Output Low) In order to turn the IGBT off, the voltage at the devices gate must simply be below the its specified threshold voltage. The chosen IGBT (Mitsubishi CM600HU-12F) has a threshold voltage of 4.5 V. Since a single supply rail op amp (LM 358) was used, the low state of the op amp could not be exactly 0 V which is deemed acceptable since the output only needs to be less than 4.5 V. Furthermore switching speeds for turn off are not of any concern as it is expected the current will have completely decayed within the chosen pulse period (Governed by the 555 IC Timer circuit). The off state voltage was thus very close to but not actually 0 V.

C.3.1.7.4 Pulse period The pulse time was chosen to greatl1y exceed the launching time. This is because unintentional turn of the IGBT during its conduction may result in failure of the device. Since time period for the tank circuit current to completely decay is in the order of milliseconds, choosing a drive pulse time of approximately 2 seconds would be more than sufficient to ensure the gate voltage would not go low during the IGBT's conduction cycle.

C.3.2 Experimental Measurements

C.3.2.1 Stator Current Real-time measurement of the tank circuit current is required for any interesting insights into the test launchers operation to be made clear. Measurement of the current will provide feedback data on 3 parameters (Namely the frequency of oscillation, the extent of damping and of course the magnitude of the current.) of the launcher which can readily be compared to the results aquired through extensive computational simulations. The current is measured using a current meter (Using a L.E.M module or current transformer to provide readings while remaining isolated from the tank circuit). Its output is 100 mV/A and could connected directly to a digital storage scope triggered on rising pulses. It is noted that waveform averaging and HF noise rejection features on the oscilloscope should also be enhance quality of the output current trace.

C.3.2.2 Capacitor voltage The initial voltage charge on the capacitor is measured directly using a digital mutlimeter. However because of the incredibly short duration of the current and voltage decay a typical multimeter cannot be used to determine the time varying voltagewave form. It is decided not to measure system voltage as it would not provided anything more meaningful/revealing than that already provided by the current measurement.

C.3.2.3 Armature velocity tracked with optical sensors It was decided vary early in the design of the test launcher that the armatures velocity would be determined using optical methodes. However in an effort to manage time effectively and prevent uncesssary work, the detailed design of the optical speed trap would only commence once the laboratory test launcher concept had been proven to launch the armature coil at a speed worth measuring.

C.3.3 Safty

C.3.3.1 Device must be properly grounded The device must be properly grounded, to prevent any points "floating" above ground which may result failure of supply circuit breakers to "trip" when a fault occurs and more dangerously user electrocution. In addition proper grounding of the device will also reduce any control circuit noise or radiation interference which may unintentionally trigger the IGBT drive circuit.

C.3.3.2 Control circuity for IGBT optically isollated For the purposes of operator safety and preventing control circuit damage, as much of the control circuit must be isolated from the actual gate drive circuit. This must be achieved using an opto-coupler to provide galvanic isolation between the 555 Timer IC control circuitry and the op-amp which provides the drive voltage of the IGBT.

C.3.3.3 IGBT properly mounted to heat sink The IGBT modules must be securely mounted to a suitable heat sink. Since the discharge period is so short this is probably more for safe sturdy location of the device than for heat dissipation.

C.3.3.4 Charging circuit must be fused The circuit used to charge capacitors must be suitably fused. The fuses are built into the variable A.C power supply and preventing it from drawing/supplying an excessive amount of current, which may occour if there is a fault in the tank circuit during charging.

C.3.3.5 Isolation transformer to protect variable A.C supply The purpose of the isolation transformer is to decouple the charging circuit and the variable A.C supply which would both otherwise share the same ground which may result in the variable AC supply's casing (which itself is grounded) "floating" to a hazardous voltage. Use of a suitable isolation transformer will prevent this from occurring.

C.3.4 Cost

C.3.4.1 Total cost The total budget allocated to each MEC4061Z undergraduate thesis project is around R1500. Additional funding is availabe, if necessary.

C.3.5 Dates for Deliverables

C.3.5.1 Parts drawings submissions Parts that require any machining must be submitted to the workshop for manufacture before the September Vacation (stating on 7th September 2007) to avoid the annual congestion of the Mechanical Engineering Department's Workshop, expected to be greater this year because of the number of students registered for the MEC4061Z course.

C.3.5.2 Final report submission A final coppy of the report is to be submitted to the mechanical engeering departmental secretary (Mrs. Thembisa Dlakiya) on Tuesday the 30st of October 2007.

C.3.5.3 Presentation A poster presentation and interview will be conducted with an external examiner on Tuesday 20th of November 2007.

D Detailed Test Results

Contents

Figures

Tables

D.1 Introduction

This appendix presents the many tank circuit waveforms found in practice for various operating voltages. These results are presented in contrast to the theoretical results predicted by computer simulations and used to develop the launcher system. The results will be compared in terms of

- Oscillation frequency [Hz]
- Peak current [Amps]
- Discharge period [sec]

It should be noted that the mechanical performance of the actual launcher is not discussed here, the reason being that notable motion of the armature was only achieved at voltages above 300 V. In which case the armature would only move approximately 15 mm, hardly enough to warrant optical velocity measurement of the armature coil. The poor mechanical performance differs from what the computer simulation had predicted, reasons explaining this are discussed in detail in Section 6 on page 47 within this reports main body.

For all the theoretical results that follow, the tank circuit uses and assumed loop resistance of 4 mΩin addition to the stator coil resistance and capacitor E.S.R of 11 mΩ and 1.67 mΩ respectively, the tank circuit capacitance used in the model was 305 μF which is the actual capacitance of the bank. Furthermore the maximum IGBT and diode voltage drop of 2.8 V is also included in the theoretical simulations.

D.2 Results

Test 1: Initial capacitor energy = 0.98 Joules @ 80 Volts

Table 30: Comparison of actual and theoretical result for the test launcher for an initial voltage of 80 V.

	Frequency of Oscillation	Period of Decay	Peak Current
Theoretical	3.2 kHz	4.5 msec	446 A
Actual	3.3 kHz	1.25 msec	375 A

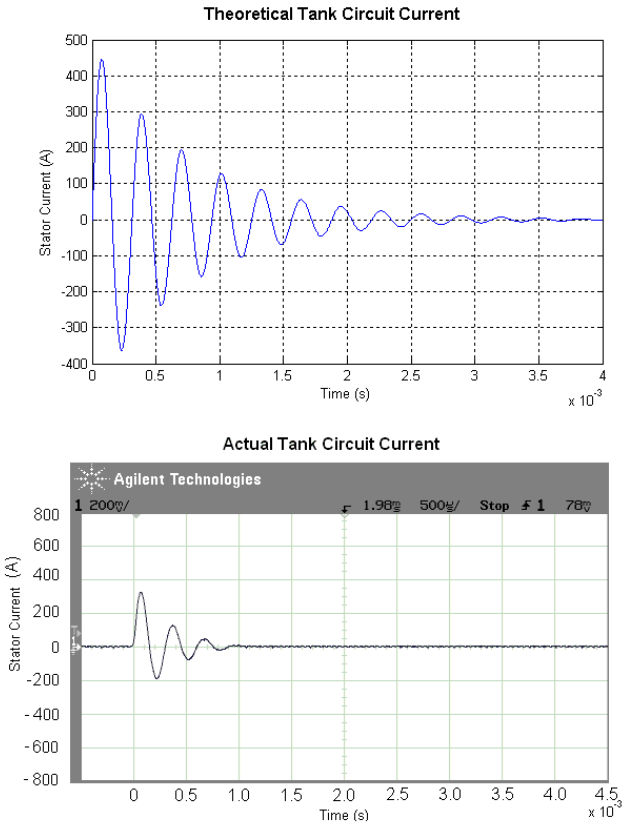

Figure 105: Comparative plots of the theoretical and actual current in the tank circuit/stator coil for an initial voltage of 80 V.

Test 2: Initial capacitor energy = 2.02 Joules @ 115 Volts

Table 31: Comparison of actual and theoretical result for the test launcher for an initial voltage of 115 V.

	Frequency of Oscillation	Period of Decay	Peak Current
Theoretical	3.2 kHz	4.5 msec	641 A
Actual	3.3 kHz	1.25 msec	600 A

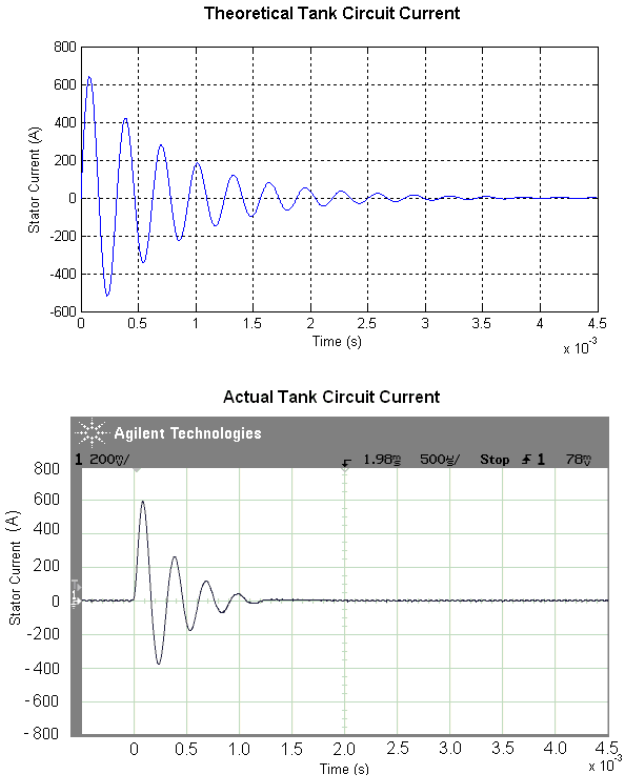

Figure 106: Comparative plots of the theoretical and actual current in the tank circuit/stator coil for an initial voltage of 115 V.

Test 3: Initial capacitor energy = 3.40 Joules @ 150 Volts

Table 32: Comparison of actual and theoretical result for the test launcher for an initial voltage of 150 V.

	Frequency of Oscillation	Period of Decay	Peak Current
Theoretical	3.2 kHz	4.5 msec	836 A
Actual	3.15 kHz	1.25 msec	740 A

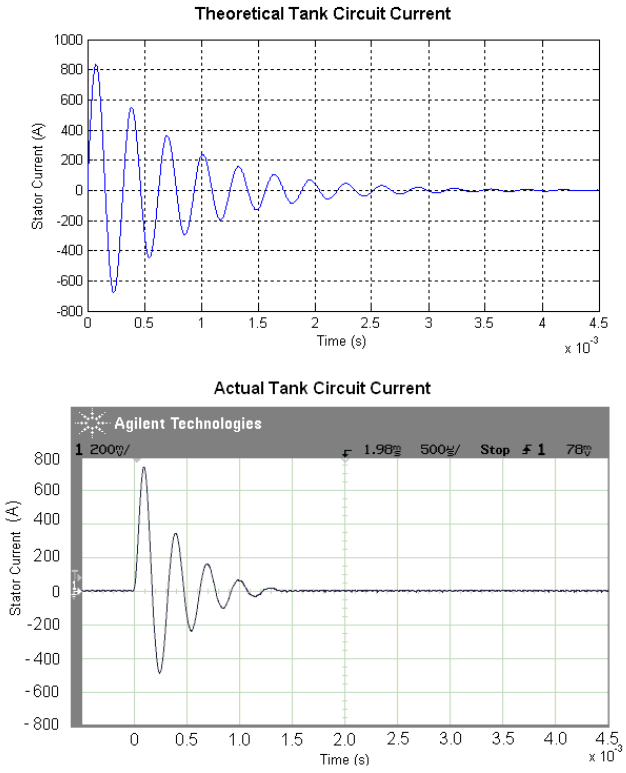

Figure 107: Comparative plots of the theoretical and actual current in the tank circuit/stator coil for an initial voltage of 150 V.

Test 4: Initial capacitor energy = 6.10 Joules @ 200 Volts

Table 33: Comparison of actual and theoretical result for the test launcher for an initial voltage of 200 V.

	Frequency of Oscillation	Period of Decay	Peak Current
Theoretical	3.2 kHz	4.5 msec	1115 A
Actual	3.0 kHz	1.5 msec	810 A

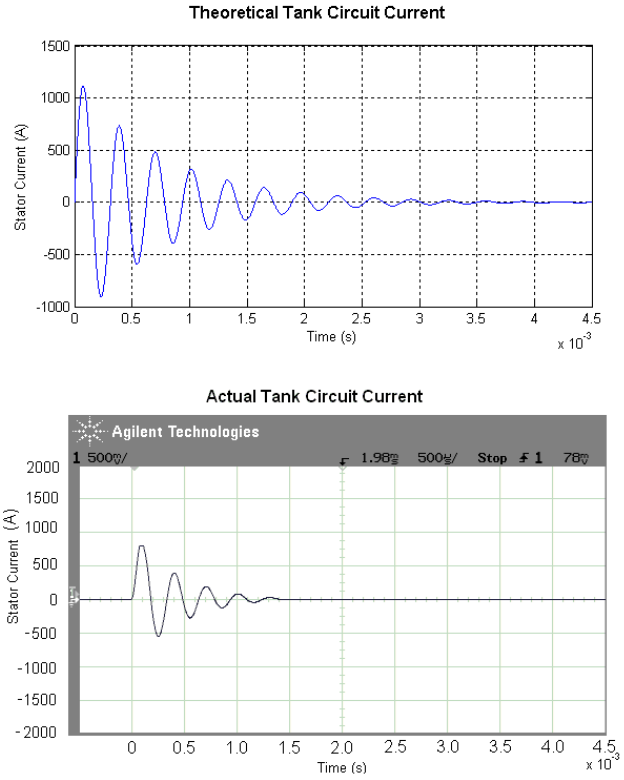

Figure 108: Comparative plots of the theoretical and actual current in the tank circuit/stator coil for an initial voltage of 200 V.

Test 5: Initial capacitor energy = 6.70 Joules @ 210 Volts

Table 34: Comparison of actual and theoretical result for the test launcher for an initial voltage of 210 V.

	Frequency of Oscillation	Period of Decay	Peak Current
Theoretical	3.2 kHz	4.5 msec	1171 A
Actual	3.15 kHz	1.75 msec	1150 A

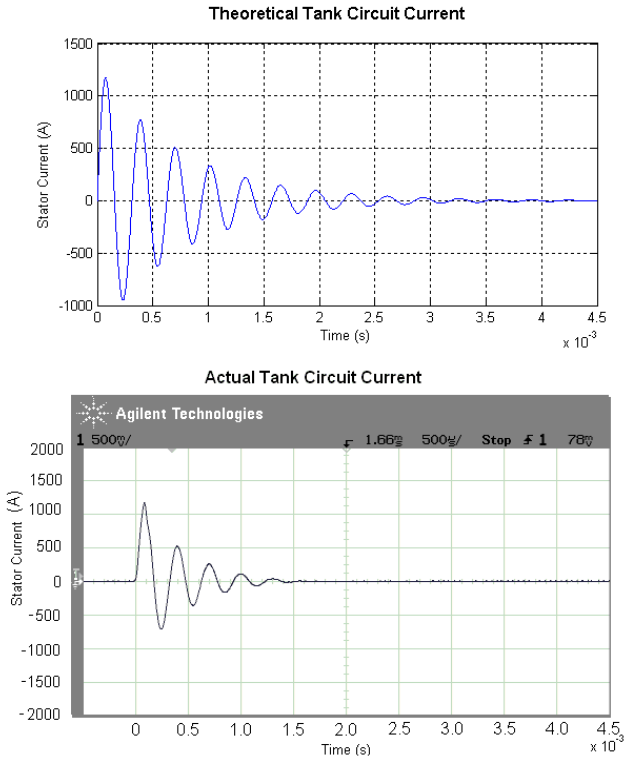

Figure 109: Comparative plots of the theoretical and actual current in the tank circuit/stator coil for an initial voltage of 210 V.

Test 6: Initial capacitor energy = 9.50 Joules @ 250 Volts

Table 35: Comparison of actual and theoretical result for the test launcher for an initial voltage of 250 V.

	Frequency of Oscillation	Period of Decay	Peak Current
Theoretical	3.2 kHz	4.5 msec	1394 A
Actual	3.3 kHz	1.25 msec	1200 A

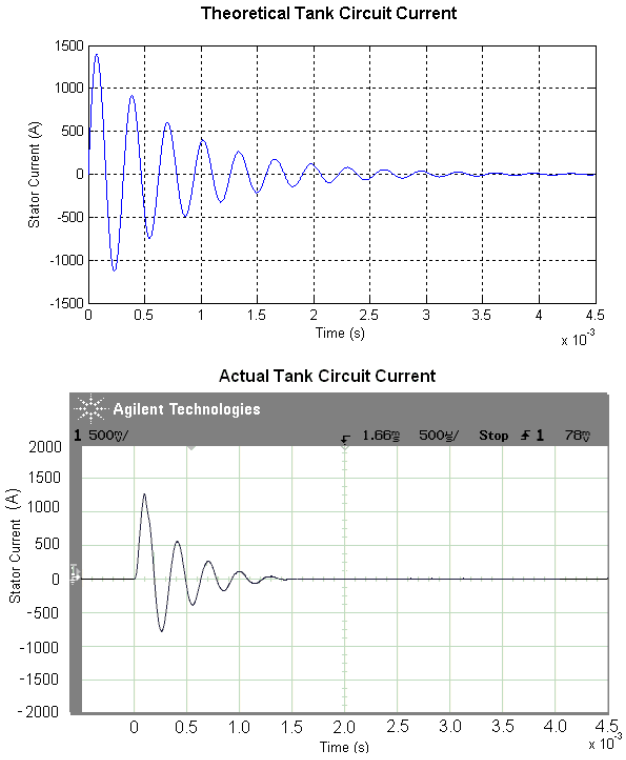

Figure 110: Comparative plots of the theoretical and actual current in the tank circuit/stator coil for an initial voltage of 250 V.

Test 7: Initial capacitor energy = 13.70 Joules @ 300 Volts

Table 36: Comparison of actual and theoretical result for the test launcher for an initial voltage of 300 V.

	Frequency of Oscillation	Period of Decay	Peak Current
Theoretical	3.2 kHz	4.5 msec	1672 A
Actual	2.8 kHz	1.8 msec	1400 A

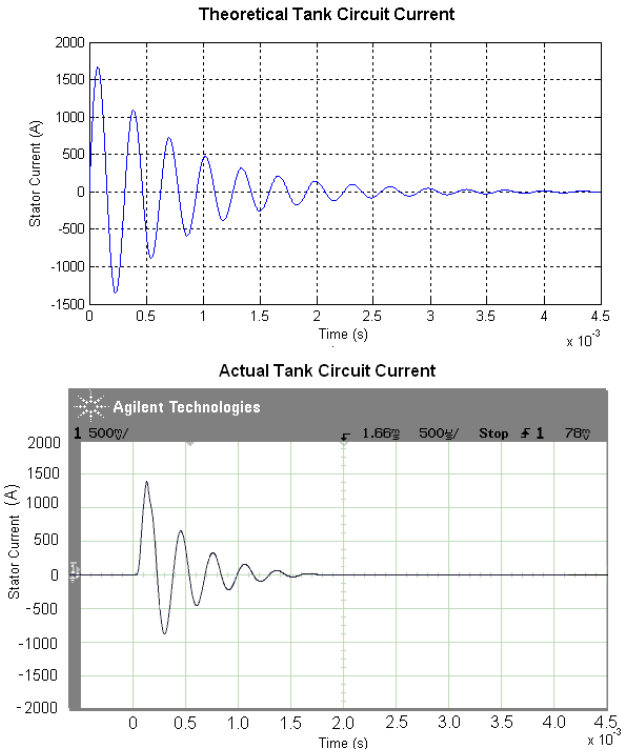

Figure 111: Comparative plots of the theoretical and actual current in the tank circuit/stator coil for an initial voltage of 300 V.

Test 8: Initial capacitor energy = 18.70 Joules @ 350 Volts

Table 37: Comparison of actual and theoretical result for the test launcher for an initial voltage of 350 V.

	Frequency of Oscillation	Period of Decay	Peak Current
Theoretical	3.2 kHz	4.5 msec	1952 A
Actual	3.3 kHz	2.25 msec	1400 A

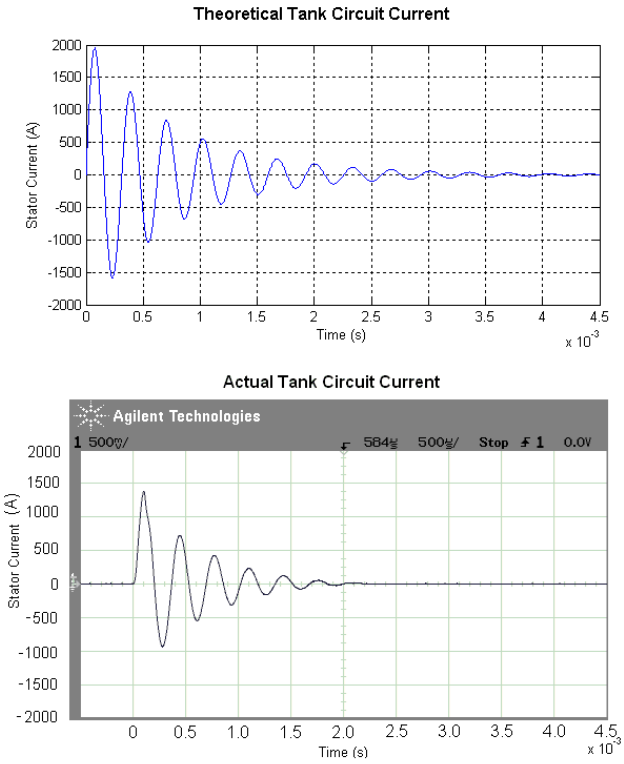

Figure 112: Comparative plots of the theoretical and actual current in the tank circuit/stator coil for an initial voltage of 350 V.

E Drawings

Table 38: List of Drawings.

Drawing number	Drawing Name	Type
1.1	Final Assembly	Assembly
1.2	Barrel Assembly	Assembly
1.2.1	Stator Coil Form	Part
1.2.2	Base	Part
1.2.3	Lower Mounting Block	Part
1.2.4	Upper Mounting Block	Part
1.3	Armature Assembly	Assembly
1.3.1	Armature Coil Form	Part
1.4	Complete Circuit Diagram	Circuit

Table 39: Electric Components List.

Item No.	Description
B	10 A; 1500V Bridge Rectifier
C_1	Capacitor 47 uF
C_2	Capacitor 0.76 uF
C_3	Capacitor 10 nF
C_4	Tank Circuit Capacitor 305 uF; 450 V
F_1	Fuse 10 A
F_2	Fuse 10 A
I	IGBT [CM600HU-12F]
IC	555 Timer IC
L	Stator Coil
OA	Op-amp [LM358]
OC	Opto-coupler [4N32]
R_1	Resistor; 10 kΩ
R_2	Resistor; 10 kΩ
R_3	Resistor; 10 kΩ
R_4	Resistor; 10 kΩ
R_5	Resistor; 10 kΩ
R_6	Resistor; 2.7 kΩ
R_7	Resistor; 500 kΩ
R_8	Resistor; 10 kΩ
R_9	Resistor; 150 kΩ
R_10	Resistor; 10 kΩ
R_11	Resistor; 5 kΩ
S	Safety Interlock
Z	Zener Diode 16 V; 5W